Università degli Studi di Palermo

AREA QUALITÀ, PROGRAMMAZIONE E SUPPORTO STRATEGICO
SETTORE STRATEGIA PER LA RICERCA
U. O. DOTTORATI

Dottorato in Information and Communication Technologies.
Dipartimento di Ingegneria
Settore Scientifico Disciplinare ING/INF 04

# ROBUST CONTROL OF NONLINEAR SYSTEMS: AN UNKNOWN INPUT OBSERVER BASED APPROACH

IL DOTTORE
**ING. SALVATORE PEDONE**

IL COORDINATORE
**PROF. ILENIA TINNIRELLO**

IL TUTOR
**PROF. ILENIA TINNIRELLO**

EVENTUALE CO TUTOR
**ING. ADRIANO FAGIOLINI**

CICLO ____XXXV___
ANNO CONSEGUIMENTO TITOLO ___2023_____

**Abstract:** This thesis addresses the robust control of complex nonlinear system via an Unknown Input Observer based approach. More specifically, through a suitable model dynamic reformulation, a generic nonlinear system has been described as the sum of two functions, the first linear and known and the second highly nonlinear and unknown, resulting from imperfect knowledge of system model parameters, exogenous disturbances and so on, which can be seen as a perturbation (disturbance) of the linear function. This simplification allows an advantageous system dynamic description in matrix form. Subsequently, a discrete-time Delayed Unknown Input Observer has been designed to asymptotically estimate both system state and disturbance at the only cost of a few sample delay. Finally, a controller actively compensates the estimated disturbance and asymptotically steers the system state to the desired one. This thesis also presents a closed-loop stability proof of the method. The proposed solution advantageously needs no a-priori information about the total perturbation boundedness, additional variables to model uncertainties, or observer parameters to be tuned. Its effectiveness and superiority to existing methods are studied in theory and practice in two different contexts, i.e. self-driving racecars and articulated soft-robots.

# Contents

# Chapter 1

# Introduction

In most control applications, it is hard to establish the mathematical models that regulate the system dynamics precisely. Indeed, some parameters process can have a different values with respect to the nominal ones or some variables can influence the process from the around environment, significantly complicating the control problem resolution.

This is the main reason for Proportional-Integral-Derivative (PID) control massive use in industrial applications along the last century because this technique does not use any mathematical model for system control [1]. Despite its simplicity, the PID control struggles to keep up with the current control engineering goals where high standards of efficiency are pursued, specially for systems that work in complex environments.

In this context, many control approaches have been proposed to handle the undesirable effects caused by unknown disturbances and system parameter uncertainties that can be summarized as follows [2]:

1. Adaptive Control: The key idea is that the model parameters of the controlled systems is first identified online, then the control parameters are tuned based on the identified model parameters to obtain good performance. Adaptive control is valid solution in dealing with model parameter uncertainties and nowadays it is widely used in practical engineering. The Adaptive Control goodness solution highly depend on the design of identification or estimation laws on time-varying model parameters. When these are difficult to identify or estimate online,

these method is not applicable.

2. Robust Control: It focuses mainly on the abilities of the controller to manage model uncertainties. The main idea of the robust control design is to consider the worst case of model uncertainties and its robustness is generally obtained getting poor system transient performance. For this reason, the classical Robust Control is often criticized to be over-conservative.

3. Sliding Mode Control: It is able to suppress the effects of parameter perturbations as well as external disturbances. Despite it, the discontinuous switching of the controller tends to produce the so-called chattering phenomena. Although the employment of some modification methods such as the saturation function method could effectively reduce the chattering problem, the advantage of prominent disturbance rejection performance is sacrificed.

4. Internal Model Control: This technique received a great deal of attention in the control theory due to its simple concept and intuitive design philosophy. However, the Internal Model Control is generally available for linear systems and the implementation of the related algorithm for high dimensional system is quite sophisticated due to the requirement of calculating the inverse of a high dimensional transfer function matrix.

Ultimately, these control approaches generally achieve the goal of disturbance rejection via feedback regulation based on the tracking error between the measured outputs and their set-points. Thus, designed controllers can not react directly and fast enough in the presence of strong disturbances [3].

## 1.1 Thesis Contributions

This thesis aims to overcome the complexity of nonlinear system modeling and control and proposed a fast disturbance rejection method via an unknown input observer-based approach. This goal has been obtained via a suitable reformulation of a generic nonlinear system to decouple the dynamics into the sum of two functions. The first, totally known and linear and the second unknown and

highly nonlinear. More specifically, consider the nonlinear discrete-time system

$$\begin{aligned} x_{k+1} &= f\left(x_k, u_k, w_k, k\right) \\ y_k &= g\left(x_k, u_k, w_k, k\right) \end{aligned} \tag{1.1.1}$$

where $f$ and $g$ are two vectorial functions and where $x_k \in \mathbb{R}^n$, $u_k \in \mathbb{R}^m$, $w_k \in \mathbb{R}^p$ are the state, the known and the unknown input vectors, respectively and finally $y_k \in \mathbb{R}^c$ is the output vector. Without loss of generality, we can affirm that the above system state can be rearranged as

$$x_{k+1} = \bar{f}\left(x_k, u_k, k\right) + \delta_k\left(\tilde{x}_k, \tilde{u}_k, \tilde{w}_k, k\right) \tag{1.1.2}$$

where $\bar{f}\left(x_k, u_k, k\right)$ is a nominal linear function that we can assume as known and where $\delta_k\left(\tilde{x}_k, \tilde{u}_k, \tilde{w}_k, k\right) = f\left(x_k, u_k, w_k, k\right) - \bar{f}\left(x_k, u_k, k\right)$ is an unknown nonlinear disturbance function that can lumped together a different kinds of uncertainties as model parameter variations, exogenous disturbances and so on. In this way, the system (1.1.2) can be described in the following simplified matrix form

$$\begin{aligned} x_{k+1} &= A\, x_k + B\, u_k + W\, \delta_k \\ y_k &= C\, x_k + D\, u_k + \Theta\, \delta_k \end{aligned} \tag{1.1.3}$$

where $A \in \mathbb{R}^{n\times n}$, $B \in \mathbb{R}^{n\times m}$, $W \in \mathbb{R}^{n\times v}$ , $C \in \mathbb{R}^{c\times n}$, $D \in \mathbb{R}^{c\times m}$ and $\Theta \in \mathbb{R}^{c\times v}$ are the corresponding system matrices. By virtue of this simplification, the starting nonlinear system (1.1.1) becomes a linear system perturbed by a disturbance signal $\delta_k \in \mathbb{R}^v$.

Once the model reformulation has been derived, the problem of the unknown input reconstruction has been addressed. This thesis solves this problem via the Delayed Unknown Input Observer theory (DUIO), [4]. It has been attacked exploiting the output history vector within an horizon of $L$ delayed sample, whose knowledge allows the design of DUIO that is able to asymptotically reconstruct both system state and disturbance signals.

Despite the estimations are delayed, the DUIO allows to relax the strict conditions that must be met in order to reconstruct the entire state vector in classical unknown input observer approach [5]. Furthermore, DUIOs do not lean on assumptions on the disturbance dynamics and its boundedness,

require no parameter tuning and have exact convergence guarantees of system state and disturbance. This allows to outperform other existing solutions such as Extended State Observers (ESO) or Extended Kalman Filter as demonstrated in chapters (3-4).

Note the disturbance signal reconstruction, a control law composed by a static state feedback and an open-loop disturbance compensation has been derived to asymptotically steer the system trajectories to the desired ones, as shown in chapter (2).

As widely presented in chapters (3-4), this technique, namely DUIO-based Control, has been validated into two different context with a closed-loop stability proof. The first, the self-driving car ones, where the proposed solution is applied to control both longitudinal and lateral vehicle dynamics. More precisely, using the measures coming from the classical vehicle on-board sensors such as a Global Positioning System (GPS) or an Encoder, two different DUIO based controller have been designed [6, 7], capable of estimating both vehicle state and disturbance signals, according to the model decomposition above-mentioned, and finally to steer the vehicle to the desired behaviour. Furthermore, a DUIO-based approach has been utilized for a wind-sensorless estimation and compensation for racecar model affected by lateral wind gusts. The simulation are carried out on the Matlab&Simulink environment using the Vehicle Dynamics Blockset, a particular tool that emulates more realistic driving conditions, via a real-time execution of the approach through the implementation on a real Raspberry PI hardware. The solution goodness is widely demonstrated, expecially with respect to the benchmark solutions as Extended Kalman Filter or Extended State Observer.

Finally, the DUIO-based control approach has been applied to the soft-robot control context, to control both stiffness and position in robot joints [8]. More specifically, a DUIO for VSA-driven robots that simultaneously estimates the input disturbance and system states is derived, with a robust controller that is able to provide perfect asymptotic tracking of position and stiffness desired trajectories. The proposed solution goodness is proved by a simulations on Matlab&Simulink environment and via an experimental validations on a multi degree-of-freedom VSA-driven articulated soft robot [9] with a successfully tracking of the desired position and stiffness references despite the existing nonlinearities and uncertainties.

# Chapter 2

# Robust Control: An Unknown Input Observer Approach

In this chapter the proposed DUIO-based control solution is presented. The first paragraph recalls the theoretical foundations of the Delayed Unknwon Input Observer [10]. The second and last paragraph, instead, shows the DUIO-based control design.

## 2.1 Delayed Unknown Input Observer

Consider the system expressed in matrix form (1.1.3). Without loss of generality, we assume that the matrix $\begin{bmatrix} W \\ \Theta \end{bmatrix}$ is full-column rank. It should be noted that this condition can be always satisfied by a suitable transformation of the unknown input signals as in [11].

It is well-known that the system response over a time delay step $L$ can be expressed as

$$y_k^L = \mathbb{O}^L x_k + \mathbb{H}^L u_k^L + \mathbb{V}^L \delta_k^L \tag{2.1.1}$$

having defined the related history vectors $y_k^L = (y_k, ..., y_{k-L})^T$, $u_k^L = (u_k, ..., u_{k-L})^T$ and $\delta_k^L = (\delta_k, ..., \delta_{k-L})^T$ and where $\mathbb{O}^L$, $\mathbb{H}^L$ and $\mathbb{V}^L$ are the $L$-step observability and invertibility matrices

that can be obtained via the following recursive definitions

$$\mathbb{O}^L = \begin{pmatrix} C \\ \mathbb{O}^{L-1} A \end{pmatrix}, \mathbb{H}^L = \begin{pmatrix} D & 0 \\ \mathbb{O}^{L-1} B & \mathbb{H}^{L-1} \end{pmatrix}, \text{ and } \mathbb{V}^L = \begin{pmatrix} D & 0 \\ \mathbb{O}^{L-1} W & \mathbb{V}^{L-1} \end{pmatrix}.$$

The existence of a Discrete-Time Unknown Input Observer (DUIO) can be summarized via the following proposition:

**Proposition 1** (Delayed Unknown-Input Observer, DUIO)**.** *Given a suitable design delay step $L$, the discrete-time linear system*

$$\begin{aligned} \hat{x}_{k+1-L} &= E\,\hat{x}_{k-L} + F\,y_k^L + B\,u_k - F\,\mathbb{H}^L\,u_k^L, \\ \hat{\delta}_{k-L} &= G \begin{pmatrix} \hat{x}_{k+1-L} - A\,\hat{x}_{k-L} - B\,u_{k-L} \\ y_{k-L} - C\,\hat{x}_{k-L} - D\,u_{k-L} \end{pmatrix}, \end{aligned} \tag{2.1.2}$$

*where $G$ is the left-pseudoinverse of $(W^T, \Theta^T)^T$, and $E$ and $F$ satisfy the conditions:*

*A1)* $F\,\mathbb{V}^L = (W, 0_{n\times m})$ *(*input decoupling*),*

*A2)* $E = A - F\,\mathbb{O}^L$ *(*initial state decoupling*),*

*A3) $E$ is Schur, i.e. having eigenvalues in the unit circle (*free solution convergence*),*

*is a DUIO for the model (1.1.3), i.e. it generates delayed state and input estimates, $\hat{x}_{k-L}$ and $\hat{\delta}_{k-L}$, asymptotically tracking the delayed ones of model in (1.1.3), or equivalently*

$$\lim_{k\to\infty} (\hat{x}_{k-L} - x_{k-L}) = 0\,, \quad \lim_{k\to\infty} (\hat{\delta}_{k-L} - \delta_{k-L}) = 0\,. \quad \square$$

*Proof.* Exploiting equations (1.1.3)-(2.1.2), a direct computation of the delayed state estimation

error shows that

$$
\begin{aligned}
e_{k-L+1} &= \hat{x}_{k-L+1} - x_{k-L+1} = \\
&= E\,\hat{x}_{k-L} + F\,y_k^L + B\,u_{k-L} - F\,\mathbb{H}^L\,u_k^L - A\,x_{k-L} - B\,u_{k-L} - W\delta_{k-L} = \\
&= Ee_{k-L} + \left(E - A - F\,\mathbb{O}^L\right)x_{k-L} + F\,\mathbb{H}^L u_k^L + F\,\mathbb{V}^L\delta_k^L - F\,\mathbb{H}^L u_k^L + \\
&- W\,\delta_{k-L} = \\
&= Ee_{k-L} + \left(E - A - F\,\mathbb{O}^L\right)x_{k-L} + F\,\mathbb{V}^L\delta_k^L - W\,\delta_{k-L}
\end{aligned}
\tag{2.1.3}
$$

that solving the conditions A1) and A2) allows to obtain the following state estimation error dynamics

$$
e_{k-L+1} = E\,e_{k-L} \tag{2.1.4}
$$

which leads to the asymptotic tracking of the delayed state of system (1.1.3) if and only if the condition A3) is satisfied. □

Therefore, the existence of a DUIO is closely related to the solvability of condition A1) for some $L$ and $F$, for which the following proposition can be stated

**Proposition 2** (System Invertibility)**.** *Given the sequence of matrix* $\{\mathbb{V}^L\}$*, for* $L = \{1, \cdots, n\}$*, condition A1) can be solved for some* $F$ *if and only if there exists* $L$ *such that*

$$
rank(\mathbb{V}^L) - rank(\mathbb{V}^{L-1}) = v\,. \tag{2.1.5}
$$

*where* $v$ *is the dimension of the unknown input vector* $\delta_k$*.*

Furthermore, another fundamental condition is that the system must be strong observable, i.e.

**Proposition 3** (Strong Observability)**.** *For any initial state and any unknown inputs sequence, there is a positive integer* $L$ *such that the initial state can be recovered from the* $L$*-output history vector. This condition is satisfied if*

$$
rank\left[(\mathbb{O}^L \;\; \mathbb{V}^L)\right] = n + rank\left(\mathbb{V}^L\right) \tag{2.1.6}
$$

*where $n$ is the system order.*

## 2.2 DUIO-based Control

Once the unknwon input reconstruction law is known, we are ready to formalize the following theorem:

**Theorem 1.** *Given the system (1.1.3), the robust control law*

$$u_k = B^{-1}\left(\hat{\Phi}_k - W\,\hat{\delta}_k\right) \tag{2.2.1}$$

*where $\hat{\Phi}_k \in \mathbb{R}^{n\times m}$ is a suitable linear state feedback control law composed by the delayed estimated state variables, ensures robust and global bounded stability of both state estimation error $e_{k-L}$ and system state $x_k$, respectively, around the origin.*

*Proof.* The first step consists to describe the full system dynamics composed by (1.1.3) and (2.1.4) as

$$\xi_{k+1} = \begin{pmatrix} A & 0_{n\times n} \\ 0_{n\times n} & E \end{pmatrix}\xi_k + \begin{pmatrix} B \\ 0_{n\times m} \end{pmatrix} u_k + \begin{pmatrix} W \\ 0_{n\times v} \end{pmatrix}\delta_k \tag{2.2.2}$$

having denoted the new state vector $\xi_k = \left(x_k^T,\, e_{k-L}^T\right)^T \in \mathbb{R}^{2n}$. First, it should be noted that according to the DUIO design the state estimation error is independent with respect to the known and unknown inputs, respectively, and its zero-convergence is guaranteed by virtue of the fact that matrix $E$ must be Schur for condition A3).

Closing the loop with the control law (2.2.1), having chosen $\hat{\Phi}_k = -K\,\hat{x}_{k-L}$, where $K \in \mathbb{R}^{n\times m}$ is a free gain matrix, and finally considering that by virtue of state estimation error definition holds that $\hat{x}_{k-L} = (e_{k-L} + x_{k-L})$, we come to the following closed-loop system

$$\xi_{k+1} = \Sigma\,\xi_k + \Psi_k \tag{2.2.3}$$

where

$$\Sigma = \begin{pmatrix} A - B_c K & -B_c K \\ 0_{n\times n} & E \end{pmatrix}, \quad \Psi_k = \begin{pmatrix} B_c \\ 0_{n\times m} \end{pmatrix} \Delta_{u_k} + \begin{pmatrix} W \\ 0_{n\times v} \end{pmatrix} \tilde{\delta}_k$$

and with

$$B_c = (0_{n-1\times m}, 1_{m\times m})^T, \quad \tilde{\delta}_k = \left(\delta_k - \hat{\delta}_{k-L}\right), \quad \Delta_{u_k} = -K\left(x_k - \hat{x}_{k-L}\right),$$

A direct computation of the closed loop matrix $\Sigma$ shows that it is in upper triangular form and consequently its eigenvalues are equal to those of the submatrices that lie on the diagonal block, i.e. $(A - B_c K)$ and $E$, respectively. In the hypothesis that the controllability matrix of the pair $(A, B_c)$, i.e. $\mathcal{R} = (B_c | A\, B_c)$, has full rank, the existence of the gain matrix $K$ is guaranteed and the eigenvalues of $(A - B_c K)$ can be placed within the unit circle to generate asymptotically stable modes. Therefore, in the absence of disturbance $\Psi_k$, the closed-loop system is asymptotically stable.

To investigate the system stability when the disturbance $\Psi_k$ perturbs it, first we place the eigenvalues of matrix $\Sigma$ inside the unit circle and around the origin, i.e. $\sigma_i \in \text{spec}(\Sigma) \approx 0$, also ensuring its diagonalizability via a suitable choice of the gain matrix $K$. In this setting, we perform the change of coordinates $z_k = T\,\xi_k$ using the non-singular matrix $T$ composed by the eigenvector of matrix $\Sigma$. Therefore system (2.2.2) becomes:

$$z_{k+1} = \Lambda\, z_k + \Omega \Psi_k \tag{2.2.4}$$

where $\Lambda = \text{diag}(\sigma_i) = T^{-1}\Sigma T$, and $\Omega = T$. Choosing the discrete time Lyapunov function

$$V_k = z_k^T\, z_k \tag{2.2.5}$$

and computing the one-step forward difference we arrive to

$$\begin{aligned} \Delta V = V_{k+1} - V_k &= z_{k+1}^T\, z_{k+1} - z_k^T\, z_k = \\ &= (\Lambda\, z_k + \Omega\Psi_k)^T\, (\Lambda\, z_k + \Omega\Psi_k) - z_k^T\, z_k = \\ &= z_k^T \left(\Lambda^T\Lambda - I_{n\times n}\right) z_k + 2\, z_k^T\, \Lambda^T \Omega \Psi_k + \Psi_k^T \Omega^T \Omega \Psi_k \end{aligned} \tag{2.2.6}$$

Having placed the eigenvalues of the relating closed-loop matrix $\Sigma$ inside the unit circle and around

the origin, it is clear that $\left(\Lambda^T\Lambda - I_{n\times n}\right) \approx -I_{n\times n}$ and therefore the terms $z_k^T z_k$ and $\Psi_k^T\Omega^T\Omega\Psi_k$ dominate the rest of equation (2.2.6) that becomes

$$\Delta V = -z_k^T z_k + \Psi_k^T\Omega^T\Omega\Psi_k \tag{2.2.7}$$

Furthermore, a direct inspection of the perturbation term $\Psi_k$ shows that it is bounded with bound proportional to the product $\lambda L$, where $\lambda$ is the relative sampling-time. Indeed, it is closely related to the absolute maximum variation of $z_k$ and $\delta_k$ between $L$ consecutive samples. Therefore, in the hypothesis that within the horizon $[k : k-L]$ both state and disturbance are fixed at their absolute maximum values, i.e. $z_{k_M}$ and $\delta_{k_M}$, respectively, the maximum allowable variations are equal to the following quantities:

$$|\alpha_k| = |\lambda\, L\, z_{k_M}|, \;\; |\beta_k| = |\lambda\, L\, \delta_{k_M}|$$

A computation of the euclidean norm shows that

$$\begin{aligned} ||\Psi||_2 &\leq ||\Omega||_2^2 \left(||B_c||_2^2\, ||K||_2^2\, ||\alpha_k||_2^2 + ||W||_2^2\, ||\beta_k||_2^2\right) \leq \\ &\leq \lambda^2 L^2\, ||\Omega||_2^2 \left(||B_c||_2^2\, ||K||_2^2\, ||z_{k_M}||_2^2 \; + ||W||_2^2\, ||\delta_{k_M}||_2^2\right) \end{aligned} \tag{2.2.8}$$

Therefore to ensure the system bouned stability it is necessary that $\Delta V \leq 0$ that is it true

$$\forall \;\; ||z_k||_2^2 \geq \lambda^2\, L^2 ||\Omega||_2^2 \left(||B_c||_2^2\, ||K||_2^2\, ||z_{k_M}||_2^2 + ||W||_2^2\, ||\delta_{k_M}||_2^2\right) \tag{2.2.9}$$

To conclude, by virtue of (2.2.9) has been demonstrated that the system solution are globally bounded. However, for small sampling time we come to the statement that $||z_k||_2^2 \approx 0 \rightarrow z_k \approx 0$, which in turn implies that $\xi_k \approx 0$. □

# Chapter 3

# DUIO-based Control for Self-Driving Car

## 3.1 Introduction

In the near future, a great number of automotive applications will become possible [12], by leveraging on the availability of denser and faster communication networks that will soon be enabled by the 5G technology [13]. Via the Vehicle-to-Everything (V2X) architecture [14], all actors of future transport systems (vehicles, passengers, and pedestrians) [15,16] will be able to cooperatively plan and optimize their travel experience [17], according to faster [18], more efficient [19], secure [20], and safer [21–23] protocols. They will be able to share evidence of possible hazards, including unexpected traffic jams in tunnels, road damages, anomalous behavior of human drivers and autonomous pilots [24, 25], thus improving the overall safety of passengers and pedestrians [26]. In this scenario, the race towards (electric) vehicles with full self-driving capacity has just begun [27–30]. However, several obstacles have to be overcome before this technology goes mainstream to the market [31], including an infrastructure modernization [32, 33], the definition of legislations addressing moral and legal issues [34, 35], and the achievement of stronger guarantees on the ability of an autonomous vehicle to detect and react to uncertainties caused by unexpected changes in the driving conditions.

The two major sources of uncertainty when modeling a vehicle's dynamics are related to the traction force and the presence of external disturbance [36]. The traction force is proportional to the instantaneous friction coefficient, whose value can be computed only using heuristic functions, experimentally identified [37, 38], that require the knowledge of the type of road (dry, wet, snowy, and icy). In a realistic scenario, in which the road surface may change unexpectedly, the road type detection can be done by using visual data, but the accuracy of this process is affected by light conditions and the asphalt reflection property. External disturbance is due to sudden wind gusts, aerodynamic drag, and rolling resistance. Modeling persistent or rapidly changing winds, such as those occurring when exiting from a tunnel, driving on viaducts and overpasses [39], or as a result of the interaction with another approaching vehicle, is not easy. Direct measurement of the wind speed can be done by using anemometer sensors, based on pitot probes, which however are less accurate at lower speed, require altitude-dependent calibration, must be installed far enough from the vehicle to catch only laminar airflow, and introduce further costs. Consequently, even though the aerodynamic drag force can be accurately modeled, its direct estimation may be imprecise as it needs the information about the vehicle's speed relative to the wind velocity. The rolling resistance force is also known approximately, and its identification is vehicle-specific and requires so-called coast-down tests.

In order to obtain safe and performant control of a vehicle's motion, one can either use robust control techniques, such as sliding mode control [40], or estimate the unknown quantities by using dynamic input-state observers. Regarding the second approach, it has been recently shown that online estimation of tire-road interaction forces can be obtained if a full model, including tires, wheels, and vehicle dynamics, is considered [41]. Observers-based solutions can estimate the instantaneous maximum available power [42] and even allow prompt intervention of drivers upon risk detection [43]. The standard way of estimating a vehicle's state is undoubtedly by using Kalman filters [44, 45], which are optimal estimators when the vehicle is moving at a constant speed for almost all time. This optimality is lost if the vehicle performs aggressive driving maneuvers, made of sequences of acceleration and deceleration phases, when the nonlinear traction force is uncertain, or when the external disturbance is far from being a Gaussian noise signal. The estimation of the traction force and the other external disturbance signals named above can be obtained by using Extended Kalman

Filters (EKF). These filters provide good results, but they require adding new states to the observers and accurate modeling of their dynamics [46–48]. Discontinuous changes in the friction coefficient can be handled with adaptive estimators, thanks to the introduction of a parameter update law [49].

To overcome this limitation and simultaneously estimate disturbance inputs and states, Extended State Observers (ESO) come in handy, which, similarly to EKFs, model the deviation with respect to a nominal behavior as additional states and only require tuning a set of control parameters [50–52]. Despite their simplicity, they involve again high-gain parameters that make them often too sensitive to measurement noise and lead to peaky estimations. Also, they assume a small or negligible change over time of the disturbance signals [53]. Closely related to the ESOs is the Active Disturbance Rejection Control (ADRC) technique [54–57]. It is a robust control method assuming that parameter and model uncertainties are modeled as a disturbance input vector, estimated via an ESO, and finally compensated via a state-feedback control law [50]. Despite its simplicity, its closed-loop stability remains strongly linked to the underlying ESO's primary assumption that the disturbance acting on the system has a negligible rate of change, which leads to worse estimation performance in systems with fast varying disturbances.

Within this context, this thesis proposes a DUIO-based control solution for self-driving racecar to reconstruct the total disturbance signals, resulting from imperfect knowledge of the time-varying tire-road interface characteristics, the presence of other nearby vehicles, wind gusts, model reduction, and uncertainty and subsequently to actively compensate the estimated disturbances to steer the tracking error to zero. This solution needs no a-priori information about the total disturbance boundedness, additional variables to model uncertainty, or tuning of observer parameters and allows faster and more accurate disturbance estimation and better dynamic response.

The organization of the chapter is as follows: In the first two paragraphs (3.2)-(3.3), the traction force and lateral wind gust estimation problems are addressed, respectively. The closed-loop stability of the method is not presented and the information coming from the Unknown Input Observer is exploited for the design of suitable continuous-time controllers which steer the system state to the desired one. Finally, in the last paragraph, concerning the control of the lateral dynamics, a deep analysis of the closed-loop stability of the DUIO-based control is presented.

## 3.2 Racecar Longitudinal Control in Unknown and Highly-Varying Driving Conditions

### 3.2.1 Introduction

This paragraph addresses the longitudinal speed control problem for a racecar under unknown and highly-varying driving conditions. The aim is to provide the controlled vehicle with the capacity to asymptotically track an aggressive maneuver, i.e. a trajectory with a constant high-speed plateau [58], preceded and followed by fast acceleration/deceleration phases (Fig. 3.1).

The problem is attacked first by using the DUIO observer, which reconstructs the uncertain and unknown time-varying quantities affecting the vehicle dynamics, then obtaining a convenient reduced-degree-of-freedom model, and finally achieving a feedback control for the sought tracking.

The contribution of this solution is at least threefold. First, constructing a DUIO observer that uses only vehicle's and wheel speed measures and that allows estimating the current traction force, the resultant of the resistance forces, and the so-called effective tire radius. An appealing feature of this approach, is its independence from the knowledge of the actual time-varying traction model, the wind model, and the vehicle-specific rolling and aerodynamic coefficients. Such an independence is inherited from the decoupling of state and input reconstruction according to the DUIO theoretical foundations. The observer is computationally light, i.e. it consists of a linear dynamic system of the same order of the vehicle dynamics and a linear mapping reconstructing the unknown inputs, it is directly implementable on embedded hardware, and it is very fast. Contrarily to this solution, the most common observer-based control techniques, require adding additional states to the estimator, or need tuning the entries of the covariance matrices and possesses no convergence guarantees, such as for EKF-based approach. As a second contribution, under the assumption of small values for the slip ratio variable (later defined), a reduced-degree-of-freedom model for the vehicle's dynamics is derived, which is independent of the traction force. Based on this model and by using data estimated by the input-state observer, this approach describes a feedback control law that allows the asymptotic tracking of aggressive maneuvers, while maintaining the slip ratio below a desired threshold, irrespectively of the presence of external disturbance and abrupt changes in the traction

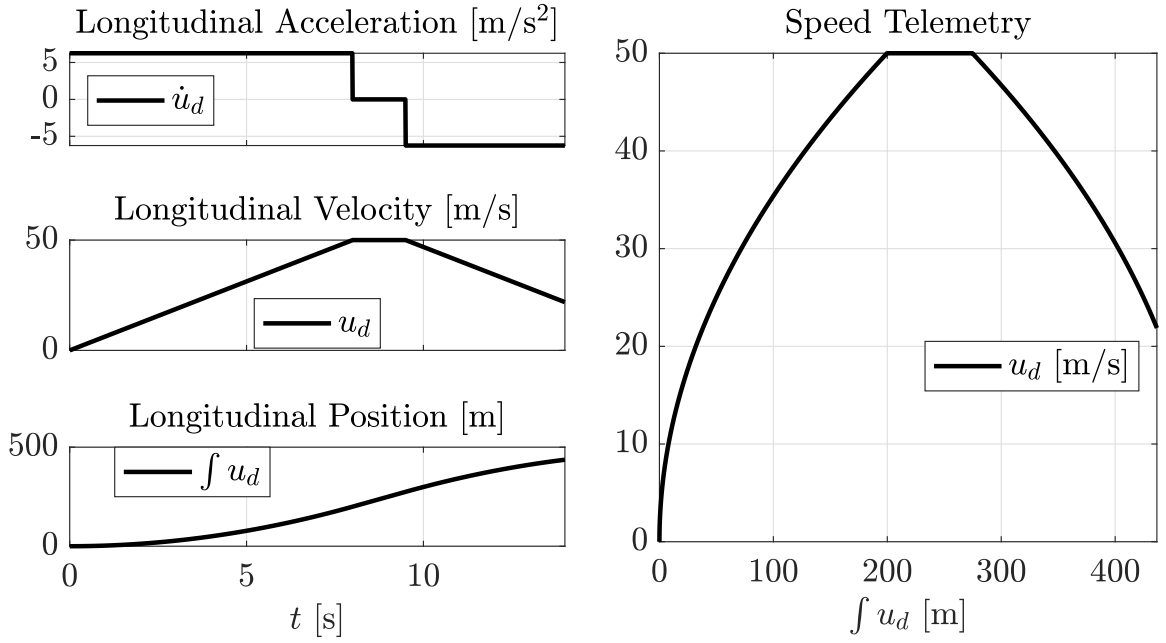


Figure 3.1: Example of a telemetry plot depicting an aggressive maneuver in which a racecar accelerates from 0 to 180 km/h (50 m/s) in 8 seconds with a constant acceleration of 6.25 m/s$^2$, then moves at a constant high speed, and finally decelerates with opposite acceleration rate.

force. Thirdly, the effectiveness and performance of the overall solution are shown through a series of simulations, carried out first with a nominal model, then adding system and measurement noise, and subsequently by using the Vehicle Dynamics Blockset. This last tool emulates more realistic driving conditions and allows showing the robustness of the proposed approach also to model uncertainties. Finally, real-time execution of the approach is proved via the implementation on a real Raspberry PI hardware.

### 3.2.2 System modeling: Longitudinal Vehicle Model

Consider a racecar with rear traction traveling along a flat and straight road. Under the common assumptions of having tires with identical geometric and inertial characteristics and traction that can be generated instantaneously, the dynamic behavior of the car is described by the so-called bicycle model [36]. Referring to such a model, by denoting with $\omega$ the speed of the virtual rear wheel and with $u$ the longitudinal velocity of the vehicle, the following dynamic equations can be

used

$$\begin{aligned} I_\omega \, \dot{\omega} &= T - R_\omega(\dot{u}) \, F_t(\omega, u, \dot{u}) \, , \\ m \, \dot{u} &= F_t(\omega, u, \dot{u}) - F_a(u) - F_r(u) \, , \end{aligned} \tag{3.2.1}$$

where $I_\omega$ is the wheel's inertia along the rotation axis, $m$ is the vehicle mass, $T$ is the input driving torque, $R_\omega$ is the so-called effective tire radius, $F_t$ is the rear traction force, $F_a$ is the aerodynamic drag force, and $F_r$ is the total rolling resistance force summing up the effects at all tires.

Though the model appears to be very compact, its complexity is actually encoded in every single term composing the dynamic expressions in Eq. (3.2.1), whose analysis reveals that the model is still in implicit form, thereby hindering the underlying estimation and control problems. More precisely, the effective tire radius $R_\omega$ relates the rotational wheel velocity $\omega$ to the linear longitudinal wheel velocity as it moves through the contact patch of the tire with the ground [59]. It can be shown that $R_\omega$ can be expressed according to the formula:

$$R_\omega = \frac{\sin(\arccos(R_d/R))}{\arccos(R_d/R)} R \, , \tag{3.2.2}$$

where $R$ and $R_d$ are the tire's undeformed and dynamic radii, respectively, the latter of which is obtained as follows:

$$R_d = R - \frac{F_z(\dot{u})}{K_t} , \tag{3.2.3}$$

with $F_z$ the vertical force acting on the rear tire and $K_t$ its stiffness along the vertical direction. In turn, the vertical force $F_z$ is obtained as a static term, depending on the geometry of the car and being present in conditions of constant longitudinal speed, and a dynamic one directly proportional to the longitudinal acceleration $\dot{u}$ and expressing the normal load transfer between front and rear axles during acceleration and braking phases. In particular, it holds [36]

$$F_z = \frac{m}{l} \left( g \, a_1 + h \, \dot{u} \right) , \tag{3.2.4}$$

with $l$ is the wheelbase, i.e. the distance between the rear and front axles, $a_1$ is the distance between the front axle and the vehicle's center of mass, and $h$ is the height of the center of gravity from to

the road. Based on this reasoning the effective tire radius is in the general case a function of the instantaneous longitudinal acceleration, i.e. $R_\omega = R_\omega(\dot{u})$.

Moreover, the rear traction force $F_t$ is highly dependent on many factors, among which are the characteristics of the road and the type of interaction between the tire and the road asphalt. At the state-of-the-art only heuristic expressions are available, which consist of static models providing the instantaneous traction force $F_t$ as a function of the wheel speed $\omega$, longitudinal velocity $u$ and acceleration $\dot{u}$, and other parameters to be ad-hoc identified (see e.g. [60]). For the sake of generality, the dynamics considered in Eq. (3.2.1) does not refer to any of such models, and as such the sought solution will do, while to evaluate the proposed solution the so-called Burckhardt's and Pacejka's formulas will be used later in paragraph (3.2.10). Similar reasoning holds for the expressions of the aerodynamic drag force $F_a$ and rolling resistance force $F_r$. Here, it is also assumed that the vehicle's pitching motion is limited and can occur only at the beginning of the acceleration or braking phase. This allows neglecting the effect of the suspensions on the vehicle's dynamic behavior, which is present only during short initial transients.

Furthermore, it can be assumed that the wheel's and longitudinal vehicle's speeds are available. Indeed, in modern cars, measurement of the wheel speed $\omega$ can be obtained from the Antilock Brake System (ABS), while that of the vehicle's longitudinal speed $u$ can be provided by speedometer sensors, whose accuracy can be improved by fusion with GPS speed data [61] and even LiDar measurement [62]. More precisely, speedometers must provide by regulation a measured speed that is always equal or greater than the real one, and never bigger than the 110% of it, plus 4 km/h [63]. In practice, digital speedometers have a lower upper bound of uncertainty of 2/3%. GPS speed accuracy can vary and be affected by e.g. weather conditions, obstruction by surrounding building, and sudden direction changes, but it increases with the vehicle speed [64], as the ratio of positional error to positional change is lower. It has been estimated, with a typical GPS equipment, that the average measurement error decreases from 4.55% at around 20 km/h down to 1.57% at 50 km/h. Combination of these sensors' data allows then even better performance.

### 3.2.3 Design of the Proposed Estimator for the Racecar Model

In order to estimate the sought unknown inputs affecting the racecar, it is first necessary to obtain a time-discretized version of the model described in Eq. (3.2.1). To this purpose, by introducing a sampling time $\delta$ and approximating all time derivatives by their first-order Euler approximations, the following discrete-time system is obtained:

$$\begin{aligned} \omega_{k+1} &= \omega_k - \frac{\delta}{I_\omega} R_{\omega,k}\, F_{t,k} + \frac{\delta}{I_\omega} T_k \,, \\ u_{k+1} &= u_k + \frac{\delta}{m}(F_{t,k} - F_{a,k} - F_{r,k}) \,, \end{aligned} \tag{3.2.5}$$

where $\omega_k = \omega(k\delta)$, $u_k = u(k\delta)$, $R_{\omega,k} = R_\omega(k\delta)$, $F_{t,k} = F_t(k\delta)$, $F_{a,k} = F_a(k\delta)$, $F_{r,k} = F_r(k\delta)$, $T_k = T(k\delta)$, and $k$ is a discrete time step. Therefore, one can define the current state sample vector as $X_k = (\omega_k, u_k)^T$.

Accordingly, Eq. (3.2.5) can be rewritten as

$$X_{k+1} = A\, X_k + B\, U_k \,, \tag{3.2.6}$$

where the remaining matrices are given by

$$A = I_{2\times 2} \,,\; B = \begin{pmatrix} \frac{\delta}{I_\omega} & 0 \\ 0 & \frac{\delta}{m} \end{pmatrix} \,,\; C = I_{2\times 2} \,,\; D = 0_{2\times 2} \,. \tag{3.2.7}$$

having defined

$$U_k = \begin{pmatrix} U_{1,k} \\ U_{2,k} \end{pmatrix} = \begin{pmatrix} T_k - R_{\omega,k}\, F_{t,k} \\ F_{t,k} - F_{l,k} \end{pmatrix} \,, \tag{3.2.8}$$

where $F_{l,k} = F_{a,k} + F_{r,k}$ is the total resistance force, exploiting that the known and unknown input matrices have an equal structure and therefore the corresponding invertibility matrices are the same.

Given the above discrete-time state form of the racecar's dynamic model, the following result can be stated:

**Theorem 2** (Traction and Resistance Forces Estimator)**.** *Given the discrete time system Eq. (3.2.6),*

*a DUIO observer estimating the state of the system and its unknown inputs is described by the iterative rule*

$$\begin{aligned} \hat{X}_{\gamma+1} &= E\,\hat{X}_\gamma + F\,\mathbb{Y}_k^L\,, \\ \hat{U}_\gamma &= G\begin{pmatrix} \hat{X}_{\gamma+1} - A\,\hat{X}_\gamma \\ Y_\gamma - C\,\hat{X}_\gamma \end{pmatrix}, \end{aligned} \tag{3.2.9}$$

*with the following design matrices*

$$\begin{gathered} E = \begin{pmatrix} \lambda_\omega & 0 \\ 0 & \lambda_u \end{pmatrix}, \quad F = \left(\begin{array}{cc|cc} -\lambda_\omega & 0 & \frac{\delta}{I_\omega} & 0 \\ 0 & -\lambda_u & 0 & \frac{\delta}{m} \end{array}\right), \\ G = \begin{pmatrix} \frac{I_\omega}{\delta} & 0 & 0 & 0 \\ 0 & \frac{m}{\delta} & 0 & 0 \end{pmatrix}, \end{gathered} \tag{3.2.10}$$

*with $\gamma = k-L$ and where $\lambda_\omega$ and $\lambda_u$ are free constants that can be chosen so as to allocate the estimation error eigenvalues. Moreover, given the estimated unknown inputs $\hat{U}_\gamma = (\hat{U}_{1,\gamma}, \hat{U}_{2,\gamma})^T$, best-effort estimates of the dynamic tire radius, the traction force and total resistance forces, respectively, are given by the following formulas:*

$$\hat{R}_{d,\gamma} = R - \frac{\hat{F}_{z,\gamma}}{K_t} = R - \frac{mga}{lK_t} - \frac{h}{lK_t}\hat{U}_{2,\gamma}\,, \tag{3.2.11}$$

*and*

$$\begin{pmatrix} \hat{F}_t \\ \hat{F}_l \end{pmatrix} = \begin{pmatrix} \dfrac{T - \hat{U}_{1,\gamma}}{\hat{R}_{\omega,\gamma}} \\ \dfrac{T - \hat{U}_{1,\gamma}}{\hat{R}_{\omega,\gamma}} - \hat{U}_{2,\gamma} \end{pmatrix}. \tag{3.2.12}$$

*Finally, a best-effort estimate of the effective tire radius $\hat{R}_{\omega,\gamma}$ is obtained by using Eq. (3.2.2) and the estimate $\hat{R}_{d,\gamma}$ from Eq. (3.2.11).*

*Proof.* The proof proceeds by determining first the required step delay $L$, then the estimators matrices, and finally proving the unknown input reconstruction formulas.

### 3.2.4 Design Step

To reconstruct the system state $X_\gamma$, it is necessary to determine the design matrices described in chapter (2). Condition A1) requires that matrix $F \in \mathbb{R}^{n \times Lp}$ is in the left nullspace of the last $Lm$ columns of the $L$-step invertibility matrix $\mathbb{V}^L$, having denoted with $m$ the unknown input vector dimension, i.e. $U_k \in \mathbb{R}^m$. This requirement translates in asking that the last $Lm$ columns of $F$ be in the left nullspace of the matrix

$$P = \begin{pmatrix} 0 \\ \mathbb{H}^{L-1} \end{pmatrix}.$$

Having then denoted with $\bar{N}$ a basis of the left nullspace of $\mathbb{V}^{L-1}$, the matrix

$$\begin{pmatrix} I_p & 0 \\ 0 & \bar{N} \end{pmatrix}$$

is a basis of the left nullspace of $P$. This means that any linearly independent combinations of the rows of $\bar{N}$ satisfy, by construction, the relation:

$$W \begin{pmatrix} I_p & 0 \\ 0 & \bar{N} \end{pmatrix} \mathbb{V}^L = W \begin{pmatrix} D & 0 \\ \bar{N}\mathbb{O}^{L-1}\, B & 0 \end{pmatrix},$$

where $W$ is a free invertible matrix collecting all the combination coefficients. Moreover, the invertibility condition implies that the rank of matrix $\begin{pmatrix} D \\ \bar{N}\mathbb{O}^{L-1}\, B \end{pmatrix}$ is $m$, and thus it is possible to choose $W = (W_1^T, W_2^T)^T$ so that its bottom $m$ rows $W_2$ and top remaining ones $W_1$ are a left inverse and in the left nullspace of the above matrix, respectively. Namely, the matrix

$$N = W \begin{pmatrix} I_p & 0 \\ 0 & \bar{N} \end{pmatrix} \tag{3.2.13}$$

is such that

$$N\,\mathbb{V}^L = \begin{pmatrix} 0 & 0 \\ I_m & 0 \end{pmatrix}.$$

This reasoning suggests that $F$ can be found by factorizing it as $F = (F_1, F_2)\, N$, which allows obtaining

$$F\, \mathbb{V}^L = (F_1, F_2) \begin{pmatrix} 0 & 0 \\ I_m & 0 \end{pmatrix} = (B, 0)\ ,$$

from which it is obvious that $F_2 = B$ and $F_1$ is a free matrix. The second condition of Prop. 8 then becomes $E = A - (F_1, B)\, S$ with

$$S = \begin{pmatrix} S_1 \\ S_2 \end{pmatrix} = N O^L\,, \tag{3.2.14}$$

where $S_2$ is composed of the bottom $m$ rows of $S$. Matrix $E$ is rewritten as

$$E = A - B\, S_2 - F_1\, S_1\,, \tag{3.2.15}$$

where $F_1$ is a free matrix which is finally chosen to ensure that all its eigenvalues are within the unit circle.

Finally, the unknown inputs can be reconstructed by rearranging the state form equations as:

$$\begin{pmatrix} X_{\gamma+1} - A\, X_\gamma \\ Y_\gamma - C\, X_\gamma \end{pmatrix} = \begin{pmatrix} B \\ D \end{pmatrix} U_k\,, \tag{3.2.16}$$

which, under the assumption that $(B^T, D^T)^T$ is full column rank, can be inverted via a matrix $G$ such that

$$G \begin{pmatrix} B \\ D \end{pmatrix} = I_m\,. \tag{3.2.17}$$

Indeed, by left-multiplying both members of Eq. (3.2.16) by $G$ and replacing $X_\gamma$ with its best available estimate $\hat{X}_\gamma$, we finally obtain the last relation in Eq. (3.2.9).

### 3.2.5 Delay Computation

As a first step, one has to determine the required delay step $L$. The sought delay can be found by searching the smallest integer $L$ satisfying proposition 2. This shows that $L = 1$ since the invertibility

matrices in 0 and 1 steps, respectively, are

$$\mathbb{V}^0 = D = 0_{2\times 2}\,,$$
$$\mathbb{V}^1 = \begin{pmatrix} D & 0 \\ CB & D \end{pmatrix} = \begin{pmatrix} 0 & 0 & 0 & 0 \\ 0 & 0 & 0 & 0 \\ \frac{\delta}{I_\omega} & 0 & 0 & 0 \\ 0 & \frac{\delta}{m} & 0 & 0 \end{pmatrix}.$$

As the first two columns of $\mathbb{V}^1$ are linearly independent while the other ones are null, or equivalently the last two columns are linearly independent while the first two are null, it holds

$$\text{rank}(\mathbb{V}^1) - \text{rank}(\mathbb{V}^0) = 2 - 0 = 2 = m\,,$$

### 3.2.6 Design of the Estimator

We can now proceed to design the one-step delayed observer for system of Eq. (3.2.6) and (3.2.7). Given that $m = 2$ and $L = 1$, condition A1) requires that matrix $F$ satisfies the equation

$$F\,\mathbb{V}^1 = (B, 0_{2\times 2})\ ,$$

which implies that $F$ has to be in the left nullspace of the last $Lm = 2$ columns of the one-step invertibility matrix $\mathbb{V}^1$. Since $\mathbb{V}^0$ is null, a basis of its left nullspace can be described by matrix $\bar{N} = I_2$. According to the reasoning expressed in paragraph (3.2.3), matrix $W$ has to be found such that

$$W \begin{pmatrix} 0 & 0 \\ 0 & 0 \\ \frac{\delta}{I_\omega} & 0 \\ 0 & \frac{\delta}{m} \end{pmatrix} = \begin{pmatrix} 0 & 0 \\ 0 & 0 \\ 1 & 0 \\ 0 & 1 \end{pmatrix}.$$

A possible choice of $W$ is thus

$$W = \begin{pmatrix} 1 & 0 & 0 & 0 \\ 0 & 1 & 0 & 0 \\ 0 & 0 & \frac{I_\omega}{\delta} & 0 \\ 0 & 0 & 0 & \frac{m}{\delta} \end{pmatrix}$$

and correspondingly

$$N = W \begin{pmatrix} I_2 & 0 \\ 0 & \bar{N} \end{pmatrix} = W \,.$$

Moreover, by using the 1-step observability matrix

$$\mathbb{O}^1 = \begin{pmatrix} 1 & 0 & 1 & 0 \\ 0 & 1 & 0 & 1 \end{pmatrix}^T$$

one can obtain from the relation $S = N\mathbb{O}^1$ (see Eq. 3.2.14) the following sub-matrices:

$$S_1 = I_2 \,, \quad S_2 = \begin{pmatrix} \frac{I_\omega}{\delta} & 0 \\ 0 & \frac{m}{\delta} \end{pmatrix} .$$

According to Eq. 3.2.15, the estimation error dynamics is given by

$$E = A - B \begin{pmatrix} \frac{I_\omega}{\delta} & 0 \\ 0 & \frac{m}{\delta} \end{pmatrix} - F_1 = \begin{pmatrix} 0 & 0 \\ 0 & 0 \end{pmatrix} - F_1 \,.$$

Since all eigenvalue of $E$ are already inside the unit circle (and indeed in the origin), matrix $F_1$ can be null. More generally, if the eigenvalues are required to be placed at $\lambda_\omega$ and $\lambda_u$, the output injection matrix $F_1$ can be chosen as in Eq. (3.2.10). Finally, having guaranteed by the choice of the unknown inputs, that the matrix $(B^T, D^T)^T$ is full column rank, it is possible to find a matrix

$G$ that satisfies Eq. (3.2.17). For the system in consideration, this relation is

$$G \begin{pmatrix} B \\ D \end{pmatrix} = G \begin{pmatrix} \frac{\delta}{I_\omega} & 0 \\ 0 & \frac{\delta}{m} \\ 0 & 0 \\ 0 & 0 \end{pmatrix} = I_2 \,,$$

whose solution can be computed via the pseudo-inverse and gives the expression reported in Eq. (3.2.10).

### 3.2.7 Refinement of the Effective tire Radius Estimate

Once the current value of the unknown input $\hat{U}_\gamma$ has been reconstructed, one can observe that its second component $\hat{U}_{2,\gamma}$ represents the total force acting along the vehicle's longitudinal direction (cf. the second equation of the model in Eq. (3.2.1)). As such, an estimate $\hat{\dot{u}}_\gamma$ of the instantaneous longitudinal acceleration $\dot{u}$ of the racecar can be obtained by dividing for its mass $m$, i.e. as

$$\hat{\dot{u}}_\gamma = \frac{\hat{U}_{2,\gamma}}{m}. \tag{3.2.18}$$

This enables first obtaining a more accurate, best-effort estimate $\hat{F}_{z,\gamma}$ of the tire's normal (vertical) load $F_z$ via Eq. (3.2.4), that is

$$\hat{F}_{z,\gamma} = \frac{m}{l}\left(g\,a + h\frac{\hat{U}_{2,\gamma}}{m}\right) = \frac{a}{l}mg + \frac{h}{l}\hat{U}_{2,\gamma}\,,$$

which can be used to reach the best-effort dynamic tire radius estimate $\hat{R}_{d,\gamma}$ described in Eq. (3.2.11), and finally the corresponding one for the effective tire radius $\hat{R}_{\omega,\gamma}$, which is more accurate than the a-priori value $R_{\omega,0}$.

### 3.2.8 Computation of the Traction and Resistance Forces

After having reconstructed the current effective tire radius $\hat{R}_{\omega,\gamma}$, based on the fact that the wheel drive torque $T$ is known, the traction and resistance forces can be algebraically derived by solving

the following system in Eq. (3.2.8) with respect to them, that is

$$\begin{pmatrix} \hat{U}_{1,\gamma} \\ \hat{U}_{2,\gamma} \end{pmatrix} = \begin{pmatrix} T - \hat{R}_{\omega,\gamma}\, \hat{F}_t \\ \hat{F}_t - \hat{F}_l \end{pmatrix},$$

which yields the formulas described in Eq. (3.2.12). □

### 3.2.9 Dynamic Model Reformulation and Control System Design

To achieve independence on the highly unknown traction force $F_t$, it is convenient to rewrite the system's model described in Eq. (3.2.1) to make this term disappear and reach an explicit form of the state dynamics. To this aim, first, solve the first expression in Eq. (3.2.1) for $F_t$, which yields:

$$F_t(\omega, u, \dot{u}) = \frac{T - I_\omega\, \dot{\omega}}{R_\omega(\dot{u})},$$

and substitute it in the second expression of Eq. (3.2.1), leading to

$$m\, \dot{u} = \frac{T - I_\omega\, \dot{\omega}}{R_\omega(\dot{u})} - F_a(u) - F_r(u)\,. \tag{3.2.19}$$

Moreover, it is known that the traction force $F_t$ depends on the slip ratio $\sigma$, a quantity that will be defined later in Eq. (3.2.34). It is worth noticing that $F_t$ reaches its maximum for slip ratio values that range between 0.06 and 0.17, depending on the tire/road surface, and then decreases for larger values [37] (Fig. 3.2). It is therefore desirable to control a car's motion, while maintaining $\sigma$ small or practically null, which becomes particularly advantageous in the context of racecars as the obtained traction force is maximized. Under this assumption, it can be shown that the effective tire radius $R_\omega$ coincides with the time-varying coefficient instantaneously translating the wheel speed $\omega$ to that of the vehicle's longitudinal velocity $u$, via the ratio [65]:

$$R_\omega = \frac{u}{\omega}. \tag{3.2.20}$$

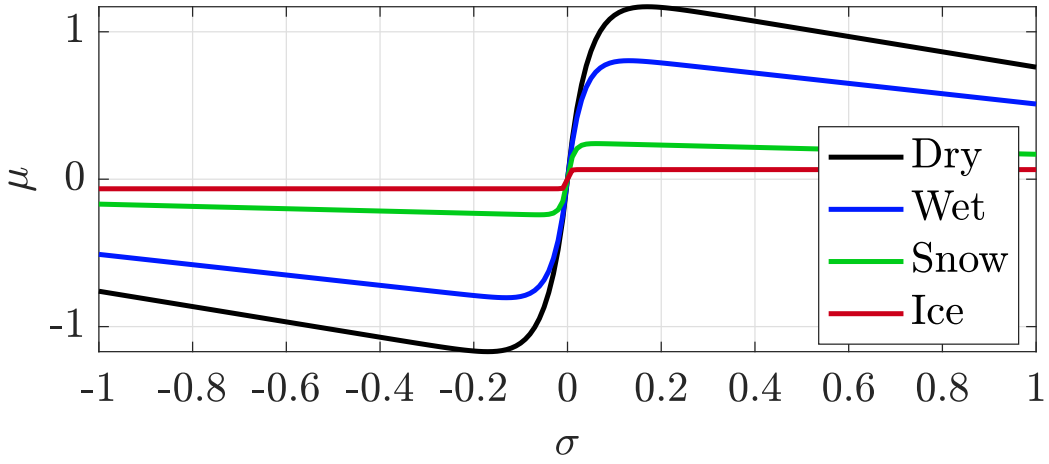


Figure 3.2: Characteristics of the friction coefficient $\mu$ for various nominal types of tire/road surface [37]. Maximum values are attained for slip ratios in the range $[0.06, 0.17]$. The instantaneous traction force $F_t$ is related to the friction coefficient via the formula in Eq. (3.2.35).

Rewriting this equation as $u = R_\omega\,\omega$ and computing its time-derivative allow obtaining

$$\dot{u} = \dot{R}_\omega(\dot{u})\,\omega + R_\omega(\dot{u})\,\dot{\omega}$$

whose solution for the wheel acceleration $\dot{\omega}$ is

$$\dot{\omega} = \frac{\dot{u} - \dot{R}_\omega(\dot{u})\,\omega}{R_\omega(\dot{u})}, \tag{3.2.21}$$

which, substituted in Eq. 3.2.19, allows achieving the expression:

$$\frac{mR_\omega^2(\dot{u}) + I_\omega}{R_\omega^2(\dot{u})}\dot{u} - \frac{\dot{R}_\omega(\dot{u})}{R_\omega^2(\dot{u})}I_\omega\,\omega - \frac{T}{R_\omega(\dot{u})} = -F_a(u) - F_r(u)\,. \tag{3.2.22}$$

While the exact differential system, described in the above equation, is still implicit, due to the nonlinear dependency on $\dot{u}$, which does not allow its factorisation as a multiplicative term, a nonlinear yet simplified model can be obtained by observing the following. First, it is worth noticing that the racecar is nominally intended to be operated at regimes with piecewise-constant (even null) longitudinal accelerations, i.e. with $\ddot{u} = 0$ for almost all times. Therefore, by this assumption, the

effective tire radius $R_\omega(\dot{u})$ becomes exactly constant and its derivative identically null. Indeed, it holds:

$$\dot{R}_\omega(\dot{u}) = \frac{\partial R_\omega(\dot{u})}{\partial \dot{u}} \ddot{u} = 0\,.$$

Therefore, indicating, as above, the total resistance force as

$$F_l(u) = F_a(u) + F_r(u)\,,$$

the following traction-force independent model of the longitudinal dynamics of a racecar is obtained:

$$\left(m + \frac{I_\omega}{R_\omega^2(\dot{u})}\right) \dot{u} = \frac{T}{R_\omega(\dot{u})} - F_l(u)\,. \tag{3.2.23}$$

**Remark 1.** *Note that, under the above assumptions, the wheel's dynamics in Eq. (3.2.21) also simplifies as $\dot{\omega} = \dot{u}/R_{\omega,0}$, thus solving the problem of trajectory tracking for $u$, also ensures tracking of the corresponding wheel tracking. Therefore, the stability of the above-obtained model guarantees that of the wheel's dynamics, namely, the system dynamics is reduced to a one degree of freedom.*

The above reformulation of the dynamic model, from Eq. (3.2.1) to Eq. (3.2.23), enables a great simplification in the derivation of a controller, as it is shown in the following result:

**Theorem 3.** *Given a racecar described by the dynamic model in Eq. (3.2.23), a desired trajectory $u_d(t)$ for the car's longitudinal velocity, and a desired convergence speed $\kappa > 0$ for the tracking error $e_u = u - u_d$, the best-effort feedback and feed-forward control law described by*

$$T = \frac{m\hat{R}_{\omega,\gamma}^2 + I_\omega}{\hat{R}_{\omega,\gamma}} \left(\dot{u}_d - \frac{\kappa}{2}(u - u_d)\right) + \hat{R}_{\omega,\gamma}\,\hat{F}_l(u)\,, \tag{3.2.24}$$

*where $\hat{R}_{\omega,\gamma}$ and $\hat{F}_l$ are the estimated effective tire radius and resistance forces obtained by means of Eq. (3.2.11) and Eq. (3.2.12), respectively, ensures exponential asymptotic tracking of $u_d$ and requires no information about the traction force $F_t$.*

*Proof.* Let us first introduce the positive quantity

$$m^*(\dot{u}) = m + \frac{I_\omega}{R_\omega^2(\dot{u})}\,.$$

In order to design a control law allowing the tracking of a desired velocity $u_d$, or equivalently, ensuring that the tracking error $e_u$ exponentially converges to zero, consider the Lyapunov control function $V(e_u) = \frac{1}{2} m^*(\dot{u})\, e_u^2$, which is positive definite around $e_u = 0$ and whose directional derivative is $\dot{V} = e_u\, m^*(\dot{u})\, \dot{e}_u$. By plugging the expression of the system's dynamics described in Eq. (3.2.23) into the quantity $m^*(\dot{u})\, e_u = m^*(\dot{u})\, \dot{u} - m^*(\dot{u})\, \dot{u}_d$, and then substituting the result into the above expression of the Lyapunov's directional derivative yields

$$\dot{V} \;=\; e_u \left( \frac{T}{R_\omega(\dot{u})} - F_l(u) - m^*(\dot{u})\, \dot{u}_d \right)\,. \tag{3.2.25}$$

To guarantee the asymptotic stability of the equilibrium point $e_u = 0$, $\dot{V}$ must be negative definite. To obtain also that a desired convergence speed of $\kappa$ is achieved, one can impose the expression in Eq. 3.2.25 to be equal to

$$\dot{V} = -\kappa\, V = e_u \left( -\frac{\kappa}{2} m^*(\dot{u})\, e_u \right)\,, \tag{3.2.26}$$

which leads to the condition

$$\frac{T}{R_\omega(\dot{u})} - F_l(u) - m^*(\dot{u})\, \dot{u}_d = -\frac{\kappa}{2} m^*(\dot{u})\, e_u$$

and, then, to the following formula for the driving torque:

$$T = m^*(\dot{u}) R_\omega(\dot{u}) \left( \dot{u}_d - \frac{\kappa}{2}(u - u_d) \right) + R_\omega(\dot{u})\, F_l(u)\,.$$

Under the assumption that the UIO described in Th. 2 has converged, one can replace the unknown quantities $R_\omega$ and $F_l$ with the estimated ones, $\hat{R}_{\omega,\gamma}$ and $\hat{F}_l$, respectively, and thus obtain the best-effort control described in Eq. (3.2.24). Indeed, despite the estimations are delayed, by choosing a

small sampling time can be stated that $R_\omega \approx \hat{R}_{\omega,\gamma}$ and $F_l \approx \hat{F}_l$, [66].

Finally, with the above choice of $T$, the solution of the differential equation described by the first two members of Eq. (3.2.26) is $V(t) = e^{-\kappa t}\, V(0)$, with $V(0) = \frac{1}{2} m^*(\dot{u}(0))\, e_u^2(0)$, that exponentially converges to zero with speed $\kappa$. This result also concludes the proof. □

**Remark 2** (Maximum Deliverable Torque)**.** *During acceleration or deceleration phases, a longitudinal wheel's slip ratio $\sigma$, which will be defined later in Eq. (3.2.34) of Sec. (3.2.10), always occurs. The reduced-degree-of-freedom model of Eq. (3.2.23) has been found under the hypothesis of a null slip, but it remains valid also for small values of such a variable. To ensure that the absolute value of the slip ratio is kept within a threshold $\bar{\sigma}$, the driving torque function in Eq. (3.2.24) is replaced by the formula*

$$T = \frac{I_\omega}{\hat{R}_{\omega,\gamma}} \hat{\dot{u}} + \hat{R}_{\omega,\gamma} \left( \hat{F}_{l,\gamma} + |\hat{F}_{t,\gamma} - \hat{F}_{l,\gamma}|\, sign(\sigma) \right) , \tag{3.2.27}$$

*whenever the condition $|\sigma| \geq \bar{\sigma}$ is detected.*

*To explain this choice, it is first convenient to find a differential equation for the slip ratio variable $\sigma$. During an acceleration phase with $u_d > u$, the (positive) slip ratio variable is $\sigma = 1 - u/(\omega R_\omega)$ (cf. the first expression of Eq. (3.2.34). Rewriting its definition as $u - (1-\sigma) w R_\omega = 0$ and differentiating it with respect to time yields $\dot{u} + \dot{\sigma}\, \omega\, R_\omega - (1-\sigma)\, \dot{\omega}\, R_\omega = 0$. Solving this last equation for $\dot{\sigma}$ and using the equivalence $\dot{u} = R_\omega\, \dot{\omega}$ (valid for small $\sigma$) gives*

$$\dot{\sigma} = -\frac{\dot{u}}{u}\, \sigma\, . \tag{3.2.28}$$

*During a deceleration phase ($u_d < u$ and $\sigma < 0$), the slip ratio is defined as $\sigma = \omega R_\omega / u - 1$ (cf. the second expression of Eq. (3.2.34). With a similar reasoning as above, one obtains $\dot{\sigma}\, u + (1+\sigma)\, \dot{u} - \dot{\omega}\, R_\omega = 0$, whose solution for $\dot{\sigma}$ gives again the formula in Eq. (3.2.28).*

*Moreover, for a vehicle moving forward ($u > 0$) with a slip ratio having reached a maximum allowed value, i.e. $\sigma \geq \bar{\sigma} > 0$, it must be ensured that the condition $\dot{\sigma} < 0$ holds, which is satisfied if $\dot{u} > 0$. A possible choice for the driving torque $T$ ensuring the above condition is $T = \frac{I_\omega}{R_\omega} \dot{u} +$*

$R_\omega\,(F_l + |F_t - F_l|)$, *which, plugged into the vehicle's longitudinal dynamics of Eq. (3.2.23), yields*

$$\left(m + \frac{I_\omega}{R_\omega^2}\right)\dot{u} = \frac{I\omega}{R_\omega^2}\dot{u} + |F_t - F_l|\,,$$

*and hence*

$$m\,\dot{u} = |F_t - F_l| \geq 0\,. \tag{3.2.29}$$

*The simultaneous satisfaction of* $\dot{\sigma} \leq 0$ *and* $\dot{u} \geq 0$ *implies that the car is controlled so that to reduce the slip ratio* $\sigma$ *while still increasing (or at least not decreasing) its speed* $u$ *toward the desired value* $u_d$*. Conversely, if the slip ratio has reached a minimum allowed value (*$\sigma \leq -\bar{\sigma} < 0$*), it must occur that* $\dot{\sigma} > 0$ *and thus that* $\dot{u} < 0$*. For this case, the choice* $T = \frac{I_\omega}{R_\omega}\dot{u} + R_\omega\,(F_l - |F_t - F_l|)$ *allows obtaining the longitudinal vehicle's speed dynamics*

$$m\,\dot{u} = -|F_t - F_l| \leq 0\,. \tag{3.2.30}$$

*The simultaneous conditions* $\dot{\sigma} \geq 0$ *and* $\dot{u} \leq 0$ *enables to maintain small the slip ratio while the car's velocity is reduced toward the desired* $u_d$*. It is straightforward to see that the above two choices for* $T$ *can be combined together, thereby leading to Eq. 3.2.27, where the unknown quantities have been replaced with their corresponding estimates. One can notice that, the condition* $F_t = F_l$*, for which* $\dot{\sigma} = \dot{u} = 0$*, can only happen for specific combinations of the tire/road surface and the vehicle's aerodynamic coefficients, and in fact it may only be present for few instants. Therefore, the inequalities in Eq. (3.2.29) and Eq. (3.2.30) are practically always satisfied in the strict sense, and so are the ones involving* $\dot{\sigma}$*.*

### 3.2.10 Simulation, Validation, and Performance Comparison

This paragraph validates the effectiveness of the proposed estimation and control approach, and it compares it to the performance achieved by using an EKF. The evaluation and comparison are carried out via simulations realized in Matlab/Simulink environment. Numerical data used to develop the simulations refer to the setting of a *Robocar*, one of the self-driving racecars participating in the Roborace Challenge [28]. Geometric and inertial parameters of the car are summarized in Table 3.3.

Table 3.1: Inertial and geometric parameters of a racecar as in the Roborace Challenge [28].

| Parameters | Value | Unit |
|---|---|---|
| Vehicle's Mass, $m$ | 1350 | [Kg] |
| Vehicle's Inertia Moment, $J$ | 1150 | [Kg $\cdot$ m$^2$] |
| Center of gravity height from ground, $h$ | 0.5 | [m] |
| Front wheelbase, $a_1$ | 1.51 | [m] |
| Rear wheelbase, $a_2$ | 1.288 | [m] |
| Wheelbase, $l$ | 2.798 | [m] |
| Effective tire Radius (Static), $R_{\omega,0}$ | 0.5 | [m] |
| Wheel's Inertial Moment, $I_\omega$ | 1.125 | [Kg $\cdot$ m$^2$] |

**Numerical Implementation of the Proposed DUIO**

Referring to the numerical values reported in Table (3.3) and choosing a sampling time $\delta = 10^{-3}$ s the effective tire radius corresponding to null acceleration $\dot{u} = 0$ is $R_{\omega,0} = 0.5$ $[m]$ and the matrices of the racecar model in Eq. (3.2.7) becomes

$$A = I_2\,,\; B = \begin{pmatrix} 8.89 \cdot 10^{-3} & 0 \\ 0 & 7 \cdot 10^{-7} \end{pmatrix}.$$

Moreover, by choosing the observer eigenvalues $\lambda_\omega = -0.02$ and $\lambda_u = 0.02$ to be small but not coincident, so that to reduce the numerical sensitivity of the filter, the UIO matrices from Th. 8 becomes

$$E = \begin{pmatrix} -0.02 & 0 \\ 0 & 0.02 \end{pmatrix},$$

$$F = \begin{pmatrix} -0.02 & 0 & 8.89 \cdot 10^{-3} & 0 \\ 0 & 0.02 & 0 & 7 \cdot 10^{-7} \end{pmatrix},$$

$$G = \begin{pmatrix} 1.1248 \cdot 10^{2} & 0 & 0 & 0 \\ 0 & 1.429 \cdot 10^{6} & 0 & 0 \end{pmatrix}.$$

**Design of the comparative EKF for Unknown Input Estimation**

Let us briefly recall in the following the theoretical framework of an EKF (cf. e.g. [67, 68]) and show how this can be used for estimating the unknown inputs of our system. Consider a generic

discrete-time process governed by a stochastic difference equation of the form

$$\begin{aligned} Z_{k+1} &= f(Z_k, U_k, W_k)\,, \\ Y_k &= h(Z_k, V_k)\,, \end{aligned} \tag{3.2.31}$$

where $Z_k$ is a state vector, $U_k$ are known inputs, $Y_k$ is the output vector, $W_k$ and $V_k$ are the process and measurement noise, respectively, $f$ and $h$ are possibly nonlinear functions describing the system dynamic and output maps. $W_k$ and $V_k$ are assumed to be independent random processes with white Gaussian distributions and time-varying covariance matrices denoted as $Q_k$ and $R_k$, respectively.

As it is known, an EKF for a dynamic system of the form in Eq. (3.2.31) consists of a two-phase algorithm during which an a-priori estimate $\hat{Z}_k^-$ of the system state $Z_k$ and an a-posteriori one $\hat{Z}_k$ are computed. More precisely, $\hat{Z}_k^-$ is calculated during the *state prediction phase* based on knowledge of the process before the arrival of the $k$-th measurement $Y_k$; afterward, the *state update phase* realizes a feedback mechanism incorporating the new measures in the a-priori estimate $\hat{Z}_k^-$ so to obtain the improved a-posteriori one $\hat{Z}_k$. The a-priori and a-posteriori estimation processes are characterized by the following covariance matrices:

$$\begin{aligned} P_k^- &= E[(Z_k - \hat{Z}_k^-)(Z_k - \hat{Z}_k^-)^T]\,, \\ P_k &= E[(Z_k - \hat{Z}_K)(Z_k - \hat{Z}_k)^T]\,, \end{aligned}$$

where $E[\cdot]$ is the expectation value operator. We also recall that, compared to a linear Kalman filter, an EKF differs in the fact that the matrices involved in the Riccati equations are obtained by linearization of the nonlinear state equations in (3.2.31), around the state estimated during the previous step. The EKF operation is summarized in Algorithm 1 [69].

Moreover, given a dynamic system in the form of Eq. (3.2.31), a common approach to use EKF for allowing, as in the scope of the present work, both state and unknown input reconstruction, requires to enhance the system state with additional variables representing such unknown inputs. To model the evolution of these newly added variables, the random walk process dynamics is assumed [70]. In the present case of the racecar, the traction force $F_t$ and resistance force $F_l$ are added as variables

**Algorithm 1** Modified EKF for Racecar Unknown Input Estimation

**loop**

$\hat{Z}^-_{k+1} = f(\hat{Z}_k, U_k)$ ◁ Compute the a-priori estimate

$\hat{Y}_k = h(\hat{Z}^-_k)$ ◁ Compute predicted measures

$A_k = \dfrac{\partial f(Z_k, U_k)}{\partial Z_k}_{Z_k=\hat{Z}^-_{k+1}}$ ◁ Compute dynamic map Jacobian

$H_k = \dfrac{\partial h(Z_k)}{\partial Z_k}_{Z_k=\hat{Z}^-_{k+1}}$ ◁ Compute dynamic map Jacobian

$P^-_{k+1} = A_k\, P_k\, A_k^T + Q_k$ ◁ Compute the a-priori error covariance

**wait untill** $Y_k$ is available

$K_k = P^-_{k+1}\, H_k^T \left(H_k\, P^-_{k+1} H_k^T + R_k\right)^{-1}$ ◁ Update Kalman gain

$\hat{Z}_k = \hat{Z}^-_k + K_k(Y_k - \hat{Y}_k)$ ◁ Update the a-posteriori estimate

$P_{k+1} = (I - K_k\, H_k)\, P^-_k$ ◁ Update the a-posteriori error covariance

**end loop**

and the system state becomes

$$Z_k = (\omega_k, u_k, F_{t,k}, F_{l,k})^T \,,$$

and, starting from the two difference relations in Eq. (3.2.5), its corresponding dynamics becomes

$$\begin{aligned} \omega_{k+1} &= \omega_k + (T_k - R_{\omega,k}\, F_{t,k})\, \delta / I_\omega + w_{1,k} \,, \\ u_{k+1} &= u_k + (F_{t,k} - F_{l,k})\, \delta / m + w_{2,k} \,, \\ F_{t,k+1} &= F_{t,k} + w_{3,k} \,, \\ F_{l,k+1} &= F_{l,k} + w_{4,k} \,. \end{aligned} \tag{3.2.32}$$

Analogously to the setting of the DUIO, the quantities available for measurement are the wheel speed $\omega_k$ and longitudinal vehicle's velocity $u_k$. Then, the output vector is obtained as

$$Y_k = \begin{pmatrix} 1 & 0 & 0 & 0 \\ 0 & 1 & 0 & 0 \end{pmatrix} Z_k + V_k \,, \tag{3.2.33}$$

where $V_k = (v_{1,k}, v_{2,k})^T$ is the output noise. The Jacobian matrices of the dynamic and output

maps from (3.2.32) are

$$A_k = \begin{pmatrix} 1 & 0 & -R_{\omega,k}\delta/I_\omega & 0 \\ 0 & 1 & \delta/m & -\delta/m \\ 0 & 0 & 1 & 0 \\ 0 & 0 & 0 & 1 \end{pmatrix}, \quad H_k = \begin{pmatrix} 1 & 0 & 0 & 0 \\ 0 & 1 & 0 & 0 \end{pmatrix}.$$

Under similar reasoning as for the DUIO in Sec. (3.2.3), once the last two entries of the augmented state vector $Z_k$, representing estimates of the traction $F_{t,k}$ and resistance $F_{l,k}$ forces, respectively, have been reconstructed by the EKF, one can obtain the instantaneous longitudinal acceleration as

$$\hat{\dot{u}} = \frac{\hat{F}_{t,k} - \hat{F}_{l,k}}{m} = \frac{\hat{Z}_{3,k} - \hat{Z}_{4,k}}{m}$$

by inverting the second relation of Eq. (3.2.1). Plugging this result in the load weight formula in Eq. (3.2.4) allows obtaining

$$\hat{F}_z = \frac{m}{l}\left(g\, a_1 + h\, \hat{\dot{u}}\right) = m\, g\, \frac{a_1}{l} + \frac{h}{l}\left(\hat{Z}_{3,k} - \hat{Z}_{4,k}\right),$$

which finally allows the reconstruction of the current effective tire radius, $\hat{R}_{\omega,k}$ from Eq. (3.2.2) and (3.2.3).

Finally, referring to the numerical value listed in Table 3.3, the Jacobian matrix of the dynamic map becomes

$$A_k = \begin{pmatrix} 1 & 0 & -\hat{R}_{\omega,k} \cdot 1.125 \cdot 10^{-3} & 0 \\ 0 & 1 & 8.89 \cdot 10^{-3} & -8.89 \cdot 10^{-3} \\ 0 & 0 & 1 & 0 \\ 0 & 0 & 0 & 1 \end{pmatrix}.$$

**Simulation Results**

To validate and assess the effectiveness of the proposed solution, the estimation and control approaches presented here have been tested in simulation within the Matlab/Simulink environment. A Robocar model characterized by the parameters listed in Tab. (3.3) has been used. Two scenarios

have been considered in which the racecar is required to track a series of aggressive maneuvers as described below.

The first scenario includes the following components:

*Traction force model $F_t$*: A well-known formula that used to describe the effect of interaction between a car's tire and the road asphalt and, more precisely, that allows obtaining the instantaneous traction force $F_t$ as a nonlinear function of the vehicle's velocity $u$, wheel speed $\omega$, and terrain properties, is the so-called Burckhardt tire model [37]. Having denoted with

$$\sigma(\omega, u) = \begin{cases} 1 - \dfrac{u}{\omega R_\omega}, & \text{if } \omega R_\omega > u \text{ (acceleration phase)}, \\ \dfrac{\omega R_\omega}{u} - 1 & \text{if } \omega R_\omega < u \text{ (braking phase)}, \end{cases} \tag{3.2.34}$$

the *longitudinal slip ratio*, the instantaneous *friction coefficient* can be described as

$$\mu(\sigma) = \mu_1 \left(1 - e^{-\mu_2 |\sigma|}\right) - \mu_3 |\sigma|,$$

where $\mu_1$ represents its maximum value, $\mu_2$ defines its curve shape, and $\mu_3$ indicates the difference between the coefficient's maximum value ($\mu_1$) and that obtained at full slip ratio with $\sigma = 1$. The values of the constants $\mu_i$ depend on the instantaneous kind of tire-asphalt interaction and thus may with time as the car moves. Then, the traction force $F_t$ can be computed as

$$F_t(\omega, u, \dot{u}) = \mu(\sigma)\, F_z(\dot{u}), \tag{3.2.35}$$

where $F_z$ is the normal component of the rear wheel load, i.e. the portion of the vehicle's weight applied to the tire, which can be obtained via Eq. (3.2.4). For the simulated scenario, the considered kinds of tire-asphalt interactions are dry-dry, dry-wet, and dry-ice. The corresponding values for all $\mu_i$ can be found e.g. in [60, 71, 72], which were obtained by curve-fitting experimentally obtained data. According to Remark 2, a conservative yet not too stringent value for the slip ratio threshold $\bar{\sigma}$ has been chosen equal to 0.08, so as to maintain the reduced-degree-of-freedom model valid.

*Resistance force model $F_l$*: The rolling resistance force $F_r$ is known to be a function of the total

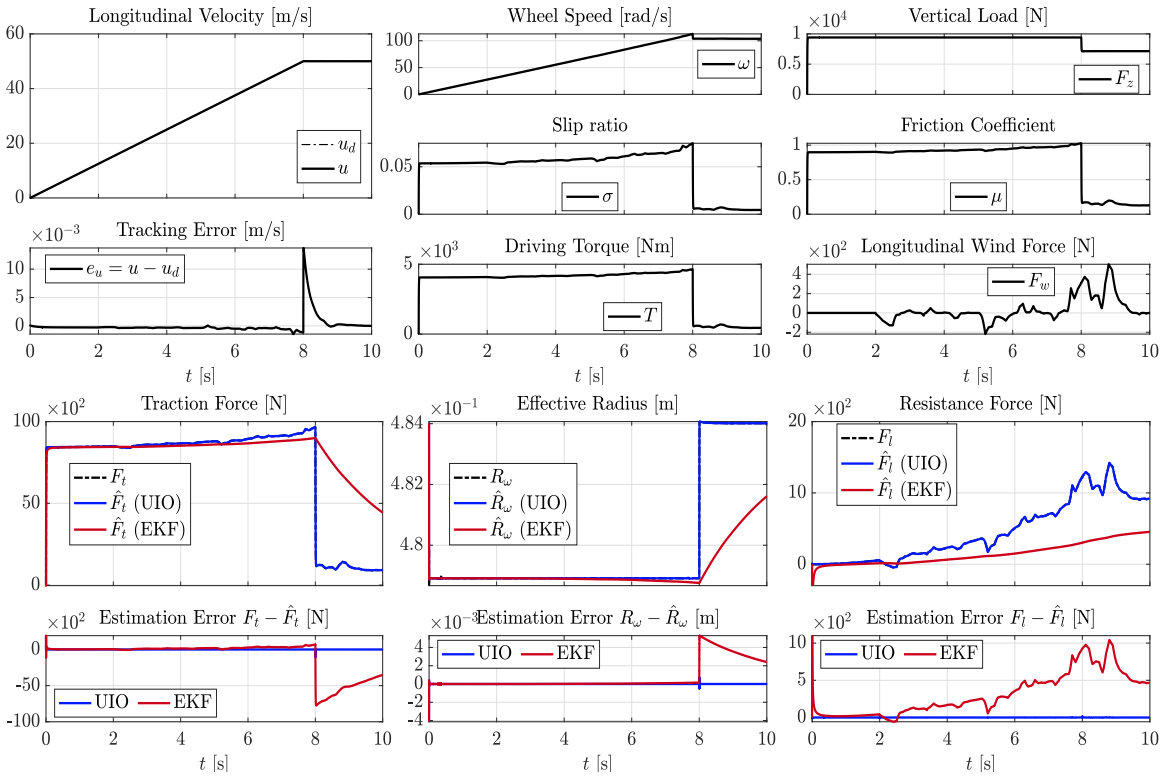


Figure 3.3: Scenario #1.1 (Dry Asphalt): Typical simulation run where the racecar travels along a straight and dry road and is required to track a longitudinal velocity profile $u_d(t)$, when a sudden wind gust hits the vehicle at $t = 2$. The DUIO is effectively able to reconstruct the unknown inputs and that the controller can track the desired trajectory and rapidly compensate for the effect of all resistances and disturbances.

normal load $F_z(\dot{u})$ acting on the tire, which in turn depends on the vehicle's velocity. However, as shown in [65], it is possible to approximate such a function by using a fourth-order Taylor expansion of the longitudinal velocity $u$, i.e.

$$F_r(u) = r_0 + r_1\, u + r_2\, u^4\,,$$

where the constants $r_i$ depend on the tire characteristics. As in [65], we have assumed that the racecar is provided with radial tire types for which typical values of these constants are used: $r_0 = 9.91{\cdot}10^{-3}$, $r_1 = 1.95{\cdot}10^{-5}$, and $r_2 = 1.76{\cdot}10^{-9}$. Moreover, the aerodynamic drag force $F_a$ is obtained according

to the well-known relationship:

$$F_a(u) = \frac{1}{2}\,\rho\, S\, C_x\ (u + u_w)^2\ ,$$

where $\rho$ is the air density, $S$ the frontal surface of the vehicle, $C_x$ the aerodynamic drag coefficient along the longitudinal axis and $u_w$ is the wind speed. Simulations address the case where the racecar travels at sea-level, and hence the air density is around $\rho = 1.225$ Kg/m$^3$, and assume the following values for the car parameters: $S = 2$ m$^2$ and $C_x = 0.3$. In the nominal cases, the resistance force is then given by

$$F_l(u) = F_r + F_a = r_0 + r_1\, u + \frac{1}{2}\,\rho\, S\, C_x\, u^2 + r_2\, u^4\,.$$

*Wind Gusts*: Simulations aim also at testing the ability of the proposed estimation and control solution to cope with disturbance due to wind gusts. Such unknown inputs are described via the Dryden turbulence model [73], according to which the linear and angular speed components of a continuous gust can be represented as spatially-varying stochastic processes. In particular, the model specifies for the longitudinal component of the gust velocity the following power spectral density

$$\Phi_u = \frac{2\sigma_u^2 L_u}{\pi V}\frac{V^2}{V^2 + L_u^2\omega_g^2}$$

where $L_u$ is the turbulence scale length, $V$ is the airspeed, $\sigma_u$ is the turbulence intensity, and $\omega_g$ is the temporal frequency of the gust.

To generate a turbulence signal that has a similar frequency spectrum as Dryden power spectral density the Dryden continuous filter is used, derived from the square roots of the Dryden power spectrum. This filter can be expressed through the following transfer function:

$$H_u(s) = \sigma_u\sqrt{\frac{2L_u}{\pi V}}\frac{1}{1 + \frac{L_u}{V}s} \tag{3.2.36}$$

We have discretized a length of the turbulence scale for a low altitude region, as described extensively in [73], having chosen: a height from sea level $h = 6\,m$, an airspeed $V = 50\frac{m}{s}$ and a level of turbulence described by $W_{2_0} = 15\,Knots$. Finally, to simulate the magnitude of the wind force,

the value of the wind speed coming from the Dryden model is added to that of the longitudinal speed in the discretization of the aerodynamic drag force.

Within this scenario, three typical simulation runs have been conducted. The first simulation reproduces a situation in which the racecar is assumed to be traveling along a straight and dry road and is required to track a longitudinal velocity profile $u_d(t)$, when a sudden wind gust instantaneously hits the vehicle. Fig. 3.3 shows the dynamic behavior of the closed-loop system, using the proposed DUIO from Th. 8 and the controller proposed in Th. 3. The simulation shows that the DUIO is effectively able to reconstruct the unknown inputs and that the controller can track the desired trajectory and rapidly compensate for the effect of the disturbances. Fig. 3.3 also show how the proposed DUIO performs better than the Kalman-based approach, while also not requiring any information about the unknown inputs. More specifically, the unknown input estimates obtained by the DUIO always converge faster than those of the EKF. This becomes more apparent when the car reaches the cruise speed at $t = 8$ seconds and the traction force $F_t$ is immediately reduced as it only needs to compensate for the dissipative forces. This slower behavior of the EKF is explained as follows. In the EKF, the unknown inputs are variables of the estimator with a random-walk dynamics. The entries of the covariance matrix $P_k$ associated with such variables converges to appropriate small quantities, thus reducing with time the adaptability of the filter to newer measures. Moreover, the performance of a more elaborate EKF, based also on the knowledge of the traction and resistance force models, would not only be dependent on the accuracy of these models and the choice of the covariance matrix, but it would also require a-priori knowledge of the type of tire-road interface, which is unnecessary for the DUIO. The second type of simulation run refers to the case where the racecar travels on a straight road with variable tire-road conditions, switching from the dry road, to wet, to snow, and finally to icy road. A sudden wind gust is also considered to show the ability of the method to cope simultaneously with different types of uncertainties. In this case, it is more evident as the proposed DUIO is more efficient than the EKF since, the latter, is not able to quickly estimate the sudden changes of tire-road friction. The obtained results are reported in Fig. 3.4. The scenario of the third simulation is identical to that of the first simulation but with the addition of measurement noise. The results reported in Fig. 3.5 show as the DUIO can estimate the traction force and the other resistance forces to vehicle's motion even in the presence of noise,

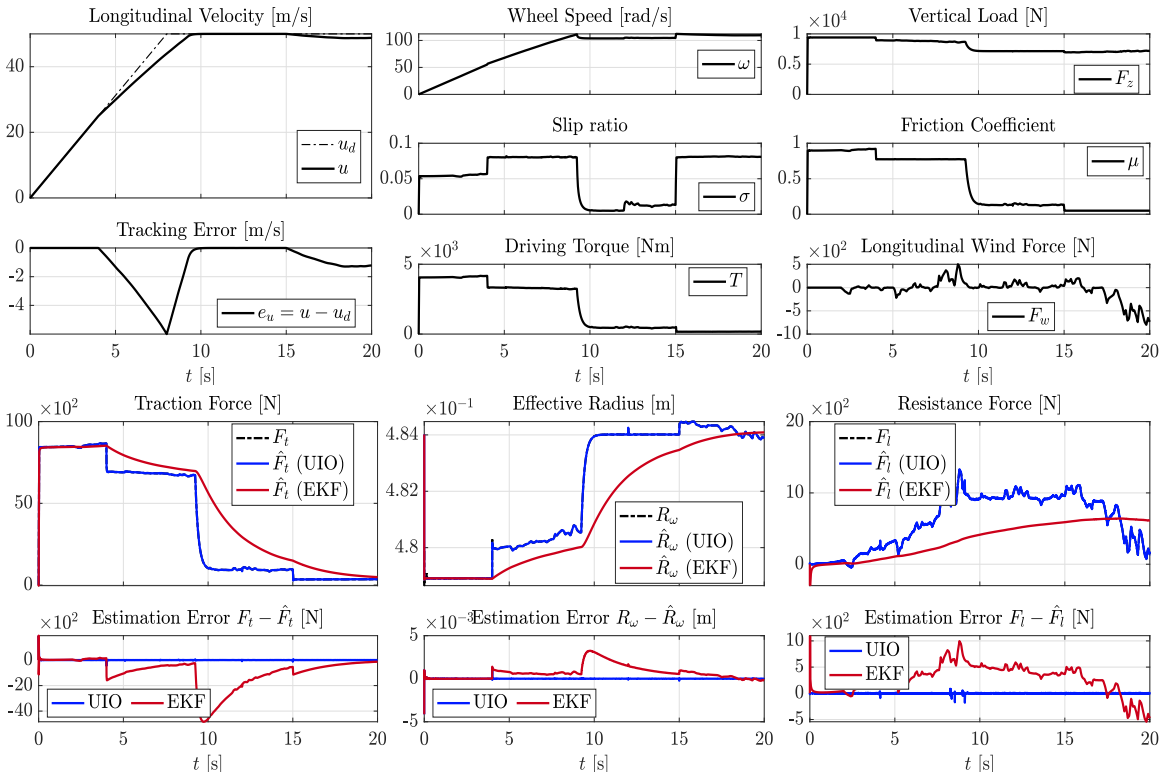


Figure 3.4: Scenario #1.2 (Changing Driving Conditions): The racecar is assumed to be traveling along a straight with variable tire-road conditions, switching from dry ($t < 4$) to wet ($4 < t < 12$) to snow ($12 < t < 15$) and finally to ice ($t > 15$). A sudden wind gust is applied at $t = 2$. The proposed estimation and control approach is capable of simultaneously coping with both types of uncertainties and disturbance.

more effectively than the EKF. It can be observed that, since both the system's states and unknown inputs become state variables of the EKF, the effect of measurement noise on their reconstruction is largely attenuated by the robust property of the filter itself. As a consequence, the estimated signals display only very small fluctuations. This is achieved at the expense of a larger observer's state and a much slower estimation error convergence. Moreover, in the case of the DUIO, only the system's states are included as observer variables, and consequently filtered, while the unknown inputs are statically reconstructed by using the formulas in Eq. (3.2.11) and (3.2.12). Consequently, the state estimates obtained via the DUIO have small fluctuations, that are comparable with those of the EKF, while the residual noise, present in such estimates, is directly propagated to the values

of estimated unknown inputs. Nonetheless, the estimation error convergence in the DUIO is much faster. It is also worth noticing that the proposed controller still guarantees the pursuit of the desired speed profile by committing a negligible tracking error. However, at steady state, small fluctuations of the tracking error can be seen with a maximum absolute value of about 0.02 m/s.

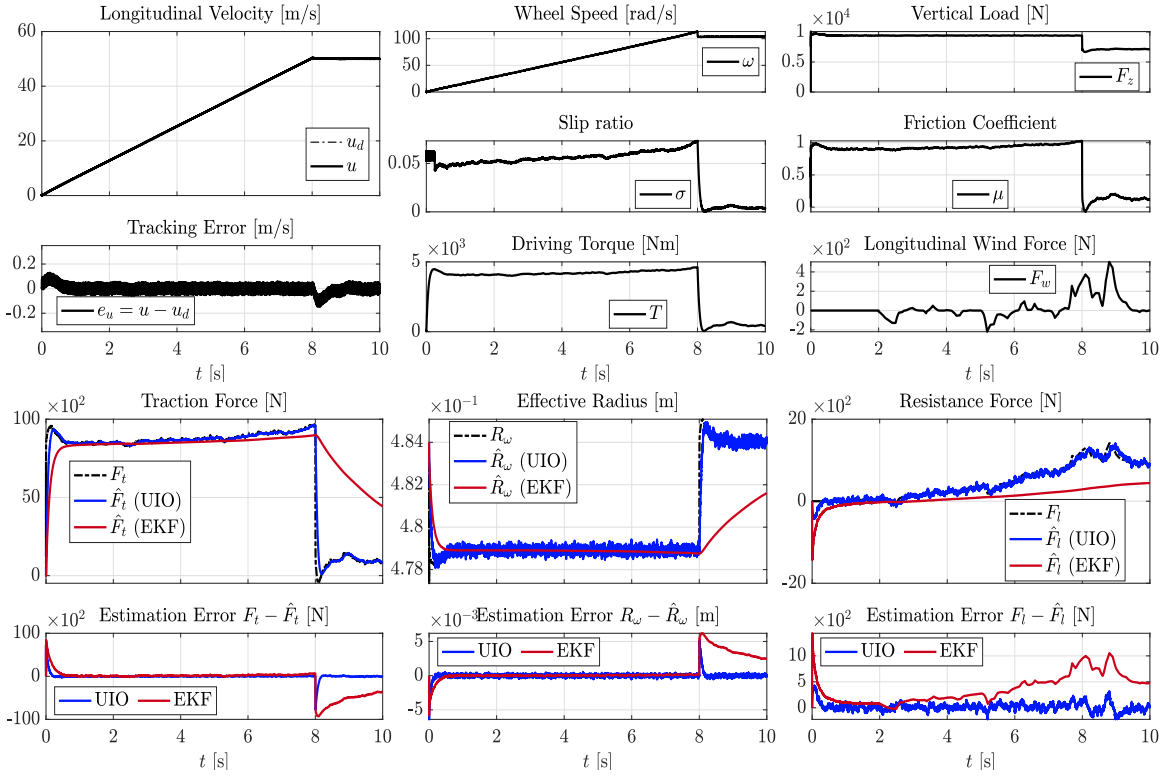


Figure 3.5: Scenario #1.3 (Measurements noise): The racecar travels along a straight and dry road and tracks a longitudinal velocity profile $u_d(t)$, when a sudden wind gust hits the vehicle at $t = 2$, in the presence of noise on the measurements. The UIO can reconstruct the unknown inputs and that the controller can track the desired trajectory with a negligible tracking error.

*Second Simulation Scenario*: In this scenario, a simulation was performed by using the Vehicle Dynamics Blockset available for Simulink. The dynamic behavior of the vehicle has been simulated through two sub-blocks: 1) Longitudinal Wheel and 2) Vehicle Body 1DOF Longitudinal. The first allows implementing the longitudinal behavior of an ideal wheel and it is also possible to specify the simulation method of the traction force and the rolling resistance as well as obtaining a series

of functional parameters, such as e.g. the torque required for a certain driving cycle. Instead, the second implements a one-degree-of-freedom (1DOF) rigid vehicle with constant mass undergoing longitudinal motion. In this simulation has been reproduced a situation in which the racecar is assumed to be traveling along a straight and dry road, simulated through Pacejka's model, in order to track a longitudinal speed profile $u_d(t)$. The accuracy of the data obtained via the Vehicle Dynamics Blockset is ensured by the use of internal nonlinear models, which are uniformly valid within the car's operating range and whose parameters have been set to the values of common driving conditions. More precisely, the so-called Pacejka's Magic Formula is used, which allows computing the longitudinal traction force $F_t$ according to the empirical four-coefficient expression:

$$F_t = D \sin\left(C \arctan\left(B\,\sigma - E\left(B\,\sigma - \arctan\left(B\,\sigma\right)\right)\right)\right) F_z\,,$$

where the dimensionless coefficients $B$, $C$, $D$, and $E$ are the stiffness, shape, peak, and curvature of the tire. Their values result from a curve-fitting process of experimental data concerning the different conditions of the tire-asphalt interface [74]. The blockset allows specifying the rolling and aerodynamic coefficients whose values, for the case of racecars, can be found in [75, 76]. The results reported in Fig. 3.6 show how the controller can follow the desired trajectory with a minimum error and the effectiveness of the disturbance estimation methodology through the DUIO, robust compared to the models that can be used to describe the forces of resistance to motion. A small deviation of at most 0.2% of the effective radius reconstructed by the DUIO with respect to the one dynamically extracted from the Vehicle Dynamics Blockset can be observed. This is caused by the dynamic deformation of the tire due to speed which is simulated within the block, but it was not considered in the formula of Eq. (3.2.11).

*Simulation of an Aggressive Maneuver as External Process on Raspberry PI*: As a final step, the proposed solution involving the input-state estimator of Th. 8 and the longitudinal control law of Th. 3 have been tested by using a low-cost hardware setup, consisting of a Raspberry PI 4 Model B system. This test has been done with the purpose to show the real-time implementability of the solution and assess the required computation time in terms of the CPU utilization. To achieve this, the Matlab/Simulink model, including the full vehicle dynamics modeled via Eq. (3.2.1),

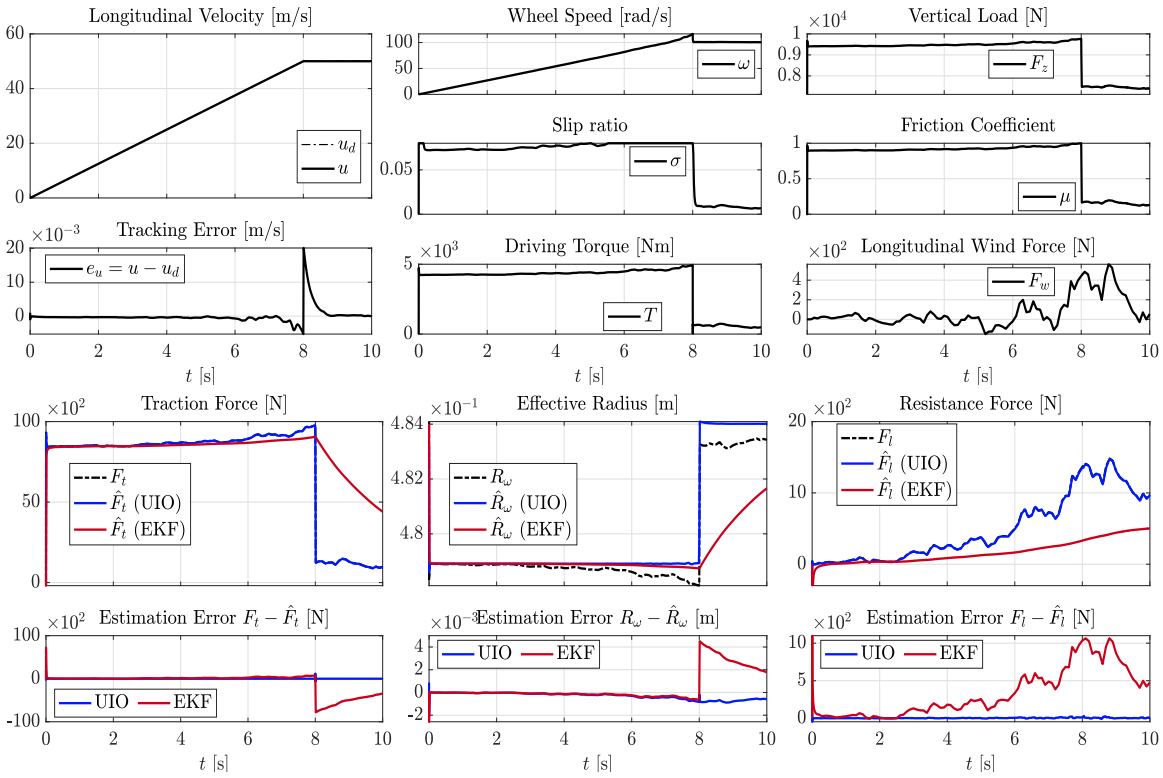


Figure 3.6: Scenario #2: (Vehicle Dynamics Blockset with Pacejka's Magic Formula): The proposed DUIO estimator and the proposed control are evaluated in a black-box test where the vehicle's dynamics model is simulated via the Vehicle Dynamics Blockset and the traction force is simulated via Pacejka's formula.

the estimator, and the control law has been compiled for the Raspberry PI hardware, via the Simulink Real-time Code Generation, and built as a standalone application. The application has been run with a scheduling time $\delta = 10^{-3}$ seconds. The inclusion of the full vehicle model in the simulation represents a further computation load that in an experimental setup would not be necessary. However, this choice allows overestimating the required CPU utilization, further ensuring the solution implementability.

Referring to Fig. 3.6, the simulated scenario is as follows. The desired longitudinal speed profile is that of an aggressive maneuver, consisting of a fast acceleration phase with $\dot{u}_d = 6.25$ m/s$^2$ ($t < 7$), a deceleration phase with $\dot{u}_d = -6.25$ m/s$^2$ ($7 \leq t < 10$), followed another acceleration phase with

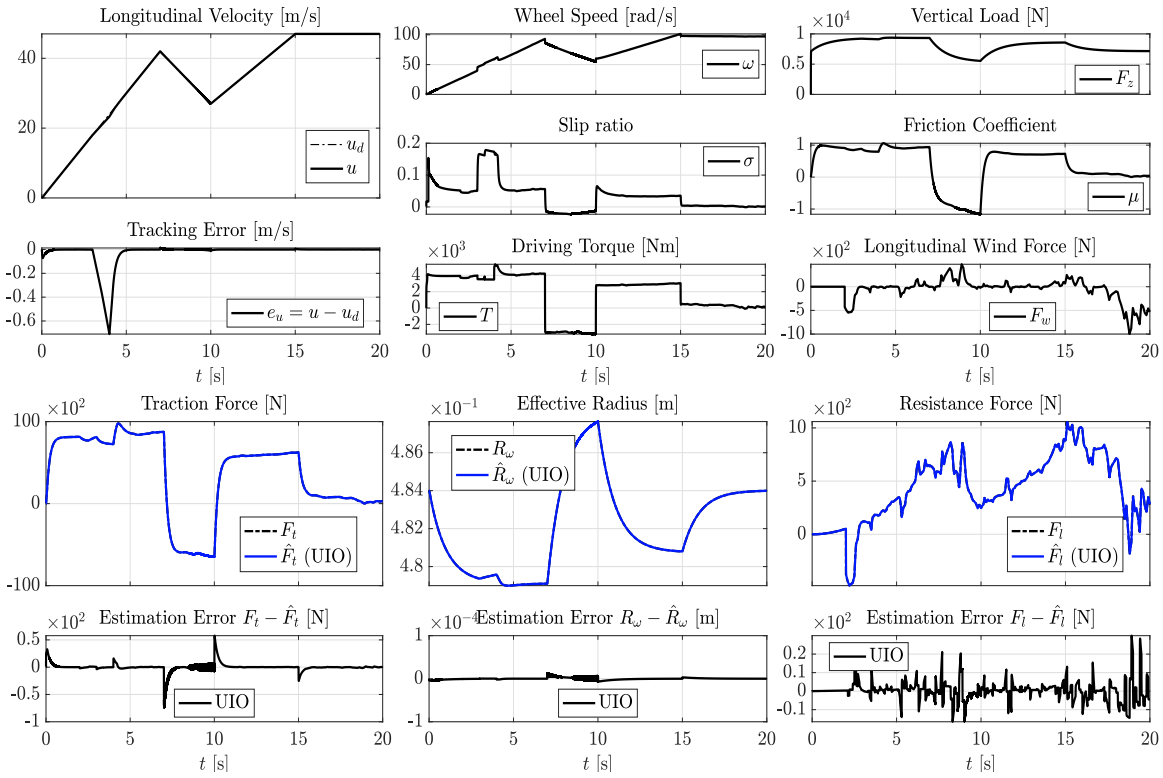


Figure 3.7: Scenario #3 (Raspberry PI 4 Model B): Results from the simulation of a complete aggressive maneuver, consisting of fast acceleration, deceleration, and constant high-speed phases, obtained with a standalone process scheduled every $\delta = 10^{-3}$ seconds. The controller successfully allows the asymptotic tracking even with a larger slip ratio threshold $\bar{\sigma} = 0.17$. As the vehicle encounters a wet surface during the interval $t \in [3, 4]$, the controller keeps increasing the longitudinal speed, while maintaining the slip ratio within the allowed range. The estimator correctly and promptly reconstructs the unknown quantities.

$\dot{u}_d = 6.25$ m/s$^2$ till the speed of 50 m/s is reached ($10 \leq t < 15$), and a final constant high-speed motion phase with $\dot{u}_d = 0$ m/s$^2$ ($15 \leq t < 20$). The road type is dry, except from during the time interval $3 \leq t < 4$ in which the car encounters a wet surface. A Dryden wind blows from the instant $t = 2$ till the end of the simulation. In order to show that the small slip ratio assumption is valid at least within the optimal interval values [37], a larger slip ratio threshold $\bar{\sigma} = 0.17$ has been chosen. While the control law is based on the reduced-degree-of-freedom model, the simulated vehicle dynamics is the full model of Eq. (3.2.1), as for the previous simulations.

Analyzing the first row of the figure, one can see the correct functioning of the controller. More

Table 3.2: Estimation Performance on the Raspberry PI 4 Model B.

| Relative Estim. Error Signal | Average | Standard Dev. |
|---|---|---|
| Traction force $F_t$ | $1.356 \cdot 10^{-2}$ | $7.823 \cdot 10^{-1}$ |
| Effective tire radius $R_\omega$ | $-4.297 \cdot 10^{-9}$ | $2.385 \cdot 10^{-6}$ |
| Resistance Force $F_l$ | $1.854 \cdot 10^{-2}$ | $1.791 \cdot 10^{-1}$ |

precisely, in the phases when the car travels on a dry road, the desired acceleration $\dot{u}_d$ requires a traction force $F_t$ that can be obtained with slip ratio values that are within the allowed range, i.e. $|\sigma| \leq \bar{\sigma}$. During these phases, the controller specifies a correct positive or negative driving torque that allows the asymptotic tracking of the desired speed $u_d$. As car meets a wet road surface, at $t = 3$, the current traction force $F_t$ instantaneously diminishes, and the asymptotic speed tracking can only be obtained with slip ratios that are out of the allowed range. The controller increases the slip ratio up to the maximum value and then applies the formula in Eq. (3.2.27), in order to make $u$ still increasing, while keeping $\sigma$ within the allowed range. As the car reaches again a dry surface at $t = 4$ and the required traction force becomes feasible, the tracking speed error quickly converges to zero.

Moving on now to the second row of the figure, it can be seen that also the estimator correctly works, thus providing accurate estimates of the unknown traction force, effective radius, and total resistance force to the controller. Specifically, it can be observed how the effective radius diminishes during the acceleration phases, increases during the deceleration ones, and reaches a constant value when moving at a constant speed. The estimation accuracy has been evaluated in terms of the relative estimation errors and the obtained results have been reported in Table 3.2. Recall that the relative estimation error of a possibly null quantity $\alpha$ estimated by $\hat{\alpha}$ is $|\alpha - \hat{\alpha}| (1 + |\alpha|)^{-1}$, where the unity is introduced to cope with the case of $\alpha = 0$.

As a final performance data, the percentage of CPU utilization has been computed by considering 25 runs of the standalone application, including the estimator, the controller, and the full vehicle's dynamics. The obtained results are reported in Fig. 3.8, which illustrates the behavior of the average of the CPU usage and of the standard deviation. The minimum and maximum utilization values within the standard deviation along the entire simulations is 4.2896% and 5.9606%, respectively, while a typical value is around 4.62%, which shows the practically implementability on the proposed

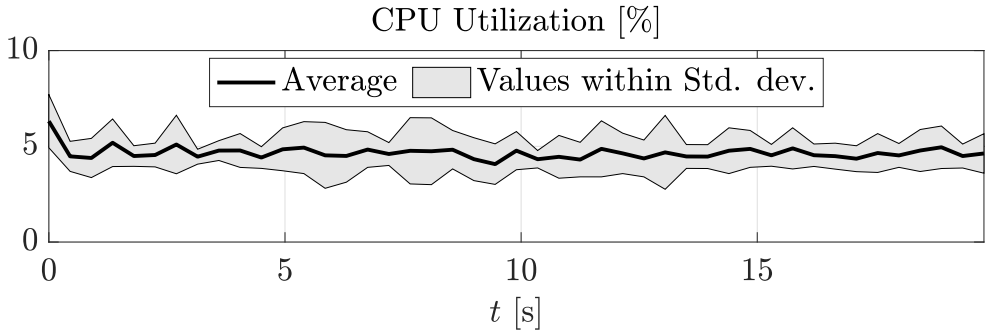


Figure 3.8: Scenario #3: Behavior of the CPU utilization percentage, computed on a dataset extracted from 25 runs of the standalone application, including the estimator, the controller, and the full vehicle's dynamics.

solution even on a low-cost platform.

### 3.2.11 Conclusion

This paragraph addressed model-free nonlinear control of the longitudinal speed for a self-driving racecar, via the use of a linear DUIO allowing the dynamic reconstruction of information on the vehicle's motion concerning the inputs acting on the system. Carried out simulations have highlighted a strong robustness of the proposed estimation and control method to the various simulation models, even in extremely changing conditions, thereby guaranteeing a much safer vehicle's motion than existing techniques. Most prominently, the estimation procedure has proven to be more efficient than EKF-based approaches, even with measurement noise, despite the simplicity of its implementation. Indeed, the approach does not require accurate knowledge of the traction force and all resistance forces. This paragraph shows that such input uncertainty as well as parametric changes in the corresponding models can be seen as disturbance inputs acting on the system, that can be accurately estimated and compensated. Future work will focus on extending this approach to the complete dynamics of the vehicle and testing it on a real Robocar.

## 3.3 Lateral Wind Estimation and Backstepping Compensation for Safer Self-driving Racecars

The present work focuses on wind-sensorless estimation and compensation for racecar models affected by lateral wind gusts. More precisely, for the estimation objective, after conveniently reformulating the nonlinear lateral model of a racecar in a form where suitable combinations of the unknown lateral wind force and moment signals act as unknown inputs, a linear input-state observer is built upon Discrete-Time Unknown Input Observer (DUIO) theory as described in paragraph (2.1). The observer uses measures of the current lateral vehicle pose, obtained via a GPS sensor, and reconstructs the full system state and unknown inputs, which is enabled by the strong observability and the system invertibility properties of the attained model when using such an output. It is worth noticing that, through this choice, our method does not use costly and robust wind sensors, yet it relies on easily accessible GPS sensors. In this respect, the framework of so-called "delayed" discrete-time UIOs has been chosen, among the others available (see e.g. [77–80]), for their advantage of involving looser existence conditions and achieving estimators with a simpler structure, explicit closed-form, direct implementability on a micro-controller, and dead-beat design, i.e. they ensure that the estimation error vanishes in a finite time, at the only expense of collecting output samples for a very small interval. Moreover, the well-known Extended Kalman Filters can be used [81], but however, they would require introducing additional state variables, representing the wind force and moment, for which an accurate dynamic model is not easy to be found both in a deterministic and stochastic framework. Finally, as for the subsequent objective of compensating the wind effect, a novel backstepping controller is proposed whose convergence is formally proved. The robustness of the proposed DUIO-based controller is tested in simulation with the model of real Robocar system [82] against the occurrence of wind gusts modeled by the well-known Dryden model [83] by using the Vehicle Dynamics Blockset [84].

### 3.3.1 Modeling

Consider a racecar with front steering and rear traction that is traveling along a flat horizontal road. Referring to Fig. 3.9, let $(X, Y)$ be the coordinates of the center of mass $G$ of the vehicle in an

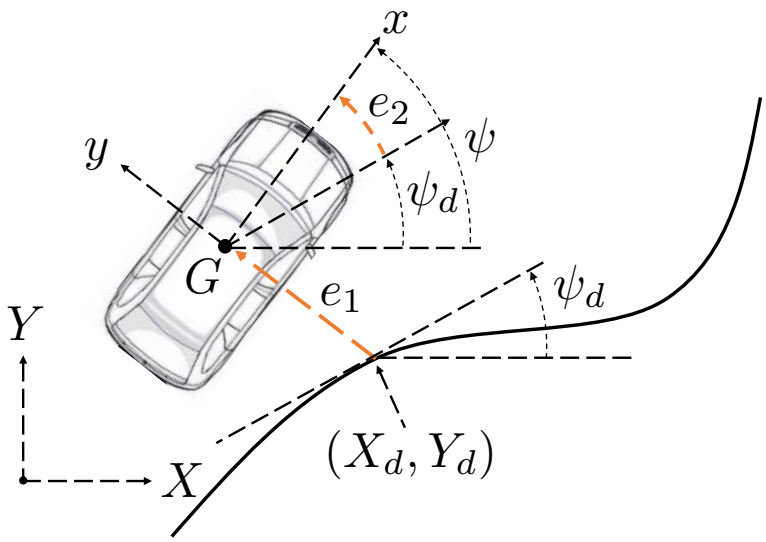


Figure 3.9: Illustration of the the vehicle schematic, desired path, and coordinate frames.

Inertial frame, and $(x, y)$ those in a body frame attached to the vehicle; let also $\psi$ be the heading direction of the vehicle with respect to the $X$-axis. Given a path to be tracked, let $(X_d, Y_d)$ be the desired position and $\psi_d$ the desired orientation, measured from the $X$-axis. Moreover, assuming that a GPS sensor is used to instantaneously measure $X$, $Y$, and $\psi$, a lateral position error variable can be introduced as the projection of the error vector $(X, Y)^T - (X_d, Y_d)^T$ along the lateral direction unit vector $(-\sin\psi, \cos\psi)^T$, i.e. $e_1 = (Y - Y_d)\cos\psi - (X - X_d)\sin\psi$; finally an orientation error can be introduced as $e_2 = \psi - \psi_d$. Assuming the absence of pitching and rolling motions, the vehicle's lateral dynamics is described by the so-called single-track model [85] which has the state-form [86]:

$$\dot{Z} = A_c(u)\, Z + B_\delta\, \delta + B_{c,r}(u)\, r_d + B_w\, F\,, \tag{3.3.1}$$

where $Z = (e_1, \dot{e}_1, e_2, \dot{e}_2)^T$, $\delta$ is the wheel's steering angle and the system's control input, $u$ is the vehicle's longitudinal speed, $r_d = \dot{\psi}_d$ is a the desired yaw rate, $F = (F_w, \tau_w)^T$ is the vector of the

Table 3.3: Nominal Inertial and Geometric Parameters of a Robocar from the Roborace Challenge [82]

| **Parameters** | **Value** | **Unit** |
|---|---|---|
| Front cornering stiffness, $\gamma_1$ | 226 | [kN,/ rad] |
| Rear cornering stiffness, $\gamma_2$ | 282 | [kN / rad] |
| Car's moment of inertia, $J$ | 1150 | [kg·m$^2$] |
| Front wheelbase, $a_1$ | 1.51 | [m] |
| Rear wheelbase, $a_2$ | 1.288 | [m] |
| Mass, $m$ | 1350 | [kg] |

lateral wind force and moment,

$$
\begin{aligned}
A_c(u) &= \begin{pmatrix} 0 & 1 & 0 & 0 \\ 0 & -\frac{\gamma_s}{mu} & \frac{\gamma_s}{m} & \frac{\gamma_m}{mu} \\ 0 & 0 & 0 & 1 \\ 0 & \frac{\gamma_p}{Ju} & -\frac{\gamma_m}{J} & -\frac{\gamma_q}{Ju} \end{pmatrix}, B_\delta = \begin{pmatrix} 0 \\ \frac{\gamma_1}{m} \\ 0 \\ \frac{\gamma_1\, a_1}{J} \end{pmatrix}, \\
B_{c,r} &= \begin{pmatrix} 0 \\ \frac{\gamma_m}{mu} - u \\ 0 \\ -\frac{\gamma_q}{Ju} \end{pmatrix}, B_w = \begin{pmatrix} 0 & 0 \\ \frac{1}{m} & 0 \\ 0 & 0 \\ 0 & \frac{1}{J} \end{pmatrix},
\end{aligned}
\tag{3.3.2}
$$

with $\gamma_s = \gamma_1 + \gamma_2$, $\gamma_p = \gamma_1\, a_1 + \gamma_2\, a_2$, $\gamma_m = \gamma_2\, a_2 - \gamma_1\, a_1$, and $\gamma_q = \gamma_1\, a_1^2 + \gamma_2\, a_2^2$, and all other geometric and inertial parameters are as in Table 3.3. Despite its simplicity, the model is known to be well suited to describe the system behavior, under the hypothesis that the vehicle moves with small steering angles. Moreover, assuming the lateral error pose can be measured via GPS sensors, one can define the following output map:

$$
Y = C\, Z + D_\delta\, \delta + D_r\, r_d + D_w\, F\,, \tag{3.3.3}
$$

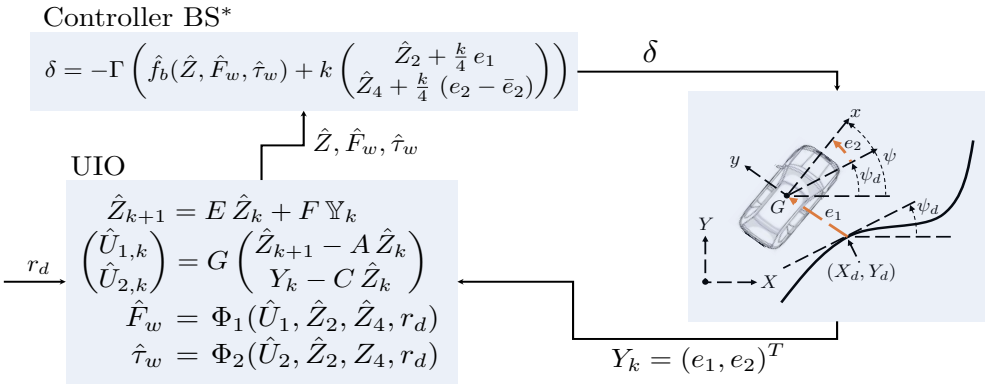


Figure 3.10: Illustration of the racecar system closed in the loop with the proposed DUIO-based estimator, and the proposed backstepping controller. Given a desired path, the desired coordinates on the curve describing such a path are $(X_d, Y_d)$, while $\psi_d$ and $r_d$ are the desired orientation and yaw rate, respectively. The outputs of the racecar are the position and orientation errors, $e_1$ and $e_2$, and are used by the DUIO-based estimator to reconstruct the current full system state $Z$ and, along with the information about $r_d$, those of the wind force and moment. Once the estimates $\hat{Z}$, $\hat{F}_w$ and $\hat{\tau}_w$ are determined, the proposed backstepping controller determines the value of the input steering angle ensuring the asymptotic convergence of the tracking errors.

with

$$C = \begin{pmatrix} 1\ 0\ 0\ 0 \\ 0\ 0\ 1\ 0 \end{pmatrix}, \quad \begin{matrix} D_\delta = D_r = 0_{2\times 1}, \\ D_w = 0_{2\times 2} \end{matrix} . \tag{3.3.4}$$

### 3.3.2 Design of the Lateral Wind Estimator

To derive the sought input-state observer, the continuous-time racecar model in (3.3.1) needs to be discretized with respect to time by using a first-order Euler approximation of the involved time derivatives. This yields the following discrete-time model:

$$\begin{aligned} Z_{k+1} &= \tilde{A}(u_k)\,Z_k + \tilde{B}(u_k)\,\tilde{U}_k\,, \\ Y_k &= C\,\tilde{Z}_k + \tilde{D}\,\tilde{U}_k\,, \end{aligned} \tag{3.3.5}$$

where the state vector is $Z_k = (e_{1,k}, \dot{e}_{1,k}, e_{2,k}, \dot{e}_{2,k})^T$, the input vector is $\tilde{U}_k = (\delta_k, r_{d,k}, F_{w,k}, \tau_{w,k})^T$, the output vector is $Y_k = (e_{1,k}, e_{2,k})^T$ and it is measurable through a GPS sensor, and the matrices

are:

$$\tilde{A} = I + T_s A_c(u_k) = \begin{pmatrix} 1 & T_s & 0 & 0 \\ 0 & 1 - \frac{\gamma_s T_s}{m u_k} & \frac{\gamma_s T_s}{m} & \frac{\gamma_m T_s}{m u_k} \\ 0 & 0 & 1 & T_s \\ 0 & \frac{\gamma_m T_s}{J u_k} & -\frac{\gamma_m T_s}{J} & 1 - \frac{\gamma_q T_s}{J u_k} \end{pmatrix},$$

$$\tilde{B} = T_s \left(B_\delta, B_{c,r}, B_w\right) = \begin{pmatrix} 0 & 0 & 0 & 0 \\ \frac{\gamma_1 T_s}{m} & \left(\frac{\gamma_m}{m u_k} - u_k\right) T_s & \frac{T_s}{m} & 0 \\ 0 & 0 & 0 & \\ \frac{\gamma_1 a_1 T_s}{J} & -\frac{\gamma_q T_s}{J u_k} & 0 & \frac{T_s}{J} \end{pmatrix},$$

where $A_c$, $B_{c,r}$ and the other control vectors are defined in (3.3.2), and finally $\tilde{D} = (D_\delta, D_{c,r}, D_w)$, that is $D = 0_{2\times 4}$.

We are now ready to obtain the first main result of this work via the following theorem:

**Theorem 4.** *Given a racecar with lateral dynamics as in (3.3.1) and a sampling time $T_s$, a delayed UIO reconstructing the wind disturbance vector $F$ is described by the iterative system:*

$$\begin{aligned} \hat{Z}_{\sigma+1} &= E\,\hat{Z}_\sigma + F\,\mathbb{Y}_k\,, \\ \hat{U}_\sigma &= \begin{pmatrix} \hat{U}_{1,\sigma} \\ \hat{U}_{2,\sigma} \end{pmatrix} = G \begin{pmatrix} \hat{Z}_{\sigma+1} - A\,\hat{Z}_\sigma \\ Y_\sigma - C\,\hat{Z}_\sigma \end{pmatrix}, \end{aligned} \tag{3.3.6}$$

*where $k$ is a discrete step time, $\sigma = k - L$ and the state vector and the output history are $\hat{Z}_\sigma = (\hat{e}_{1,\sigma}, \dot{\hat{e}}_{1,\sigma}, \hat{e}_{2,\sigma}, \dot{\hat{e}}_{2,\sigma})^T$ and $\mathbb{Y}_k = (Y_{k-2}, Y_{k-1}, Y_k)^T$, respectively, the $C$ is as in (3.3.4) and the other*

*matrices are*

$$E = \begin{pmatrix} 1 & T_s & 0 & 0 \\ -\frac{1}{T_s} & -1 & 0 & 0 \\ 0 & 0 & 1 & T_s \\ 0 & 0 & -\frac{1}{T_s} & -1 \end{pmatrix}, \; F = \begin{pmatrix} 0 & 0 & 0 & 0 & 0 & 0 \\ 0 & 0 & 0 & 0 & \frac{1}{T_s} & 0 \\ 0 & 0 & 0 & 0 & 0 & 0 \\ 0 & 0 & 0 & 0 & 0 & \frac{1}{T_s} \end{pmatrix},$$
$$G = \begin{pmatrix} 0 & \frac{1}{T_s} & 0 & 0 & 0 & 0 \\ 0 & 0 & 0 & \frac{1}{T_s} & 0 & 0 \end{pmatrix}, \; A = \begin{pmatrix} 1 & T_s & 0 & 0 \\ 0 & 1 & \frac{\gamma_s T_s}{m} & 0 \\ 0 & 0 & 1 & T_s \\ 0 & 0 & -\frac{\gamma_m T_s}{J} & 1 \end{pmatrix}. \tag{3.3.7}$$

*Finally, the best-effort wind input vector estimate* $\hat{F}_\sigma = (\hat{F}_{w,\sigma}, \hat{\tau}_{w,\sigma})^T$ *can be obtained by the formulas:*

$$\begin{aligned} \hat{F}_{w,\sigma} &= m\,\hat{U}_{1,\sigma} + \tfrac{\gamma_s}{u_k}\,\hat{Z}_{2,\sigma} - \tfrac{\gamma_m}{u_k}\,\hat{Z}_{4,\sigma} + \\ &- \gamma_1\,\delta_k + \left(m\,u_k - \tfrac{\gamma_m}{u_k}\right) r_{d,k}\,, \\ \hat{\tau}_{w,\sigma} &= J\,\hat{U}_{2,\sigma} - \tfrac{\gamma_m}{u_k}\,\hat{Z}_{2,\sigma} + \tfrac{\gamma_q}{u_k}\,\hat{Z}_{4,\sigma} + \\ &- \gamma_1 a_1\,\delta_k + \tfrac{\gamma_q}{u_k}\,r_{d,k}\,. \end{aligned} \tag{3.3.8}$$

*Proof. (State Reconstruction)* Let us start with the procedure to obtain a delayed estimation of the current system's state $Z_k$. The considered lateral vehicle dynamics model includes terms depending on the longitudinal vehicle's speed $u_k$, which is externally controlled, and the desired yaw rate $r_d$, which is specified at a higher level based on required changes in the vehicle's direction. These two variables can be assumed to be known yet time-varying, thereby leading to time-varying matrices $\tilde{A}(u_k)$ and $\tilde{B}(u_k)$. The strategy that can be adopted here is that of collecting all time-varying or nonlinear quantities into a product $B\,U_k$, where $B$ and $U_k$ are a suitable control matrix and an input vector. Indeed, the quantity $B\,U_k$ can model nonlinearities, parametric uncertainties, etc [87]. To obtain this, one can first observe that matrix $\tilde{A}$ can be additively separated as

$$\tilde{A} = A + \begin{pmatrix} 0 & 0 & 0 & 0 \\ 0 & -\frac{\gamma_s T_s}{m u_k} & 0 & \frac{\gamma_m T_s}{m u_k} \\ 0 & 0 & 0 & 0 \\ 0 & \frac{\gamma_m T_s}{J u_k} & 0 & -\frac{\gamma_q T_s}{J u_k} \end{pmatrix} = A + A^*(u_k)\,,$$

where $A$ is defined in (3.3.7). Then, one can impose the following identity:

$$A^*(u_k)\, Z_k + \tilde{B}(u_k)\, \tilde{U}_k = B\, U_k\,,$$

which, thanks to the structure of $A^*$ and the control matrix $\tilde{B}$, can be satisfied by the following choice:

$$B = \begin{pmatrix} 0 & 0 \\ T_s & 0 \\ 0 & 0 \\ 0 & T_s \end{pmatrix}\,, \quad U_k = \begin{pmatrix} U_{1,k} \\ U_{2,k} \end{pmatrix}\,, \tag{3.3.9}$$

with

$$\begin{aligned} U_{1,k} &= -\tfrac{\gamma_s}{m u_k}\,\dot{e}_1 + \tfrac{\gamma_m}{m u_k}\,\dot{e}_2 + \tfrac{\gamma_1}{m}\,\delta_k + \\ &\quad + \left(\tfrac{\gamma_m}{m u_k} - u_k\right) r_{d,k} + \tfrac{1}{m}\,F_{w,k}\,, \\ U_{2,k} &= \tfrac{\gamma_m}{J u_k}\,\dot{e}_1 - \tfrac{\gamma_q}{J u_k}\,\dot{e}_2 + \tfrac{\gamma_1 a_1}{J}\,\delta_k + \\ &\quad - \tfrac{\gamma_q}{J u_k}\, r_{d,k} + \tfrac{1}{J}\,\tau_{w,k}\,. \end{aligned} \tag{3.3.10}$$

This leads us to a time-invariant linear system, where $A$ is described in (3.3.7), $B$ is in (3.3.9), $C$ is in (3.3.4), and $D$ is a null matrix of suitable dimensions. Direct calculation shows that the system model is strongly observable Prop. 3 and invertible Prop. 2 with a delay value of $L = 2$. Indeed, given the sequence

$$\mathbb{V}^1 = 0_{4\times 4}\,, \quad \mathbb{V}^2 = \begin{pmatrix} 0_{4\times 2} & 0_{4\times 4} \\ T_s^2\, \mathbb{I}_2 & 0_{2\times 4} \end{pmatrix}\,,$$

it holds $\mathrm{rank}(\mathbb{V}^1) = 0$, $\mathrm{rank}(\mathbb{V}^2) = 2$ and hence $\mathrm{rank}(\mathbb{V}^2) - \mathrm{rank}(\mathbb{V}^1) = 2 = m$, where $m$ is the dimension of our $U_k$, and then it also holds $\mathrm{rank}([\mathbb{O}^2, \mathbb{V}^2]) - \mathrm{rank}(\mathbb{V}^2) = 4 = n$, where $n$ is the dimension of $Z_k$. Therefore, the derivation of the sought input-state observer can now be done as described below, by the reasoning described in [88]. The third condition A3) listed in the previous chapter, for $m = 2$ and $L = 2$, requires that matrix $F$ satisfies the equation

$$F\, \mathbb{V}^2 = (B, 0_{4\times 2})\,. \tag{3.3.11}$$

The above relation first implies that $F \in \mathbb{R}^{4\times 6}$ must be in the left nullspace of the last $Lm = 4$

columns of $\mathbb{V}^2$. This condition is satisfied for every $F$ since the last 4 columns of $\mathbb{V}^2$ are $\begin{pmatrix} 0 \\ \mathbb{V}^1 \end{pmatrix} = 0_{6\times4}$. Furthermore, Eq. 3.3.11 also implies that

$$F \begin{pmatrix} 0_{4\times2} & 0_{4\times4} \\ T_s^2\,\mathbb{I}_2 & 0_{2\times4} \end{pmatrix} = \begin{pmatrix} 0 & 0 \\ T_s & 0 \\ 0 & 0 \\ 0 & T_s \end{pmatrix}.$$

The simplest choice of $F$ satisfying the above condition is the one reported in (3.3.7). Moreover, given the 2-step observability matrix

$$\mathbb{O}^2 = \begin{pmatrix} 1 & 0 & 0 & 0 \\ 0 & 0 & 1 & 0 \\ 1 & T_s & 0 & 0 \\ 0 & 0 & 1 & T_s \\ 1 & 2\,T_s & \frac{\gamma_s T_s^2}{m} & 0 \\ 0 & 0 & 1-\frac{\gamma_m T_s^2}{J} & 2\,T_s \end{pmatrix},$$

the second condition A2), Sec.(2.1), yields the estimation error dynamic matrix $E$ reported in (3.3.7). Direct verification shows that all eigenvalues of $E$ are in the origin, which guarantees that the obtained estimator is asymptotically stable and has dead-beat property. Finally, since matrix $(B^T, D^T)^T$ is full column rank, it is possible to find a matrix $G$ that satisfies (3.2.17), with $m = 2$, whose solution can be computed via the pseudo-inverse and gives the expression reported in (3.3.7).

*(Input Reconstruction)*: By inverting (3.3.10) and substituting the state variables with the corresponding observer's variables, that is $\hat{\hat{e}}_1 = \hat{Z}_{2,\sigma}$ and $\hat{\hat{e}}_2 = \hat{Z}_{4,\sigma}$, one obtains the best-effort estimate of the unknown wind vector described in (3.3.8). □

### 3.3.3 Design of the Backstepping Controller with Wind Compensation

This subsection focuses on the design of a backstepping control law allowing the stabilization of the system model, with compensation of the effect of the estimated wind vector. First of all, it should

be recalled that, when the vehicle is required to align to a path with a given yaw rate $r_d \neq 0$, it is not possible to steer both variables $e_1$ and $e_2$ to zero. Assuming that $e_1$ has a priority over the other variable, meaning that the lateral position error must vanish, the resulting steady-state value $\bar{e}_2$ is necessarily not zero. The specific value of $\bar{e}_2$ as a function of the desired yaw rate $r_d$ can be found in [89] and is given by:

$$\bar{e}_2 = \tfrac{a_1}{a_1+a_2}\tfrac{m\,a_y}{\gamma_2} - \tfrac{a_2}{R} = \tfrac{a_1}{a_1+a_2}\left(\tfrac{m}{\gamma_2}\,u - \tfrac{a_2}{u}\right) r_d\,, \tag{3.3.12}$$

where the expressions for the instantaneous curvature radius, $R = u/r_d$, and lateral acceleration $a_y = u^2/R = u\,r_d$, respectively, have been used. It is worth noticing that this property arises from the nature of the physical system and is independent of the type of control used. Intuitively, the proposed backstepping approach, described below, uses the system's input $\mu = \delta$ to control the state $\xi = (\xi_1, \xi_2)^T = (\dot{e}_1, \dot{e}_2)^T$ of the velocity error subsystem, and exploits afterward such velocities to regulate the state $\eta = (\eta_1, \eta_2)^T = (e_1, e_2 - \bar{e}_2)^T$ of the position error one. This is based on the fact that the system dynamics in (3.3.1) can be written in the cascade form:

$$\begin{aligned} \dot{\eta} &= f_a(\eta) + g_a(\eta)\,\xi\,, \\ \dot{\xi} &= f_b(\eta,\xi) + g_b(\eta,\xi)\,\mu\,, \end{aligned} \tag{3.3.13}$$

where $f_a(\eta) = (0,0)^T$, $g_a(\eta) = \mathbb{I}_2$, $f_b(\eta,\xi) = (f_{b,1}, f_{b,2})^T$, with

$$\begin{aligned} f_{b,1} &= \tfrac{\gamma_s}{m}\,(\eta_2 + \bar{e}_2) - \tfrac{\gamma_s}{mu}\,\xi_1 + \tfrac{\gamma_m}{mu}\,\xi_2 + r_d\left(\tfrac{\gamma_m}{mu} - u\right) + \tfrac{F_w}{m}\,, \\ f_{b_2} &= -\tfrac{\gamma_m}{J}\,(\eta_2 + \bar{e}_2) + \tfrac{\gamma_m}{Ju}\,\xi_1 - \tfrac{\gamma_q}{Ju}\,\xi_2 - \tfrac{\gamma_q}{Ju}\,r_d + \tfrac{\tau_w}{J}\,, \end{aligned}$$

and

$$g_b(\eta,\xi) = \begin{pmatrix} \frac{\gamma_1}{m} \\ \frac{\gamma_1 a_1}{J} \end{pmatrix}.$$

Following the approach developed in [90] and also described in [91], we can prove the second main result of the work:

**Theorem 5.** *Given the racecar model in (3.3.1), or equivalently in (3.3.13), and given also a desired*

*convergence speed $k > 0$ and an estimate $\hat{F} = (\hat{F}_{w,\sigma}, \hat{\tau}_{w,\sigma})^T$ of the wind vector $F$, a backstepping-based best-effort control law for the steering angle $\delta$, ensuring convergence of the lateral position error $e_1$ to zero, is given by*

$$\delta = -\Gamma \left( \hat{f}_b + k \begin{pmatrix} \hat{Z}_{2,\sigma} + \frac{k}{4}\, e_1 \\ \hat{Z}_{4,\sigma} + \frac{k}{4}\, (e_2 - \bar{e}_2) \end{pmatrix} \right) \tag{3.3.14}$$

*where $\bar{e}_2$ is described in (3.3.12) and where*

$$\begin{aligned} \Gamma &= \frac{Jm}{\gamma_1 (J^2 + m^2 a_1^2)} (J, m a_1)\ , \\ \hat{f}_b &= \begin{pmatrix} \frac{\gamma_s}{m}\, e_2 - \frac{\gamma_s}{mu}\, \hat{Z}_{2,\sigma} + \frac{\gamma_m}{mu}\, \hat{Z}_{4,\sigma} + r_d \left( \frac{\gamma_m}{mu} - u \right) + \frac{\hat{F}_{w,\sigma}}{m} \\ -\frac{\gamma_m}{J}\, e_2 + \frac{\gamma_m}{Ju}\, \hat{Z}_{2,\sigma} - \frac{\gamma_q}{Ju}\, \hat{Z}_{4,\sigma} - \frac{\gamma_q}{Ju}\, r_d + \frac{\hat{\tau}_{w,\sigma}}{J} \end{pmatrix}. \end{aligned} \tag{3.3.15}$$

*Proof.* To begin with, having denoted with $\phi(\eta)$ a commanded error velocity to be designed as a feedback control law ensuring the convergence to zero of the position error vector $\eta$, and with $\delta\xi = \xi - \phi(\eta)$ the difference between the error velocity and commanded one, one can rewrite the system model in the following cascade form:

$$\begin{aligned} \dot{\eta} &= f_a(\eta) + g_a(\eta)\, (\phi(\eta) + \delta\xi)\,, \\ \delta\dot{\xi} &= f_b(\eta, \delta\xi) + g_b(\eta, \delta\xi)\, \mu - \dot{\phi}(\eta)\,. \end{aligned} \tag{3.3.16}$$

The first design step requires making the first set of variables $\eta$ asymptotically stable, which is to render the first set of differential relations in (3.3.16) convergent. For this purpose, it is possible to choose the Lyapunov control function

$$V(\eta) = \tfrac{1}{2}\eta^T \eta = \tfrac{1}{2} e_1^2 + \tfrac{1}{2}(e_2 - \bar{e}_2)^2\,,$$

whose time-derivative is given by

$$\dot{V}(\eta) = \eta^T (f_a(\eta) + g_a(\eta)\, (\phi(\eta) + \delta\xi))\,.$$

Imposing for $\delta\xi = 0$ that the above expression is equal to the desired behavior, $\dot{V}(\eta) = -k\,V(\eta)$, where $k$ is the sought convergence speed, leads to the feedback law

$$\phi(\eta) = -\tfrac{k}{2}\,\eta = -\tfrac{k}{2}\,\left(e_1, e_2 - \bar{e}_2\right)^T\,. \tag{3.3.17}$$

This ensures a convergence speed of $k$, which can also be seen by the fact that the first set of relations in (3.3.16) becomes $\dot{\eta} = -k\,\eta$.

Having verified that condition $\phi(0) = 0$ holds, the second design step consists in performing analogous reasoning for the stabilization variable $\delta\xi$, that is in making the second set of relations in (3.3.16) to be convergent. To this purpose, it is worth noting that the choice of the following Lyapunov control function $V_c = V + \frac{1}{2}\delta\xi^T\delta\xi$ would be inconclusive. This occurs since the system is underactuated, i.e. it has a scalar input $\mu$, multiplied by not right-invertible control vector $g_b(\eta,\xi)$, and a two-dimensional substate variable $\delta\xi$ to be stabilized. To overcome this problem, one can observe that $g_b$ is left-invertible for all states, which in turn implies that the matrix $\Gamma = (g_b^T g_b)^{-1} g_b^T$ always exists. Then, one can choose the Lyapunov control function

$$V_c(\eta,\delta\xi) = V + \tfrac{1}{2}\delta\xi^T\,\Gamma^T\,\Gamma\,\delta\xi\,,$$

which is positive semi-definite with respect to $(\eta^T, \delta\xi^T)^T$. Its time-derivative is

$$\dot{V}_c = \eta^T\,(f_a + g_a(\phi + \delta\xi)) + \delta\xi^T\,\Gamma^T\Gamma\left(f_b + g_b\,\mu - \dot{\phi}\right)\,,$$

where the dependency of the functions on their input arguments is avoided for brevity. Substituting in the above formula the expression of (3.3.17) yields:

$$\begin{aligned}
\dot{V}_c &= -\tfrac{k}{2}\eta^T\eta + \delta\xi^T\Gamma^T\Gamma\left(f_b + g_b\,\mu - \dot{\phi}\right) = \\
&= -\tfrac{k}{2}\eta^T\eta + \delta\xi^T\Gamma^T\Gamma\left(f_b - \dot{\phi}\right) + \delta\xi^T\,\Gamma^T\mu = \\
&= -\tfrac{k}{2}\eta^T\eta + \delta\xi^T\Gamma^T\left(\Gamma\left(f_b - \dot{\phi}\right) + \mu\right)\,,
\end{aligned}$$

where the simplification $\Gamma\,g_b = (g_b^T g_b)^{-1} g_b^T g_b = 1$ has been used. This has first avoided the problem of non-right-invertibility of the control vector $g_b$ multiplying input $\delta$. By imposing now that the time-

derivative $\dot{V}_c$ equals a desired behavior, namely that it satisfies the differential equation $\dot{V}_c = -k\, V_c$ finally leads to the expression

$$\mu = -\Gamma \left( f_b - \dot{\phi} \right) - \tfrac{k}{2}\, \Gamma\, \delta\xi = -\Gamma \left( f_b - \dot{\phi} + \tfrac{k}{2} \delta\xi \right) , \tag{3.3.18}$$

and also ensures a total convergence speed of $k$. Direct computation of the involved terms gives:

$$\begin{aligned}
\Gamma = \frac{\left(\frac{\gamma_1}{m}, \frac{\gamma_1 a_1}{J}\right)}{\frac{\gamma_1^2 (J^2 + m^2 a_1^2)}{m^2 J^2}} &= \frac{Jm}{\gamma_1 (J^2 + m^2 a_1^2)} (J, m a_1) \ , \\
-\dot{\phi} + \tfrac{k}{2}\delta\xi \quad &= \quad \tfrac{k}{2} \begin{pmatrix} \dot{e}_1 \\ \dot{e}_2 \end{pmatrix} + \tfrac{k}{2} \begin{pmatrix} \dot{e}_1 + \frac{k}{2} e_1 \\ \dot{e}_2 + \frac{k}{2}(e_2 - \bar{e}_2) \end{pmatrix} = \\
&= \quad k \begin{pmatrix} \dot{e}_1 + \frac{k}{4}\, e_1 \\ \dot{e}_2 + \frac{k}{4}\, (e_2 - \bar{e}_2) \end{pmatrix} ,
\end{aligned}$$

where $\Gamma$ coincides with its expression in (3.3.15). Replacing the velocity terms and the wind vector components in (3.3.18) with the best available estimates, provided by the state-input observer described in Th. 4, i.e. $\dot{e}_1 = \hat{Z}_{2,\sigma}$, $\dot{e}_2 = \hat{Z}_{4,\sigma}$, $F_w = \hat{F}_{w,\sigma}$, and $\tau_w = \hat{\tau}_{w,\sigma}$, and then rewriting the so-obtained expression in the original state variables leads to the steering control law of (3.3.14), which concludes the proof. □

**Remark 3.** *It is worth noticing that, in general, if estimates of $\dot{e}_1$ and $\dot{e}_2$ are not available from an observer, they can still be calculated by replacing them with the corresponding equations in the dynamics. Therefore, the proposed controller uses in any case no information about velocities.*

### 3.3.4 Simulation Validation Results

This section presents a validation of the proposed estimation and control approach and compares its performance to that of existing solutions. The numerical values of the car parameters, that are typical of the cars now participating in the Roborace challenge [82], are reported in Table 3.3. The full nonlinear car's dynamics has been implemented by using the Vehicle Dynamics Blockset of Matlab/Simulink [84].

To the purpose of showing the effectiveness of the estimator proposed in Th. 4, the following scenario has been considered. The racecar accelerates up to $\bar{u} = 50$ m/s $= 180$ Km/h and decelerates various times, while the road yaw rate $r_d$ abruptly changes. A Dryden wind gust signal acts laterally to the car starting from an initial time of $t = 0.5$ s. The wind speed vector is generated via Dryden's model [83], according to which the velocity of a continuous wind gust is represented as spatially-varying stochastic processes that specify their power spectral densities. Then, the corresponding wind force $F_w$ affecting the car can be obtained via the formula $F_w = \frac{1}{2}\,\rho\,S\,c_y\,w^2$, where $w$ is the crosswind speed, $\rho = 1.225\frac{Kg}{m^3}$ is the density of air at sea level, $S$ is the reference area and $c_y$ is the lateral force coefficient. The wind moment $\tau_w$ is computed as the net moment applied over the entire lateral car's surface. The lever arm $l \in [-a_2, a_1]$ of the wind force $F_w$ is also randomly generated so as to obtain the instantaneous wind moment $\tau_w = l\,F_w$. Noise is added to the lateral and orientation error positions as white signals with zero mean value and standard deviations of 0.01 m and 0.017 rad, respectively, to simulate measurements. (cf. e.g. [92]). Fig 3.11 illustrates how the proposed DUIO can promptly and accurately reconstruct the wind's force and moment. It also shows how it outperforms an EKF [81], which has been designed by modeling the wind as a random walk process. This choice correctly ensures that the derivations of both the DUIO and the EKF are independent of the mathematical wind model. It is noticeable that the DUIO remains accurate even in the presence of measurement noise.

Moreover, to prove the effectiveness of the backstepping controller proposed in Th. 5, and in fact of the entire solution of this work, the racecar system is closed in the loop with such controller and the input-state estimator of Th. 4. The performance of the present controller is compared to those of a traditional PI controller [91] and the backstepping controller proposed in [93] (later referred to as BS). Compared to the former, the current backstepping approach symmetrically regulates both linear and angular position errors, during the first step of design (cf. the theorem's proof), instead of only the linear one. Fig. 3.12 illustrates the obtained results and shows how our controller, referred to in the figure as BS$^*$, successfully allows tracking the desired path, irrespective of the wind presence and the road curvature. As expected from [89], the steady-state orientation error is given by (3.3.12). It can finally be noticed that our backstepping controller has a faster rise time and smaller overshoot than the other two controllers (cf. the first-row plot), thereby achieving faster and

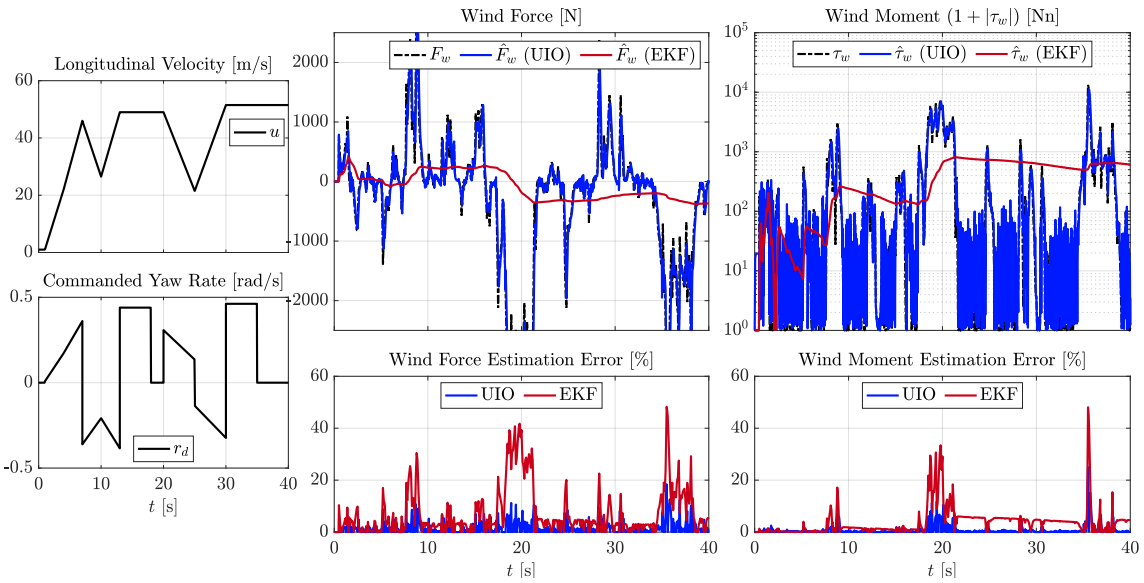


Figure 3.11: Estimation Performance with Dryden wind gusts with noisy measurement: (left column) The racecar accelerates up to $\bar{u} = 50$ m/s $= 180$ Km/h and decelerates various times, while the road yaw rate $r_d$ abruptly changes; (middle and right columns) wind force $F_w$ and moment $\tau_w$ estimated by the DUIO proposed in Th. 4 and an EKF. The figures show greater accuracy and faster tracking of the unknown wind signal by the DUIO-based solution over the EKF.

more accurate tracking (the second and third plots). Finally, Fig. 3.13 reports the results obtained with the three considered controllers, using the EKF estimates. It can be observed that EKF-based controllers work worse than DUIO ones; moreover, the proposed backstepping controller (BS$^*$) has better performance than the other two.

### 3.3.5 Conclusion

This work addressed the wind gust estimation and compensation problem for a racecar. It proposed an innovative solution based on DUIO theory and backstepping control. Despite the simplicity of the described linear state-input estimator, the proposed approach was shown to be able to quickly reconstruct even wind vector signals that are rich in frequency components, such as the ones generated via a Dryden gust model. Moreover, the backstepping-based controller could compensate for the effect of the wind and guarantee any desired convergence speed for the lateral pose error. The solution was validated via simulations with characteristics similar to those of the vehicles competing

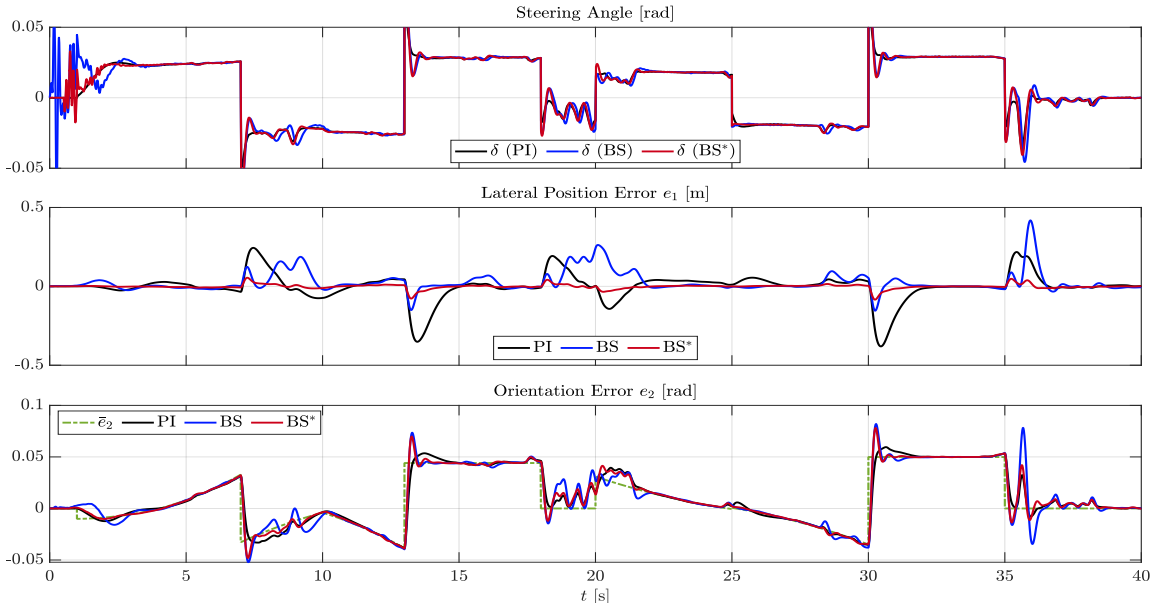


Figure 3.12: Controller's Performance with DUIO-based Closed-loop Estimation: The racecar is performing the same maneuver as in Fig. 3.11, while the estimates of the unknown wind signal $\hat{F} = (\hat{F}_w, \hat{\tau}_w)^T$ and state variables, obtained via the proposed DUIO, are used to determine the steering signal $\delta$ according to Th. 5 (first row); the second and third rows show how the commanded orientation error $e_{2,c}$ is accurately tracked by $e_2$ and the lateral error $e_1$ is kept close to zero. It is worth noticing that the proposed backstepping controller (BS*) has a faster rise time and smaller overshoot than the other two controllers (cf. the detail in the first-row plot), thereby achieving faster and more accurate tracking (second and third plots).

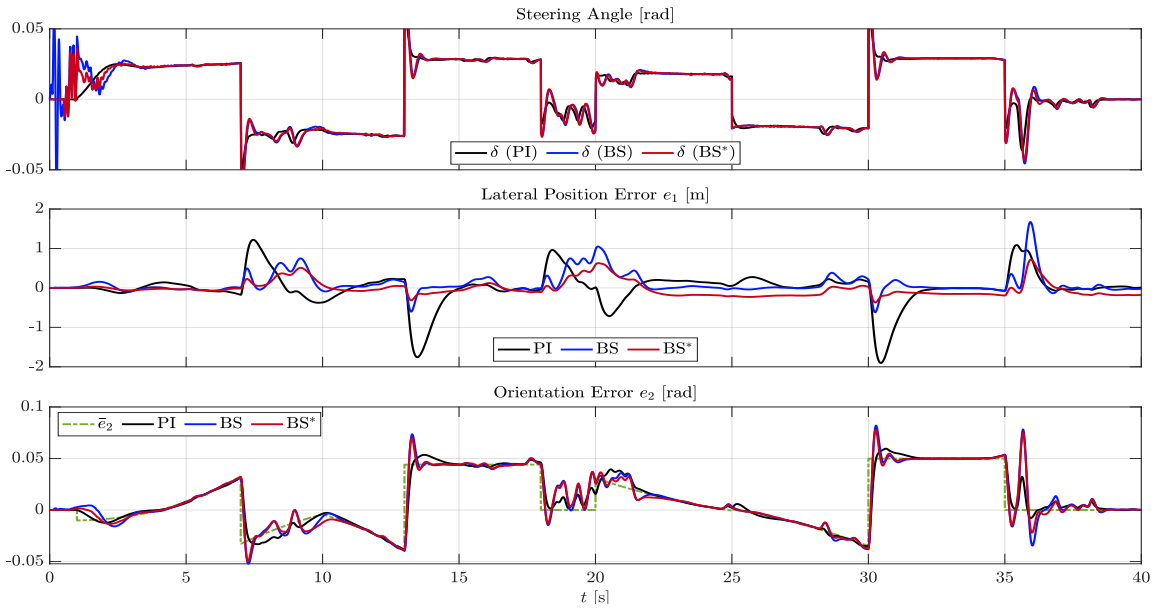


Figure 3.13: Controller's Performance with EKF-based Closed-loop Estimation: The racecar is performing the same maneuver as in Fig. 3.11, while the estimates of the unknown wind signal $\hat{F} = (\hat{F}_w, \hat{\tau}_w)^T$ and state variables are obtained via the EKF. It can observed that EKF-based controllers work worse than DUIO ones; moreover the proposed backstepping controller (BS$^*$) has better performance than the other two.

in the Roborace challenge. Results show that the proposed estimator outperforms an EKF, and the proposed backstepping controller compensates for the effect of the wind better. While the current work has focused on lateral wind gusts, future work will consider the entire system dynamics with winds coming from any direction.

## 3.4 Robust Discrete-time Lateral Control of Racecars by Unknown Input Observers

### 3.4.1 Introduction

This paragraph addresses the robust lateral control problem for self-driving racecars. It proposes a discrete-time estimation and control solution consisting of a delayed unknown input-state observer and a robust tracking controller. Based on a nominal vehicle model, describing its motion with respect to a generic desired trajectory and requiring no information about the surrounding environment, the observer reconstructs the total force disturbance signal, resulting from imperfect knowledge of the time-varying tire-road interface characteristics, presence of other vehicles nearby, wind gusts, and other model uncertainty. Then, the controller actively compensates the estimated force and asymptotically steers the tracking error to zero. It also presents a closed-loop stability proof of the method, ensuring perfect asymptotic estimation and tracking by the controlled vehicle. The proposed solution advantageously needs no a-priori information about the total disturbance boundedness, additional variables to model uncertainty, or observer parameters to be tuned. Its effectiveness and superiority to existing methods are studied in theory and shown in simulations where a full racecar model, based on the Vehicle Dynamics Blockset, is required to track aggressive maneuvers. Through a faster and more accurate disturbance estimation, the solution robustly ensures better dynamic responses even with measurement noise.

The contribution is at least fourfold. First, by starting from the so-called double-track system, a nominal model of the lateral racecar dynamics is derived, in a form where the input-disturbance and state estimation can be addressed by using DUIO theory; secondly, a robust control law is devised which uses state and disturbance estimates to ensure perfect asymptotic tracking of any desired trajectory, and the full state closed-loop asymptotic stability is formally proved with convergence speed guarantees; thirdly, the superiority of the proposed method to existing state-of-the-art solutions is shown; finally, the effectiveness, the robustness, and the real-time implementability of the proposed solution are tested by using the models of Matlab/Simulink's Vehicle Dynamics Blockset and a Raspberry PI 4 system.

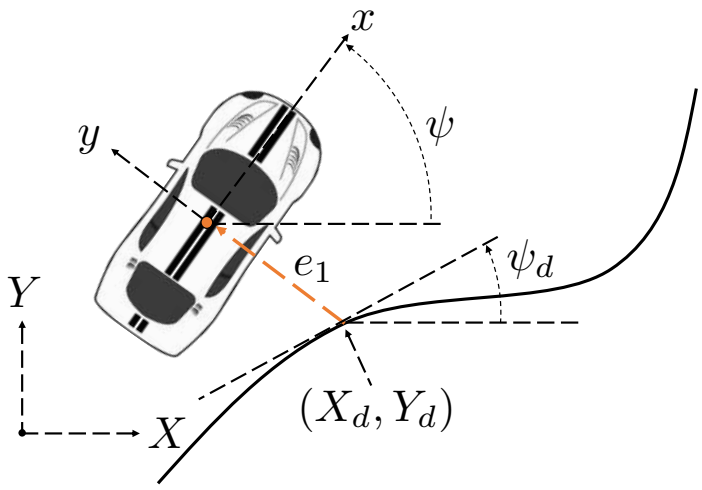


Figure 3.14: Depiction of the vehicle schematic, desired path, and coordinate frames.

### 3.4.2 Model Formalization

Consider a rear-wheel drive and front-steering racecar with mass $m$ and inertia $J$, moving along a flat horizontal road, i.e. with zero bank angle. The in-plane lateral dynamics of the vehicle can be described, in a non-inertial frame attached to it, by the double-track model [94] that reads

$$\begin{aligned} m\,(\ddot{y} + u\,\dot{\psi}) &= Y_1(\delta_v) + Y_2(\delta_v) + F_w\,, \\ J\,\ddot{\psi} &= a_1\,Y_1(\delta_v) + a_2\,Y_2(\delta_v) + \chi_w\,, \end{aligned} \tag{3.4.1}$$

where $y$ is its lateral position, $\psi$ is its heading angle, $a_1$ and $a_2$ are its wheelbases, $Y_1$ and $Y_2$ are the front and rear lateral forces applied at its center of mass, $\delta_v$ is the front steering angle and system input, $F_w$ and $\chi_w$ are the lateral wind force and moment, and $u$ is its longitudinal speed, which can be considered as a time-varying parameter, resulting from the control of its longitudinal dynamics. The lateral forces $Y_1$ and $Y_2$ can be decomposed as

$$\begin{aligned} Y_1 &= F_{y_{11}}(\delta_v)\cos\left(\delta_{11}(\delta_v)\right) + F_{y_{12}}(\delta_v)\cos\left(\delta_{12}(\delta_v)\right)\,, \\ Y_2 &= F_{y_{21}} + F_{y_{22}}\,, \end{aligned}$$

where $F_{y_{ij}}$ are the front ($i = 1$) and rear ($i = 2$) forces applied at the left ($j = 1$) and right ($j = 2$) tires, respectively, and are nonlinear functions of the front wheel steer angles $\delta_{1j}$. Moreover,

refer to Fig. 3.14 and assume that a GPS sensor is used to measure the $(X, Y)$ coordinates of the vehicle center of mass in an Inertial frame. Given the $(X_d, Y_d)$ coordinates of a point on a desired trajectory to be tracked, with a curvature radius $R$, if the vehicle is required to track such trajectory and, simultaneously, vanish its lateral position $y$, while moving at a longitudinal speed $u$, a lateral position error $e_1$ can be introduced as the projection of the error vector $(X, Y)^T - (X_d, Y_d)^T$ along the lateral direction unit vector $(-\sin\psi, \cos\psi)^T$, i.e. $e_1 = (Y - Y_d)\cos\psi - (X - X_d)\sin\psi$. Indicating with $a_{y_d} = u^2/R = u\,\dot{\psi}_d$ an approximated desired lateral acceleration in body frame, the corresponding lateral acceleration error reads [94]:

$$\begin{aligned} \ddot{e}_1 &= a_y - a_{y_d} = \ddot{y} + u\,\dot{\psi} - a_{y_d} = \\ &= \tfrac{1}{m}\left(Y_1(\delta_v) + Y_2(\delta_v) + F_w\right) - a_{y_d}\,, \end{aligned} \tag{3.4.2}$$

where the actual lateral acceleration $a_y$ has being expanded as $a_y = \ddot{y} + \dot{\psi}\,u$ and the first equation in (3.4.1) has been used.

Furthermore, achieving precise and complete characterization of the nonlinear and possibly time-varying functions $Y_1$ and $Y_2$ requires ad-hoc identification procedures which also need to be repeated over time [94]. Beyond that, the wind force and moment signals are only predictable via statistical models and hence their actual values over time remain unknown. Therefore, it is convenient to obtain a nominal vehicle model based on quantities that can be easily identified. For this purpose, one recalls that the lateral forces at the tires depend on the respective wheel slip angles $\alpha_{ij}$, for $i, j = 1, 2$; such dependence can be approximated, for small $\alpha_{ij}$, as $F_{y_{ij}} = C_{ij}\,\alpha_{ij}$, where $C_{ij}$ are the tires' cornering stiffness coefficients, which are known with good accuracy. Moreover, the wheel slip angles can be expressed by the following formulas:

$$\begin{aligned} \alpha_{1j} &= \delta_{1j}(\delta_v) - \arctan\left((v + r\,a_1)/(u + (-1)^j r\,t_1/2)\right)\,, \\ \alpha_{2j} &= -\arctan\left((v - r\,a_2)/(u + (-1)^j r\,t_2/2)\right)\,, \end{aligned}$$

with $t_1$ and $t_2$ being the front and rear vehicle tracks, $v = \dot{y}$ and $r = \dot{\psi}$ are the lateral and yaw speeds. While the functions $\delta_{1j}(\delta_v)$ are highly nonlinear, for small values of their argument, the

following second-order Taylor expansions can be used [94]:

$$\delta_{1j}(\delta_v) = (-1)^j\,\delta_1^0 + \tau\,\delta_v + (-1)^{j-1}\,\tfrac{\beta t_1}{2l}\tau^2\,\delta_v^2 + \nu\ ,$$

with $\delta_1^0$, $l$, $\tau$, and $\beta$ being the static toe angle, the total wheelbase, the steering gear ratio, and the Ackermann coefficient, respectively, and $\nu$ the approximation error signal. In light of the above reasoning, the following nominal model can be assumed, involving only the nominal values of the vehicle mass $\bar{m}$, the cornering coefficient $\bar{C}_1 = \bar{C}_{11} + \bar{C}_{12}$, and the steering gear ratio $\bar{\tau}$:

$$\ddot{e}_1 = \left(\bar{C}_1\bar{\tau}/\bar{m}\right)\delta_v + w\,, \tag{3.4.3}$$

where $w$ is a disturbance signal lumping together the effects due to parameter and model uncertainties, and even exogenous unknown inputs. Moreover, given a sampling time $\lambda$ and a discrete time step $k$ and defined the sampled state vector and disturbance with $Z_k = (e_{1k}, \dot{e}_{1k})^T = (e_1(k\lambda), \dot{e}_1(k\lambda))^T$ and $w_k = w(k\lambda)$, respectively, the model in (3.4.3) can be discretized via Euler's method and finally written in state form as

$$\begin{aligned} Z_{k+1} &= A_k\,Z_k + B_k\,\delta_k + \Gamma_k\,w_k\,,\\ y_k &= C_k\,Z_k + D_k\,\delta_k + \Theta_k\,w_k\,, \end{aligned} \tag{3.4.4}$$

where $\delta_k = \delta_v(k\lambda)$ is the input sample signal, $y_k = y(k\lambda)$, and the involved matrices are

$$A_k = \begin{pmatrix} 1 & \lambda \\ 0 & 1 \end{pmatrix},\ B_k = \lambda \begin{pmatrix} 0 \\ \bar{C}_1\bar{\tau}/\bar{m} \end{pmatrix},\ \Gamma_k = \lambda \begin{pmatrix} 0 \\ 1 \end{pmatrix},$$
$$C_k = \begin{pmatrix} 1 & 0 \end{pmatrix},\ D_k = \Theta_k = 0\,.$$

It should be noted that, even though part of the expression of the disturbance $w$ is known, the discrete-time signal $w_k$ is assumed to be fully unknown.

### 3.4.3 DUIO-based Control for Lateral Vehicle Dynamics

In this paragraph the proposed DUIO-based control for the lateral vehicle dynamics is designed. First, a DUIO observer that is able to estimate both system state and disturbance is derived.

Finally, exploiting the information deriving from the observer a robust control is designed.

**Discrete-Time Unknown Input Observer Design**

Consider the racecar model in (3.4.4) with inputs given by the steering angle $\delta_k$ and the unknown disturbance $w_k$, generated by model deviations from the nominal behavior as well as external signals, and the output given by the lateral position error $e_k$. The following first main result can be proved:

**Theorem 6** (UIO Design)**.** *The discrete-time linear system described by the iterative rule*

$$\begin{aligned} \hat{Z}_{k-L+1} &= E\,\hat{Z}_{k-L} + F\,\mathbb{Y}_k^L - F\,\mathbb{H}^L\,\delta_k^L + B_k\,\delta_{k-L}, \\ \hat{w}_{k-L} &= G\begin{pmatrix} \hat{Z}_{k-L+1} - A_k\,\hat{Z}_{k-L} - B_k\,\delta_{k-L} \\ y_{k-L} - C_k\,\hat{Z}_{k-L} \end{pmatrix}, \end{aligned} \tag{3.4.5}$$

*where $\mathbb{H}^L$ is the invertibility matrix relating to the known input and where $\hat{Z}_{k-L} = (\hat{e}_{k-L}, \hat{\dot{e}}_{k-L})^T$, $\mathbb{Y}_k^L = (e_k, e_{k-1}, e_{k-2})^T$, $\delta_k^L = (\delta_k, \delta_{k-1}, \delta_{k-2})^T$ and*

$$\begin{gathered} E = \begin{pmatrix} \sigma_1 & 0 \\ 0 & \sigma_2 \end{pmatrix},\ F = \begin{pmatrix} -\sigma_1 & 1 & 0 \\ \frac{\sigma_2}{\lambda} & -\frac{1+\sigma_2}{\lambda} & \lambda \end{pmatrix}, \\ G = \begin{pmatrix} 0 & \frac{1}{\lambda} & 0 \end{pmatrix}, \end{gathered} \tag{3.4.6}$$

*with $\sigma_1$ and $\sigma_2$ being free constants such that $|\sigma_1|, |\sigma_2| < 1$, is a DUIO for the model in (3.4.4) with reconstruction delay $L = 2$. That is, the filter in (4.4.3) can asymptotically reconstruct the full system state $Z_{k-L} = (e_{k-L}, \dot{e}_{k-L})^T$ and the unknown disturbance $w_{k-L}$.*

*Proof.* The smallest integer satisfying Prop. 2 is $L = 2$, for which it holds $\text{rank}(\mathbb{V}^2) - \text{rank}(\mathbb{V}^1) = 1 = m$ since $\mathbb{V}^1 = 0_{2\times 2}$ and

$$\mathbb{V}^2 = \begin{pmatrix} \Theta_k & 0 & 0 \\ C_k\Gamma_k & \Theta_k & 0 \\ C_kA_k\Gamma_k & C_k\Gamma_k & \Theta_k \end{pmatrix} = \begin{pmatrix} 0 & 0 & 0 \\ 0 & 0 & 0 \\ \lambda^2 & 0 & 0 \end{pmatrix}.$$

Consequently, the output history can be chosen as $\mathbb{Y}_k^2 = (e_k, e_{k-1}, e_{k-2})^T$. Condition A1) in Prop. (1) implies that matrix $F$ belong to the left-nullspace of the last columns of matrix $\mathbb{V}^2$, which are given

by $P = \begin{pmatrix} 0_{2x2} \\ \mathbb{V}^1 \end{pmatrix}$. To determine $F$, consider first a matrix $\bar{N}$ whose rows form a basis for the left-nullspace of $\mathbb{V}^1$, so that $\begin{pmatrix} I_p & 0_{p\times 2} \\ 0_{2\times p} & \bar{N} \end{pmatrix}$ is a matrix whose rows form a basis for the left-nullspace of $P$. Constant $p$ equals the unity since the system output $e_k$ is scalar. Given the null value of $\mathbb{V}^1$, for this system, it suffices to choose $\bar{N} = I_{2x2}$. Furthermore, for any invertible matrix $W$, we can define a matrix $N = W \begin{pmatrix} 1 & 0_{1\times 2} \\ 0_{2\times 1} & \bar{N} \end{pmatrix} = W\, I_{3x3}$, whose rows also form a basis for the left nullspace of $P$. Therefore, given the one-step observability matrix (see Sec. 1), $\mathbb{O}^1 = \begin{pmatrix} C_k \\ C_k A_k \end{pmatrix} = \begin{pmatrix} 1 & 0 \\ 1 & \lambda \end{pmatrix}$, to find $W$, one can first note that $N \begin{pmatrix} \Theta_k & 0 \\ \mathbb{O}^1 \Gamma_k & \mathbb{V} \end{pmatrix} = W \begin{pmatrix} \Theta_k & 0 \\ \bar{N}\,\mathbb{O}^1 \Gamma_k & 0_{2\times 1} \end{pmatrix}$. Moreover, as Prop. 2 is satisfied for a delay $L = 2$, the first columns of $\mathbb{V}^2$ are linearly independent, which implies that the matrix $\begin{pmatrix} \Theta_k & 0 \\ \bar{N}\,\mathbb{O}^1 \Gamma_k & 0_{2\times 1} \end{pmatrix}$ have rank equal to the unity. Direct computation of the above matrix shows indeed that $\begin{pmatrix} \Theta_k & 0 \\ \bar{N}\,\mathbb{O}^1 \Gamma_k & 0_{2\times 1} \end{pmatrix} = \begin{pmatrix} 0 & 0 & \lambda^2 \\ 0 & 0 & 0 \end{pmatrix}^T$. Now, one can choose matrix $W$ so that the last rows form a left-inverse of the last above matrix, while the upper ones form a basis of its left-nullspace. A possible choice for $W$ is then $W = \mathrm{diag}(1, 1, 1/\lambda^2)$, which leads also to a matrix $N$ satisfying the expression

$$N\,\mathbb{V}^2 = \begin{pmatrix} 0 & 0 & 0 \\ 0 & 0 & 0 \\ 1 & 0 & 0 \end{pmatrix} .$$

This fact finally leads to derive that it holds $N = W$. Furthermore, based again on Condition A1, matrix $F$ can be factorized as $F = \bar{F}\, N$, with $\bar{F} = (\bar{F}_1, \bar{F}_2)$ and $\bar{F}_2$ being a vector. Explicitly writing Condition A1) yields

$$\begin{pmatrix} \bar{F}_1 & \bar{F}_2 \end{pmatrix} \begin{pmatrix} 0 & 0 & 1 \\ 0 & 0 & 0 \end{pmatrix}^T = \begin{pmatrix} \Gamma_k & 0_{2\times 1} & 0_{2\times 1} \end{pmatrix} = \begin{pmatrix} 0 & 0 & 0 \\ \lambda & 0 & 0 \end{pmatrix} ,$$

which allows obtaining the solution $\bar{F}_2 = \Gamma_k = (0, \lambda)^T$ and $\bar{F}_1$ a still free design matrix.

Moving now on to the satisfaction of Condition A2, we can directly obtain $E = A - F\,\mathbb{O}^2 = A - (\bar{F}_1, \Gamma_k)\,N\mathbb{O}^2$. Splitting the rows of the matrix $N\mathbb{O}^2$ on the right-hand side into two sub-matrices $S_1$ and $S_2$, that is

$$N\mathbb{O}^2 = \begin{pmatrix} 1 & 0 & 0 \\ 0 & 1 & 0 \\ 0 & 0 & 1/\lambda^2 \end{pmatrix} \begin{pmatrix} 1 & 0 \\ 1 & \lambda \\ 1 & 2\lambda \end{pmatrix} = \begin{pmatrix} 1 & 0 \\ 1 & \lambda \\ 1/\lambda^2 & 2/\lambda \end{pmatrix} = \begin{pmatrix} S_1 \\ S_2 \end{pmatrix}$$

with $S_1 = \begin{pmatrix} 1 & 0 \\ 1 & \lambda \end{pmatrix}$, $S_2 = \begin{pmatrix} 1/\lambda^2 & 2/\lambda \end{pmatrix}$, allows further expanding the expression of matrix $E$ as

$$E = A - \Gamma_k S_2 - \bar{F}_1 S_1 = \begin{pmatrix} 1 & \lambda \\ -1/\lambda & -1 \end{pmatrix} - \bar{F}_1 \begin{pmatrix} 1 & 0 \\ 1 & \lambda \end{pmatrix}.$$

To finally satisfy also Condition A3, one can impose matrix $E$ to be given by a Schur diagonal matrix as in (4.4.4). This condition can be attained by choosing the remaining part of matrix $F$ as $\bar{F}_1 = \begin{pmatrix} -\sigma_1 & 1 \\ \sigma_2/\lambda & -(1+\sigma_2)/\lambda \end{pmatrix}$. By the above choices, the solution of the dynamics for the estimation error $\tilde{e}_k = \hat{Z}_{k-L} - Z_{k-L}$ is

$$\tilde{e}_{k+1} = E\,\tilde{e}_k \tag{3.4.7}$$

which has a convergent behavior with a speed of convergence directly dependent on the free parameters $\sigma_1$ and $\sigma_2$.

Having guaranteed the convergence of the state estimation error, the unknown input disturbance $w_k$ can be retrieved as follows. First, (3.4.4) can be rearranged as

$$\begin{pmatrix} Z_{k-L+1} - A_k\,Z_{k-L} - B_k\,\delta_{k-L} \\ y_{k-L} - C\,Z_{k-L} - D_k\,\delta_{k-L} \end{pmatrix} = \begin{pmatrix} \Gamma_k \\ \Theta_k \end{pmatrix} w_{k-L} \tag{3.4.8}$$

and its both sides can be left-multiplied by the pseudo-inverse of $(\Gamma_k^T, \Theta_k^T)^T$, i.e. matrix $G$ in (4.4.4).

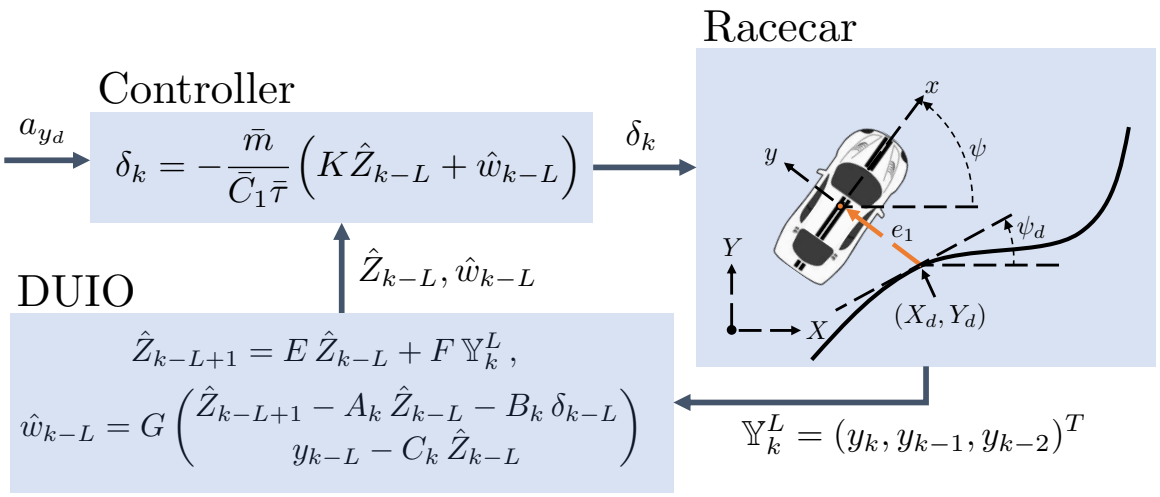


Figure 3.15: Schematic of the estimation and control strategy. The output $y_k = e_{1k}$ of the racecar is buffered in the output history vector $\mathbb{Y}_k$, which is used by the DUIO to estimate the racecar delayed state $Z_{k-L}$ and unknown input $w_{k-L}$; this information along with the desired acceleration $a_{y_d}$ are finally used by the controller to asymptotically steer the vehicle on the desired trajectory.

Doing so and then replacing the state with its estimate finally yields

$$\hat{w}_{k-L} = G \begin{pmatrix} \hat{Z}_{k-L+1} - A_k\, \hat{Z}_{k-L} - B_k\, \delta_{k-L} \\ y_{k-L} - C\, \hat{Z}_{k-L} - D_k\, \delta_{k-L} \end{pmatrix} \tag{3.4.9}$$

and it concludes the proof. □

**Robust Lateral Position Control**

As a second step, leveraging on the data reconstructed by the above designed DUIO, a robust lateral position controller for the steering angle input $\delta_k$ is derived, which ensures $e_k$'s convergence independently of all model uncertainty and external disturbance. This is formalized in the following second main result:

**Theorem 7.** *Given the dynamics of the racecar model in (3.4.4), the feedback steering angle control law*

$$\delta_k = -\frac{\bar{m}}{\bar{C}_1 \bar{\tau}} \left( K \hat{Z}_{k-L} + \hat{w}_{k-L} \right), \tag{3.4.10}$$

*where $\hat{Z}_{k-L}$ and $\hat{w}_{k-L}$ are the state and disturbance estimates from the DUIO in (4.4.3) and where*

*$K = (k_1, k_2)$ is a free control gain matrix, ensures robust and global asymptotic convergence of the state estimation error $\tilde{e}_k$ and robust and global uniform bounded stability of the racecar state $Z_k$ around the origin, with a bound decreasing at least linearly with the sampling time $\lambda$.*

*Proof.* The full dynamics of the racecar in (3.4.4) and the DUIO in (4.4.3) is

$$\begin{pmatrix} Z_{k+1} \\ \tilde{e}_{k+1} \end{pmatrix} = \begin{pmatrix} A_k & 0_{2x2} \\ 0_{2x2} & E \end{pmatrix} \begin{pmatrix} Z_k \\ \tilde{e}_k \end{pmatrix} + \begin{pmatrix} B_k\,\delta_k + \Gamma_k\,w_k \\ 0_{2x1} \end{pmatrix}, \tag{3.4.11}$$

in which the state estimation error dynamics is independent of the controlled input $\delta_k$ and the disturbance signal $w_k$ (cf. the last set of equations). This fact implies that the convergence of $\tilde{e}_k$ in the closed-loop system is again ensured by $E$ being Schur, and that, after convergence, $\hat{Z}_{k-L} \simeq Z_{k-L}$ and $\hat{w}_{k-L} \simeq w_{k-L}$. Consequently, the feedback law in (3.4.10) becomes $\delta_k \simeq -\bar{m}/(\bar{C}_1\bar{\tau})(KZ_{k-L} + w_{k-L})$. Hence, closing the loop on (4.5.4) with such a feedback law yields

$$\begin{pmatrix} Z_{k+1} \\ \tilde{e}_{k+1} \end{pmatrix} = \begin{pmatrix} A_k & 0_{2x2} \\ 0_{2x2} & E \end{pmatrix} \begin{pmatrix} Z_k \\ \tilde{e}_k \end{pmatrix} - \begin{pmatrix} B_v \\ 0_{2x1} \end{pmatrix} (KZ_{k-L} - \tilde{w}_k)\ , \tag{3.4.12}$$

where $B_v = \lambda\,(0,1)^T = \Gamma_k$ and $\tilde{w}_k = w_k - w_{k-L}$ is the disturbance estimation error. Using the factorization $A_k\,Z_k - B_vK\,Z_{k-L} + B_v\,\tilde{w}_k = (A_k - B_vK)\,Z_k + \phi_k$, with $\phi_k = B_v(K(Z_k - Z_{k-L}) + \tilde{w}_k)$ allows rewriting (3.4.12) as

$$\begin{pmatrix} Z_{k+1} \\ \tilde{e}_{k+1} \end{pmatrix} = A_c \begin{pmatrix} Z_k \\ \tilde{e}_k \end{pmatrix} + \begin{pmatrix} \mathbb{I}_{2\times2} \\ 0_{2x1} \end{pmatrix} \phi_k\,, \tag{3.4.13}$$

with

$$A_c = \begin{pmatrix} A_k - B_vK & -B_vK \\ 0_{2x2} & E \end{pmatrix} = \begin{pmatrix} 1 & \lambda & 0 & 0 \\ -\lambda k_1 & \gamma_1 & -\lambda k_1 & -\lambda k_2 \\ 0 & 0 & \sigma_1 & 0 \\ 0 & 0 & 0 & \sigma_2 \end{pmatrix},$$

and $\gamma_1 = 1 - \lambda k_2$. It should be first noticed that the free solution of (3.4.13) can be made convergent, by properly allocating the eigenvalues of $A_c$. In this respect, matrix $A_c$ is upper-block triangular

and hence the set of its eigenvalues comprises those of the DUIO, $\sigma_1$ and $\sigma_2$, and those of $A_k - B_v K$. The controllability matrix of the pair $(A_k, B_v)$ is $\mathcal{R} = (B_v | A_k B_v) = \begin{pmatrix} 0 & \lambda^2 \\ \lambda & \lambda \end{pmatrix}$ and has full rank, which ensures the existence of a matrix $K$ so that $A_k - B_v K$ has all eigenvalues within the unit circle and then generates asymptotically stable modes only. Furthermore, recall from [66] that for a small enough sampling time $\lambda$, it holds, for consecutive samples, $\hat{Z}_k \simeq \hat{Z}_{k-1}$ and $w_k \simeq w_{k-1}$ or equivalently,

$$||Z_k - Z_{k-1}||_2 < p_Z(\lambda)\,,\ ||w_k - w_{k-1}||_2 < p_w(\lambda)\,, \tag{3.4.14}$$

with $p_Z, p_w \in \mathbb{R}^+$ diminishing with the decrease of $\lambda$ and where $||\cdot||_2$ is the Euclidean norm. From the property in (3.4.14), derived from [66], it also follows $\delta_k \simeq \delta_{k-1} \simeq \delta_{k-L}$, which solves the algebraic dependence of $w_k$ from $\delta_k$. Analogously, it holds $y_k \simeq y_{k-1} \simeq y_{k-L}$. Moreover, recalling that $L = 2$, the term $\phi_k$ can be rewritten as $\phi_k = K(Z_k - Z_{k-1}) + K(Z_{k-1} - Z_{k-2}) + w_k - w_{k-1} + w_{k-1} - w_{k-2}$, and thus can be upper bounded as follows:

$$\begin{aligned} ||\phi_k||_2 \leq\ & ||B_v||_2\,||K||_2\,||Z_k - Z_{k-1}||_2 + \\ & + ||B_v||_2\,||K||_2\,||Z_{k-1} - Z_{k-2}||_2 + \\ & + ||w_k - w_{k-1}||_2 + ||w_{k-1} - w_{k-2}||_2\ = \\ & = \lambda\,(2\,||K||_2\,p_Z(\lambda) + 2\,p_w(\lambda))\ . \end{aligned}$$

From the first set of equations in (3.4.13), we have

$$\begin{aligned} ||Z_{k+1}|| \leq\ & ||A_c Z_k|| + ||\phi_k|| \leq \\ & \leq ||A_c Z_k|| + \lambda\,(2\,||K||_2\,p_Z(\lambda) + 2\,p_w(\lambda))\ . \end{aligned}$$

Since $A_c$ is Schur, the first addend in the equation above is contracting, i.e. $||A_c Z_k|| < ||Z_k||$ and hence, after a transient, the norm of the racecar state is only excited by the forcing term $\phi_k$ which decreases at least linearly with the decrease of $\lambda$.

Furthermore, as for the convergence of disturbance estimation error, $\tilde{w}_k$, from its definition, one

can write

$$\tilde{w}_k = G \begin{pmatrix} Z_{k+1} - A_k\, Z_k - B_k\, \delta_k \\ y_k - C\, Z_k - D\, \delta_k \end{pmatrix} + \\ - G \begin{pmatrix} \hat{Z}_{k-L+1} - A_k\, \hat{Z}_{k-L} - B_k\, \delta_{k-L} \\ y_{k-L} - C\, \hat{Z}_{k-L} - D\, \delta_{k-L} \end{pmatrix},$$

which, after having defined the signals $\nu_k = \hat{Z}_{k-L} - Z_k$, $\eta_k = \delta_{k-L} - \delta_k$, and $\xi_k = y_{k-L} - y_k$, becomes finally

$$\tilde{w}_k = G \begin{pmatrix} A_k\, \nu_k + B_k\, \eta_k - \nu_{k+1} \\ C\, \nu_k - \xi_k \end{pmatrix}. \tag{3.4.15}$$

Again under the hypothesis of [66] for small delays, the signals $\nu_k$, $\eta_k$, and $\xi_k$ are bounded, i.e. there exist constant upper-bounds, $S, V, T \in \mathbb{R}^+$, such that $||\nu_k||_2 \leq S$, $||\eta_k||_2 \leq V$, and $||\xi_k||_2 \leq T$, for all $k$, and also convergent due to (3.4.14), i.e. for increasing values of $k$ the upper bounds can be chosen as $S, V, T \to 0$. As a consequence, from (3.4.15), one can obtain

$$\begin{aligned} ||\tilde{w}_k||_2^2 &\leq ||G||_2^2 \left|\left| \begin{matrix} A_k\nu_k + B_k\eta_k - \nu_{k+1} \\ C\hat{\nu}_k - \xi_k \end{matrix} \right|\right|_2^2 \\ &\leq G_2^2 \left(||A_k\nu_k + B_k\eta_k - \nu_{k+1}||_2 + ||C\nu_k - \xi_k||_2\right)^2 \\ &\leq G_2^2 \left(||A_k||_2 S + ||B_k||_2 V + S + ||C||_2 S + T\right)^2 \\ &\leq G_2^2 \left((\rho_A + 2)S + (\lambda \bar{C}_1 \bar{\tau}/\bar{m})V + T)\right)^2 \end{aligned}$$

with $G_2 = 1/\lambda$ and $\rho_A = \sqrt{\rho(A_k^T A_k)}$, where $\rho(\cdot)$ indicates the spectral radius of a matrix. Therefore, the fact that $S, V, T \to 0$ also implies $||\tilde{w}_k||_2 \to 0$ and, in turn, $\tilde{w}_k \to 0$. Hence, the disturbance estimation error $\tilde{w}_k$ asymptotically converges to zero with the same speed of the state estimation error $\tilde{e}_k$, which is specified by the free constants $\sigma_1$ and $\sigma_2$ of the DUIO. This concludes the proof. □

Therefore, the DUIO-based control observes the system state and inputs at the time-step $k - L$, reconstructs the unknown disturbance $\hat{w}_{k-L}$, and finally determines the control action for the time step $k$ steering the closed-loop system in (4.5.4) and allowing the sought asymptotic convergence to

Table 3.4: Nominal Inertial and Geometric Parameters of a Robocar from the Roborace Challenge [95]

| | | |
|---|---|---|
| Total Front cornering stiffness | $C_1$ | $2.26 \cdot 10^5$ N/rad |
| Total Rear cornering stiffness | $C_2$ | $2.82 \cdot 10^5$ N/rad |
| Front wheelbase | $a_1$ | 1.510 m |
| Rear wheelbase | $a_2$ | 1.288 m |
| Front track | $t_1$ | 1.714 m |
| Rear track | $t_2$ | 1.692 m |
| Vehicle mass | $\bar{m}$ | 1350 Kg |
| Vehicle Inertia | $\bar{J}_z$ | 1150 Kg $\cdot$ m$^2$ |
| Steering gear ratio | $\tau$ | 1/10 |

Table 3.5: Magic Formula's coefficients for typical road conditions

| Surface Type | B | C | D | E |
|---|---|---|---|---|
| Dry tarmac | 10 | 1.9 | 1 | 0.97 |
| Wet tarmac | 12 | 2.3 | 0.82 | 1 |
| Snow | 5 | 2 | 0.3 | 1 |

zero.

### 3.4.4 Simulation and Validation

The correctness and robustness of the proposed method are shown in this paragraph, along with a comparison of its effectiveness for a benchmark using a standard disturbance rejection technique.

**Simulation Modeling** To show the effectiveness and robustness of the proposed method, the implementation of a real Robocar model is used by using the Vehicle Dynamics Blockset of the Matlab/Simulink environment. The geometric and inertial parameters of the vehicle are listed in Table 3.4.

The interaction with the road surface is modeled by generating all lateral wheel forces, $F_{yij}$, via the nonlinear Pacejka tire model, the so-called the Magic Formula [96], i.e. $F_{yij} = F_{zij}\,\mu_{ij}$, with

$$\mu_{ij} = D \sin(C \arctan(B\alpha_{ij} - E(B\alpha_{ij} - \arctan(B\alpha_{ij})))) \,, \tag{3.4.16}$$

where $B$, $C$, $D$, and $E$ are dimensionless coefficients whose values depend on the road surface (cf. Table 3.5) for the typical values, also used here, to represent dry, wet, snow, and icy surfaces,

and where are the vertical forces applied at each wheel. These last forces are given by

$$F_{z1j} = (m/2l)(g\,a_2 - a_x\,h) + (-1)^j \Delta Z_1\,,$$
$$F_{z2j} = (m/2l)(g\,a_1 + a_x\,h) + (-1)^j \Delta Z_2\,,$$

for $j = 1, 2$, where $g$ is the gravity acceleration, $h$ is the height of the vehicle center of gravity with respect to the road and $a_x$ is the vehicle's longitudinal acceleration in body frame, and $Z_i$ are the lateral load transfers due to the suspensions, which are given by

$$\Delta Z_1 = (d_1/t_1 l)(Y\,a_2 + N) + (k_{\phi_1}/k_\phi)(h - d)Y\,,$$
$$\Delta Z_2 = (d_2/t_1 l)(Y\,a_1 - N) + (k_{\phi_2}/k_\phi)(h - d)Y\,,$$

where $l$ is the vehicle wheelbase, $d_1$ and $d_2$ are the front and rear no-roll center height, $k_\phi = k_{\phi_1} + k_{\phi_2}$, with $k_{\phi_1}$ and $k_{\phi_2}$ being the front and rear suspension roll stiffness, respectively, and finally $d = (a_2 d_1 + a_1 d_2)/l$, $Y = Y_1 + Y_2$, $N = Y_1 a_1 - Y_2 a_2$. It should be noted that the roll and suspension effects on vehicle dynamics are taken into account via the lateral load transfers described above. Numerical values for the front and rear no-roll center height are $d_1 = 0.025m$ and $d_2 = 0.045m$, respectively, with $k_{\phi_1} = 21740.6\frac{N}{rad}$ and $k_{\phi_2} = 22322.2\frac{N}{rad}$.

Moreover, the wind force signal is obtained by modeling the wind speed $u_w$ according to the stochastic Dryden model [97]. Specifically, the wind speed signal $u_w(t)$ is chosen to replicate turbulence at low altitudes, characterized by a height from the sea level of $h = 6$ m, an airspeed of $V = 50$ m/s, and a turbulence level of $W_{2_0} = 15$ kn. Moreover, to generate the wind moment signal, the lever arm $x_w$ of the wind force is assumed to be a stochastic process with uniform distribution over the length of the vehicle, i.e. $-a_2 \leq x_w \leq a_1$. Accordingly, the wind force $F_w$ and wind moment $\chi_w$ are obtained via the expressions

$$F_w = \tfrac{1}{2}\rho\,S\,C_y\,u_w^2\,,\quad \chi_w = F_w\,x_w\,,$$

where $\rho = 1.225$ Kg/m$^3$ is the air density at sea level, $S = 2$ m$^2$ the so-called vehicle's lateral wetted area, $C_y = 1.5$ its lateral aerodynamic coefficient. Overall, the second equation of the lateral dynamics in 3.4.1 becomes $J\,\ddot{\psi} = a_1\,Y_1(\delta_v) + a_2\,Y_2(\delta_v) + \chi_w + N_x$, where $N_x = \Delta X_1\,t_1 + \Delta X_2\,t_2$,

with $\Delta X_1 = \frac{1}{2}(F_{y11}\sin\delta_{11} - F_{y12}\sin\delta_{12})$ and $\Delta X_2 = \frac{1}{2}(F_{x22} - F_{x21})$, respectively.

**Derivation of the DESO-based Benchmark**

The following benchmark based on the well-established theory described in [50] has been developed to compare the performance of our method with a *de-facto* standard disturbance rejection technique. It consists of a discrete-time implementation of the system obtained by the application of such method, according to which an Active Disturbance Rejection Controller (ADRC), based on an Extended State Observer (ESO), can be obtained as follows. First, consider an augmented state $\epsilon_k = (Z_k^T, w_k)^T$, including as an additional variable the disturbance $w_k$ for which a dynamics must also be introduced. Assuming, as for our method, that only lateral position error measures, $y_{\epsilon_k} = e_k$, are available, a Discrete-time ESO (DESO) is described by the iterative rule

$$\hat{\epsilon}_{k+1} = A_\epsilon \hat{\epsilon}_k + B_\epsilon \delta_k + L\left(y_{\epsilon_k} - C_\epsilon \hat{\epsilon}_k\right), \tag{3.4.17}$$

with

$$A_\epsilon = \begin{pmatrix} 1 & \lambda & 0 \\ 0 & 1 & \lambda \\ 0 & 0 & 1 \end{pmatrix},\ B_\epsilon = \lambda \begin{pmatrix} 0 \\ \bar{C}_1\bar{\tau}/\bar{m} \\ 0 \end{pmatrix},\ C_\epsilon = \begin{pmatrix} 1 & 0 & 0 \end{pmatrix},$$

where $L \in \mathbb{R}^3$ is such that the closed-loop dynamic matrix $A_{\tilde{\epsilon}} = A_\epsilon - LC_\epsilon$ is Schur, ensures the asymptotic boundedness of the augmented state estimation error $\tilde{\epsilon}_k = \hat{\epsilon}_k - \epsilon_k$, if, and only if, the following conditions are met: 1) $(A_k, C_k)$ is fully observable; 2) $w_k$ evolves as in $w_{k+1} = w_k + \lambda\,\kappa(\epsilon_k, w_k, k)$, where $\kappa(\epsilon_k, w_k, k)$ is a time-varying bounded function, i.e. $\exists\, M > 0$ s.t. $|\kappa(\epsilon_k, w_k, k)| \leq M\ \forall k$. As a second step, once an estimate $\hat{\epsilon}_k = (\hat{Z}_k^T, \hat{w}_k)^T$ of the augmented state $\epsilon_k$ is retrieved via the DESO in (3.4.17), the steering control law

$$\delta_k = -\frac{\bar{m}}{\bar{C}_1\bar{\tau}}\left(K\hat{Z}_k + \hat{w}_k\right), \tag{3.4.18}$$

with $K = (k_1, k_2)$ a free control gain, ensures the bounded stability of the full system

$$\begin{pmatrix} Z_{k+1} \\ \tilde{\epsilon}_{k+1} \end{pmatrix} = \begin{pmatrix} A_k & 0_{2x3} \\ 0_{3x3} & A_{\tilde{\epsilon}} \end{pmatrix} \begin{pmatrix} Z_k \\ \tilde{\epsilon}_k \end{pmatrix} + \begin{pmatrix} B_k \\ 0_{3x1} \end{pmatrix} \delta_k + \\ - W_\epsilon \, \kappa(\epsilon_k, w_k, k) \, , \tag{3.4.19}$$

with $W_\epsilon = \lambda \, (0_{1\times 4}, 1)^T$, if, and only if, the signal $\kappa(\epsilon_k, w_k, k)$ is bounded. The convergence proof straightforwardly follows from standard arguments typical of the ADRC technique, but it is omitted here for the sake of space.

Finally, to obtain comparable behaviors for the proposed DUIO-based approach and the DESO-based one, the respective free control gains have been chosen so that the eigenvalues of the closed-loop matrix in (4.5.4) and that of (3.4.19) closed in the loop with (3.4.18) are in the similar locations. More specifically, without loss of generality, the speed of convergence of the lateral tracking errors has been tuned, via the control gain $K$, so that the eigenvalues of $A_k - B_v K$ are in $p_1 = (0.1, -0.1)$; simultaneously, the speed of convergence of the observers has been chosen to be ten times faster. In the DUIO case, this is obtained by placing the eigenvalues in $p_2 = (-0.01, 0.01)$ (and hence choosing $\sigma_1 = -0.01$ and $\sigma_2 = 0.01$) and, for the DESO, this is obtained by placing the eigenvalues in $p_3 = (-0.01, -0.01, 0.01)$ (and hence choosing $l_1$, $l_2$, and $l_3$ accordingly).

**Simulation and Testing with Vehicle Dynamics Blockset and Raspberry PI board**

The testing and validation scenario is reported in Fig. 3.16. The Robocar system is required to track a trajectory with a time-varying longitudinal speed $u(t)$ and curvature radius signal $\rho(t)$, under the presence of sudden wind gusts. The longitudinal speed profile reproduces a typical telemetry profile with acceleration and braking phases [6]; the time-varying road friction is modeled via appropriate variation of the Magic-Formula coefficients.

The goal of the testing is at least fourfold. First, it aims at showing the effectiveness of the proposed method as well as its robustness to unmodeled dynamics, parameter uncertainty, and measurement noise. For this purpose, the Robocar system is implemented as a double-track racecar by using the Vehicle Body 3-DoF block of Vehicle Dynamic Blockset in Matlab/Simulink. Nominal values for the vehicle mass $\bar{m}$ with a maximum variation of 45% from the real value are used in

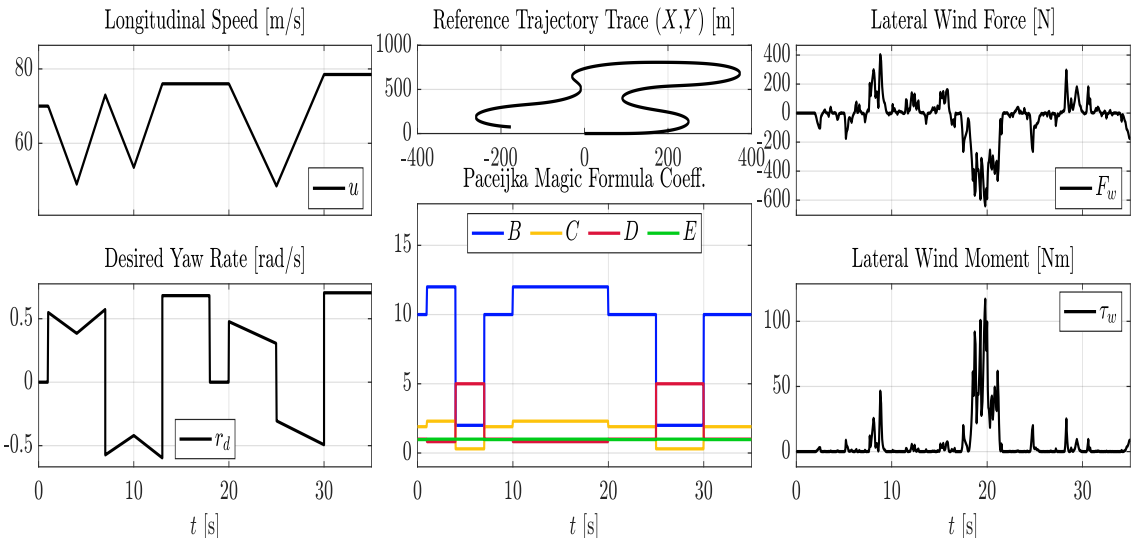


Figure 3.16: Simulation scenario designed to test and assess the effectiveness and performance of the proposed methods. The longitudinal speed profile has alternating phases of acceleration and deceleration, and two plateau phases at quasi-constant velocities. The road surface ranges from dry, wet, and snow, while also highly-varying wind gust force and moment have to be handled.

the numerical implementation of the estimators and controllers. Measurement noise is also added to the system outputs via the Matlab/Simulink Random Source block, which generates pseudo-random Gaussian distributions. Secondly, the testing aims at comparing the proposed approach with the above-described benchmark. Thirdly, it aims at proving the real-time implementability of the solution and assessing the required computation time in terms of the CPU utilization, through a low-cost hardware setup, consisting of a Raspberry PI 4 Model B system. To achieve this, the proposed DUIO-based solution and the DESO-based benchmark are compiled for the Raspberry PI hardware, via the Simulink Real-time Code Generation, and built as standalone applications. The inclusion of both control methods represents a further computational load of the micro-controller, leading to an overestimate of the required CPU utilization and a further guarantee of the solution implementability. Finally, the testing intends to show if, all the above-mentioned properties, are maintained even when enlarging sampling time. For this reason, the scheduling times of the involved processes are chosen as $\lambda = 10^{-3}$ seconds and later as $\lambda = 10^{-2}$ seconds.

Fig. 3.17 and 3.18 report the results of the testing with $\bar{m}/m = 1.45$ and with scheduling times

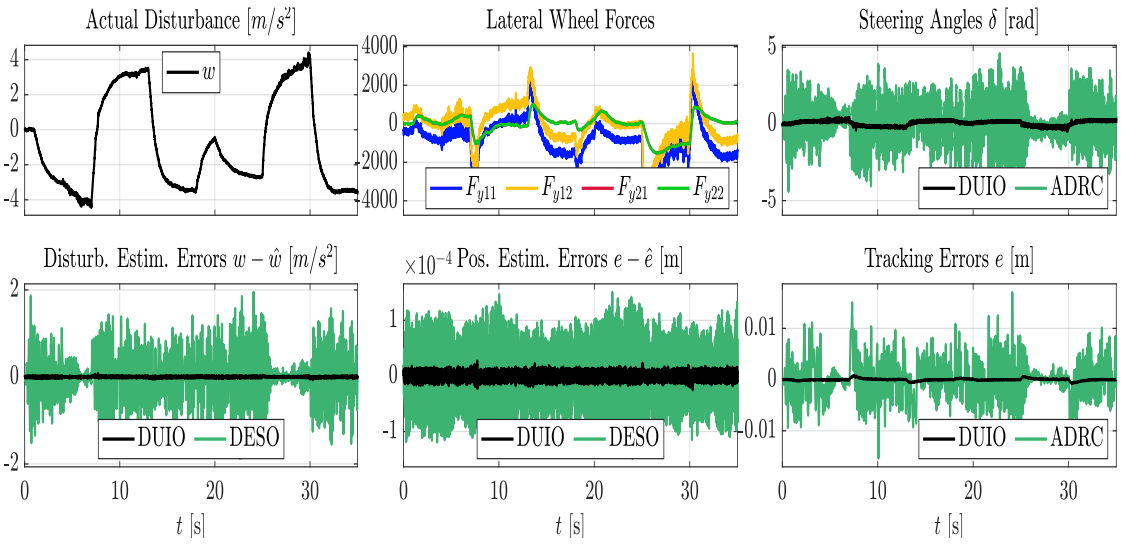


Figure 3.17: Raspberry PI 4 Testing with $\lambda = 10^{-3}$: Results with noisy measures and a nominal mass $\bar{m}/m = 1.45$. The DUIO always estimate better estimates the state and the disturbance, at least of an order of magnitude. The resulting control signal is also much less affected by the noise, better copes with the disturbance, and achieves improved tracking performance.

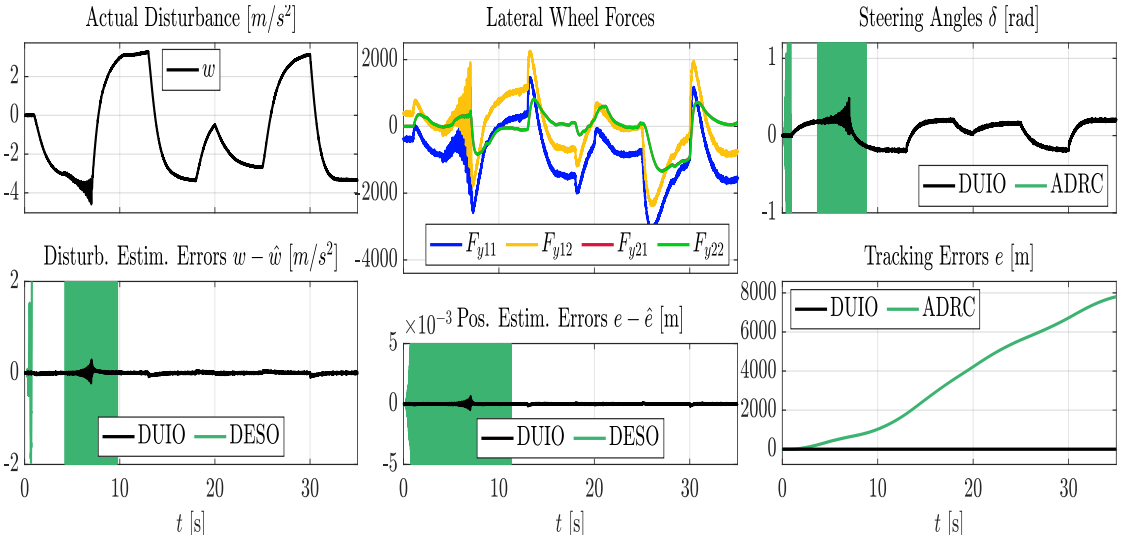


Figure 3.18: Raspberry PI 4 Testing with $\lambda = 10^{-2}$ the DESO-based benchmark is unable to correctly estimate and cope with the disturbance, which leads the system to instability (see the diverging green line of the tracking error). On the contrary, our proposed DUIO-based solution allows still a nice transient behavior and maintains stability.

Table 3.6: ITAE index comparison for DUIO and DESO based approaches, respectively, with sampling time $\lambda = 10^{-3}$.

| Method | ITAE($e_{1k}$) | ITAE($\hat{w}_k$) |
|---|---|---|
| DUIO | 0.0791 | 5.523 |
| DESO | 2.031 | 294.8 |

of $\lambda = 10^{-3}$ and $\lambda = 10^{-2}$, respectively. More precisely, Fig. 3.17 shows the DUIO always better estimates the state and the disturbance, at least by an order of magnitude. The resulting control is also much less affected by the noise and can better cope with the disturbance. Numerically speaking, the Integral Time Absolute Error (ITAE) index computed on the tracking error and the disturbance estimation error shows a clear superiority of the DUIO-based solution over the benchmark one (cf. Table 3.4.4). The total CPU utilization, during the testing, for the two estimation and control processes is always less than 12.7% with a mean value of about 6.9%. Finally, Fig. 3.18 shows that when the scheduling time is increased to $\lambda = 10^{-2}$ seconds, the DESO-based benchmark is unable to correctly estimate and cope with the disturbance, which leads the system to instability (see the diverging green line of the tracking error). On the contrary, our proposed DUIO-based solution allows still a nice transient behavior and maintains stability.

### 3.4.5 Conclusion

A robust lateral controller for self-driving racecars was proposed using a delayed unknown input-state observer. It showed robustness to time-varying tire-road interface characteristics, wind gusts, and model uncertainty. Its closed-loop asymptotic stability was proven and its performance was compared to that of a disturbance estimation and rejection technique, for which only asymptotic boundedness was obtained. The solution requires no a-priori knowledge of the boundedness or the statistical properties of the system and measurement noises. Testing results confirmed the superior performance of the DUIO over a DESO, as expected from the literature [98]. Simulations further highlighted its superiority by showing that the DUIO-based control generates smoother control signals for the steering angle, leading to smaller and less spiky tracking errors than those of the ADRC methodology.

# Chapter 4

# Articulated Soft Robots

## 4.1 Introduction

Endowed with intrinsic flexibility, Articulated Soft Robots (ASR) can reach competitive skills, such as adaptation to unstructured environment [99], effective energy storage and release [100], and stable interaction with static environment [101], that are typical of biomechanical systems. To fully match the skills of vertebrates, a class of articulated soft robots with Variable Stiffness Actuation (VSA) technology has been developed, capable of modifying robot joint stiffness with time [102]. The potential capacity to regulate simultaneously, and in a decoupled manner, joint position and stiffness [103–105], empowers them with even more dynamic manipulation capabilities, allowing them to perform tasks that involve for example throwing and catching [106] of objects, that were not attainable by rigid robots just a few decades ago.

Being biologically inspired and of a less complex mechanical design compared to other VSAs, agonistic-antagonistic VSAs are often applied technology in ASR systems [107]. However, the gained advantage of a simpler mechanical design is traded-off with the need for a more elaborated controller that can allow decoupled position and stiffness regulation. Moreover, the agonistic-antagonistic actuators introduce nonlinearities into the model since a nonlinear force-deformation dependency is needed to achieve a time-varying stiffness [108], while the existence of elastic tendons introduces hysteresis and additional nonlinearities since tendons change their characteristic over time due to

wear-off and working temperature, or even break [109].

To tackle the challenge of controlling an ASR, the first line of research consists of model-based approaches, which leverage on precise knowledge of either the full robot dynamics or the actuator's model. Relevant examples of the first setting are the ones obtained by feedback linearization [103], gain-scheduling control [110], and backstepping control [111], while adaptive control [105] and control based on damping injection [112] have been used in the latter one. A second, also very promising, line of research is model-free and involves techniques that aim at iteratively learning the position or torque control of an ASR, by using the minimum knowledge about the system while preserving its compliance through a feedforward control component [104, 113], yet without guaranteeing stability. Moreover, compared to the state feedback control in [114] this work avoids using torque sensors. In this context, this thesis proposes a DUIO-based robust control that ensures the performance even under lack of system knowledge or presence of strong external disturbance. More precisely, habe been considered arbitrary values of the parameters that construct the robot's inertia matrix, chosen under the constraint that the inertia matrix is non-singular. The proposed solution allows to estimate and compensate the model's uncertainties after only a few samples, compared to the dozen iterations needed for learning-based approaches. Compared to other existing solutions such as Extended State Observers (ESO), DUIOs do not lean on assumptions on the disturbance dynamics and its boundedness, require no parameter tuning, have exact convergence guarantees, and outperform them [98] despite their simplicity. Moreover, the controllers' robustness to the robot and actuator model uncertainties facilitates its application and avoids the necessity for extensive a-priori model identification.

## 4.2 Soft Robot Background

The structure of an articulated soft robot with $n$ links and $n$ flexible joints, driven by electromechanical VSA devices, is illustrated in Fig. 4.1. The actuation of the $i$-th robot joint is obtained as the result of mechanical deflections of elastic elements within each VSA, which are generated by internal pairs of electric motors. Such pairs are arranged in so-called agonistic-antagonistic configuration so as to enable simultaneous setting of the link position and joint stiffness. Indicating with $q_i$ the $i$-th

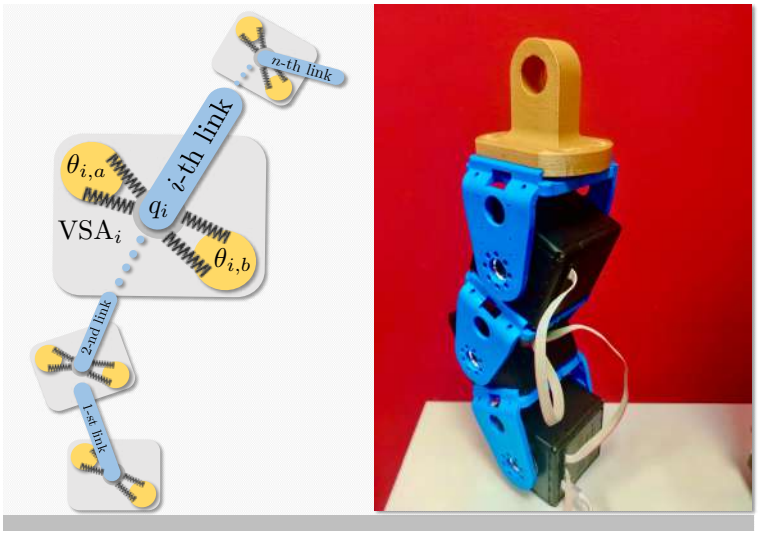


Figure 4.1: Depiction of an *articulated soft robot* with $n$ rigid links and $n$ flexible joints driven by electromechanical VSA devices (left) and picture of the 3-degree-of-freedom hardware setup used to validate the proposed solution (right).

link position and with $\theta_{i,a}$ and $\theta_{i,b}$ the internal motor positions of the $i$-th VSA device, the $i$-th pair of deflections are

$$\phi_{i,a} = q_i - \theta_{i,a}\,, \quad \phi_{i,b} = q_i - \theta_{i,b}\,, \tag{4.2.1}$$

and produce an agonistic elastic torque $\tau^e_{i,a}(\phi_{i,a})$ and an antagonistic elastic torque $\tau^e_{i,b}(\phi_{i,b})$, that are simultaneously applied at the $i$-th link. The total elastic torque applied at the $i$-th link is then

$$\tau^e_i = \tau^e_{i,a}(\phi_{i,a}) + \tau^e_{i,b}(\phi_{i,b})\,. \tag{4.2.2}$$

Defining the robot configuration vector $q = (q_1, \cdots, q_n)^T$, the motor position vectors and elastic torque vectors, $\theta_j = (\theta_{1,j}, \cdots, \theta_{n,j})^T$ and $\tau^e_j = (\tau^e_{1,j}, \cdots, \tau^e_{n,j})^T$, for $j = a, b$, respectively, and the total elastic torque vector $\tau^e = \tau^e_a + \tau^e_b$, the robot's dynamic model, including the link position dynamics and those of the motors within the VSA devices, is given by [108]:

$$\begin{aligned} M(q)\,\ddot{q} + h(q,\dot{q}) + \tau^e(\phi_a, \phi_b) &= \tau_{\text{ext}}\,, \\ J_a\,\ddot{\theta}_a + \Delta_a\,\dot{\theta}_a - \tau^e_a(\phi_a) &= \tau_a\,, \\ J_b\,\ddot{\theta}_b + \Delta_b\,\dot{\theta}_b - \tau^e_b(\phi_b) &= \tau_b\,. \end{aligned} \tag{4.2.3}$$

where $M \in \mathbb{R}^{n\times n}$ is the robot's inertia matrix, $h(q,\dot{q}) \in \mathbb{R}^n$ is a vector field collecting the centrifugal, Coriolis, and gravity terms, $\tau_{\text{ext}} \in \mathbb{R}^n$ is an externally applied torque vector, $J_a$ and $J_b$ are the motors' inertia, $\Delta_a$ and $\Delta_b$ are damping coefficients, and $\tau_a$ and $\tau_b$ are the electrically-induced motor torques. Accordingly, the $i$-th joint stiffness is given by definition

$$\sigma_i = \tfrac{\partial}{\partial \phi_{i,a}} \tau^e_{i,a}(\phi_{i,a}) + \tfrac{\partial}{\partial \phi_{i,b}} \tau^e_{i,b}(\phi_{i,b})\,, \tag{4.2.4}$$

and the joint stiffness matrix is $\sigma = \text{diag}(\sigma_1, \cdots, \sigma_n)$.

## 4.3 Compound Configuration Dynamics of ASR - Factorization and Decomposition

The purpose of this section is twofold: first, to describe a convenient and general way to factorize the actuation-related terms, in the position and stiffness dynamics of an articulated soft robot, with respect to a generic basis of functions; then, to introduce a general decomposition of the obtained model as an arbitrarily simple yet invertible nominal dynamics, affected by uncertain input signals.

### 4.3.1 Actuation Model Factorization

Virtually all VSA devices are provided with an integrated and fast control loop allowing a practically instantaneous regulation of the actuation motors. Based on this, the agonistic and antagonistic motor positions, indicated in our model by the vectors $\theta_a$ and $\theta_b$, can be viewed as input variables for the robot dynamics. As a result, the robot model in (4.2.3) can be restricted to the link equation only:

$$M(q)\,\ddot{q} + h(q,\dot{q}) + \tau^e(\phi_a,\phi_b) = \tau_{\text{ext}}\,, \tag{4.3.1}$$

where $\phi_j = (\phi_{1,j}, \cdots, \phi_{n,j})^T$, for $j = a, b$, with each $\phi_{i,j} = q_i - \theta_{i,j}$ is the $j$-th deflection at the $i$-th joint.

Assuming that all VSA devices in the robot are homogeneous, i.e. they are made of similar copies of the same agonistic/antagonistic actuation mechanism, the entries of the elastic torque vectors $\tau^e_a$

and $\tau_b^e$ can be expressed as combinations of suitable basis functions, $\{y_1, \cdots, y_p\}$, of the $(i,j)$-th pair of deflection variables $\phi_{i,j}$ (cf. e.g. the basis choice in [115]), i.e.

$$\tau_{i,a}^e = \sum_{k=1}^p \alpha_{i,k}\, y_k(\phi_{i,a})\,,\ \tau_{i,b}^e = \sum_{k=1}^p \beta_{i,k}\, y_k(\phi_{i,b})\,,$$

for $i = 1, \cdots, n$, with $\alpha_{i,k}$ and $\beta_{i,k}$ being the coefficients of the combinations. Note that since the functions $y_k$ belong to a basis, they can be assumed to be linearly independent. From (4.2.2) and considering the separability of the elastic torque factors, the total elastic torque vector $\tau^e$ can be factorized as in the following:

$$\tau^e = \begin{pmatrix} \tau_{1,a}^e(\phi_{1,a}) + \tau_{1,b}^e(\phi_{1,b}) \\ \vdots \\ \tau_{n,a}^e(\phi_{n,a}) + \tau_{n,b}^e(\phi_{n,b}) \end{pmatrix} = \Pi\, \Gamma(\phi_1, \phi_2)\,,$$

with

$$\Pi = \mathrm{diag}(\Pi_1, \cdots, \Pi_n) \in \mathbb{R}^{n \times 2np}\,,$$
$$\Gamma = (\gamma_1(\phi_{1,a}, \phi_{1,b})^T, \cdots, \gamma_n(\phi_{n,a}, \phi_{n,b})^T)^T \in \mathbb{R}^{2np}\,,$$

and each

$$\Pi_i = (\alpha_{i,1}, \cdots, \alpha_{i,p}, \beta_{i,1}, \cdots, \beta_{i,p}) \in \mathbb{R}^{1 \times 2p}\,,$$
$$\gamma_i = (y_1(\phi_{i,a}), \cdots, y_p(\phi_{i,a}), y_1(\phi_{i,b}), \cdots, y_p(\phi_{i,b}))^T \in \mathbb{R}^{2p}\,.$$

Moreover, to attain a similar decomposition for the dynamic behavior of the joint stiffness matrix $\sigma$ and, in parallel, avoid using link and motor speed data, it is algebraically convenient to adopt the time-integral $S_i$ of the total $i$-th joint stiffness $\sigma_i$, i.e. $S_i = \int_0^t \sigma_i(\tau) d\tau$, as a state variable. Then, its time derivative is $\dot{S}_i = \sigma_i$, which, by virtue of (4.2.4), is the sum of two addends depending on the $i$-th agonistic and antagonistic deflections, respectively. Hence, such a derivative can be expressed via the same basis functions used above, i.e.

$$\dot{S}_i = \sigma_i = \sum_{k=1}^p (\mu_{i,k}\, y_k(\phi_{i,a}) + \nu_{i,k}\, y_k(\phi_{i,b}))\,,$$

where $\mu_{i,k}$ and $\nu_{i,k}$ are suitable coefficients. Accordingly, one can write $\dot{S} = \Sigma\, \Gamma(\phi_1, \phi_2)$, with

$\Sigma = \text{diag}(\Sigma_1, \cdots, \Sigma_n) \in \mathbb{R}^{n \times 2np}$ and each

$$\Sigma_i = (\mu_{i,1}, \cdots, \mu_{i,p}, \nu_{i,1}, \cdots, \nu_{i,p}) \in \mathbb{R}^{1 \times 2p}\,.$$

Finally, putting all together, the dynamics of the *compound* configuration vector $(q^T, S^T)^T$ can be written in the following form with actuation factorization:

$$\begin{aligned} M(q)\,\ddot{q} + h(q, \dot{q}) &= \tau_{\text{ext}} - \Pi\,\Gamma(\phi_a, \phi_b)\,, \\ \dot{S} &= \Sigma\,\Gamma(\phi_a, \phi_b)\,, \end{aligned} \tag{4.3.2}$$

where the basis functions used to decompose the total elastic torque and its partial derivative operate as input functions.

### 4.3.2 Nominal and Uncertain Model Decomposition

The dynamics in (4.3.2) includes functions that may be uncertain or even unknown, i.e. the inertia matrix $M(q)$, the functions appearing in $h(q, \dot{q})$, the coefficients of $\Pi$ and $\Sigma$ in the actuation-related terms, and the external torque $\tau_{\text{ext}}$ are only partially known. Under this hypothesis, we seek for a convenient decomposition of (4.3.2) separating a minimal yet exactly known dynamics from the remainder uncertain one.

To this purpose, it can be assumed, without loss of generality, that $M(q)^{-1}$ can be expanded as the sum of an *invertible* known matrix $\bar{M}(q)^{-1}$ and a remainder uncertain one $\Delta M(q)^{-1}$. In addition, as the basis functions used to factorize the actuation-related terms can be freely chosen, they are available and, thus, the only uncertainty affects the values of the involved coefficients $\Pi$ and $\Sigma$. Finally, no assumptions on the separability of known and unknown terms in $h(q, \dot{q})$ are made. In summary, it holds:

$$\begin{aligned} M(q)^{-1} &= \bar{M}(q)^{-1} + \Delta M(q)^{-1}\,, \\ \Pi = \bar{\Pi} + \Delta\Pi\,,&\quad \Sigma = \bar{\Sigma} + \Delta\Sigma\,, \end{aligned} \tag{4.3.3}$$

with $\bar{\Pi}$ and $\bar{\Sigma}$ being nominal known values and $\Delta\Pi$ and $\Delta\Sigma$ the uncertain ones. Having stated the previous assumptions, one can left-multiply the first equation of (4.3.2) by $M(q)^{-1}$ and, using (4.3.3),

obtain

$$\begin{aligned}
\ddot{q} &= M(q)^{-1}\left(\tau_{\text{ext}} - h\left(q,\dot{q}\right)\right) - M(q)^{-1}\,\Pi\,\Gamma(\phi_a,\phi_b) = \\
&= \left(\bar{M}(q)^{-1} + \Delta M(q)^{-1}\right)\left(\tau_{\text{ext}} - h(q,\dot{q})\right) \;\; + \\
&- \left(\bar{M}(q)^{-1} + \Delta M(q)^{-1}\right)\Delta\Pi\;\Gamma(\phi_a,\phi_b) \;\; + \\
&- \Delta M^{-1}(q)\;\bar{\Pi}\;\Gamma(\phi_a,\phi_b) - \bar{M}^{-1}(q)\;\bar{\Pi}\;\Gamma(\phi_a,\phi_b) \;\; , \\
\dot{S} &= \bar{\Sigma}\;\Gamma(\phi_a,\phi_b) + \Delta\Sigma\;\Gamma(\phi_a,\phi_b)\,.
\end{aligned}$$

As a next step, one can separate the terms that are fully known from the remaining ones that can be lumped together into a vector signal $w = (w_q^T, w_S^T)^T$, which will be considered as unknown disturbance. Specifically, defining

$$\begin{aligned}
w_q &= M(q)^{-1}\left(\tau_{\text{ext}} - h(q,\dot{q})\right) \;\; + \\
&\quad - \left(M(q)^{-1}\Delta\Pi + \Delta M(q)^{-1}\;\bar{\Pi}\right)\Gamma(\phi_a,\phi_b)\,, \\
w_S &= \Delta\Sigma\;\Gamma(\phi_a,\phi_b)\,,
\end{aligned}$$

where matrix $M(q)^{-1}$ has been recombined where possible for compactness, leads to the sought nominal model with explicit unknown input disturbance:

$$\begin{aligned}
\ddot{q} &= -\bar{M}(q)^{-1}\;\bar{\Pi}\;\Gamma(\phi_a,\phi_b) + w_q\,, \\
\dot{S} &= \bar{\Sigma}\;\Gamma(\phi_a,\phi_b) + w_S\,.
\end{aligned} \tag{4.3.4}$$

**Remark 4.** *As shown later, the inertia inverse $\bar{M}(q)^{-1}$ can be chosen quite arbitrarily, provided that it is invertible, thereby avoiding information loss on the right hand-side of* (4.3.1)*. Accordingly, to make the synthesis of a linear input-state observer feasible, as done in the next section, $\bar{M}(q)^{-1}$ is further assumed to be constant, i.e. $\bar{M}(q)^{-1} = \bar{M}^{-1}$. The remainder part of the inertia inverse is then $\Delta M(q)^{-1} = M(q)^{-1} - \bar{M}^{-1}$.*

## 4.4 Input-State Observer Design for ASR

The second step of our strategy is to dynamically reconstruct the unknown signal $w$ (or better its discrete-time version), acting in (4.3.4), so as to enable its subsequent compensation by a suitable robust controller later derived. Leveraging on the model reformulation described in the previous

section, $w$ can be estimated by a linear unknown input-state observer using a nominal state form of such model.

To this aim, given a sampling period $T$ and a discrete time $k$, let the compound configuration vector be the system output, i.e. $Y = (q^T, S^T)^T \in \mathbb{R}^{2n}$, the output of the robust controller be the system (manipulable) input, i.e. $U = \Gamma(\phi_a, \phi_b) \in \mathbb{R}^{2np}$, and $w = (w_q^T, w_S^T)^T \in \mathbb{R}^{2n}$ be an unknown disturbance (note that no link speed data is used); defining the state vector $X = (q^T, \dot{q}^T, S^T)^T$ , (4.3.4) is written as $\dot{X} = A_c X + B_c U + W_c w$, with $A_c = \begin{pmatrix} 0_n & \mathbb{I}_n & 0_n \\ 0_{2n\times n} & 0_{2n\times n} & 0_{2n\times n} \end{pmatrix}$ , $B_c = (0_{np\times n}, -(\bar{M}^{-1}\,\bar{\Pi})^T, \bar{\Sigma}^T)^T$, $W_c = (0_{n\times 2n}^T, \mathbb{I}_{2n})^T$. Assuming $U$ and $w$ be constant between two consecutive discrete times and using the approach in [116] and the fact that $A_c$ is nilpotent of order 2, i.e. $A_c^k = 0$ for $k \geq 2$, it is straightforward to obtain the linear discrete-time state form

$$X_{k+1} = A\,X_k + B\,U_k + W\,w_k\,, \quad Y_k = C\,X_k\,, \tag{4.4.1}$$

where $X_k = X(kT)$, $Y_k = Y(kT)$, $U_k = U(kT)$, and $w_k = w(kT)$ and where

$$\begin{aligned} A = e^{A_c T} = \mathbb{I}_{3n} + T A_c = \begin{pmatrix} \mathbb{I}_n & T\,\mathbb{I}_n & 0_n \\ 0_n & \mathbb{I}_n & 0_n \\ 0_n & 0_n & \mathbb{I}_n \end{pmatrix}, C = \begin{pmatrix} \mathbb{I}_n & 0_n & 0_n \\ 0_n & 0_n & \mathbb{I}_n \end{pmatrix} \\ B = J\,B_c = \begin{pmatrix} 0_{n\times np} \\ -T\bar{M}^{-1}\,\bar{\Pi} \\ T\bar{\Sigma} \end{pmatrix}, W = J\,W_c = \begin{pmatrix} 0_{n\times 2n} \\ T\,\mathbb{I}_{2n} \end{pmatrix}, \end{aligned} \tag{4.4.2}$$

being $J = A_c^{-1}(e^{A_c T} - \mathbb{I}_{3n}) = T$.

Now, indicating with $\hat{X}_k = (\hat{q}(kT)^T, \dot{\hat{q}}(kT)^T, \hat{S}(kT)^T)^T$ an estimate of $X_k$, with $\hat{w}_k$ an estimate of $w_k$, with $\mathbb{Y}_k = (Y_{k-2}^T, Y_{k-1}^T, Y_k^T)^T$ the output history vector of the latest 3 values of $Y_k$, and with $\{\lambda_1, \cdots, \lambda_{3n}\}$ a set of constants that can be freely chosen within the unit circle of the complex plane, the linearity of (4.4.1) allows designing the following delayed estimator:

**Theorem 8** (DUIO Design for ASR)**.** *Given the reformulated model of an articulated soft robot described in* (4.4.1)*, with matrices A, B, and C as in* (4.4.2)*, a* 2*-sample delayed state estimate* $\hat{X}_{k-2}$

*can be computed via the iterative rule*

$$\hat{X}_{k-2+1} = E\,\hat{X}_{k-2} + B\,U_{k-2} + F\,(\mathbb{Y}_k + \mathbb{N}_k)\,, \tag{4.4.3}$$

*in which*

$$E = diag(\lambda_1, \cdots, \lambda_{3n})\,,$$
$$F = \left(\begin{array}{c|c|c|c|c|c} F_1 - \mathbb{I}_n & \frac{1}{T}\mathbb{I}_n & 0_n & 0_n & 0_n & 0_n \\ \hline -F_1 - \frac{1}{T}\mathbb{I}_n & \mathbb{I}_n & \frac{1}{T}F_3 & 0_n & \frac{1}{T}\mathbb{I}_n & 0_n \\ \hline \frac{1}{T}\mathbb{I}_n & F_2 + \mathbb{I}_n & 0_n & \mathbb{I}_n & 0_n & 0_n \end{array}\right) \tag{4.4.4}$$

*with* $F_1 = diag(\lambda_1, \cdots, \lambda_n)$, $F_2 = diag(\lambda_{n+1}, \cdots, \lambda_{2n})$, $F_3 = diag(\lambda_{2n+1}, \cdots, \lambda_{3n})$, *and in which*

$$\mathbb{N}_k = (0_{2n}, (N_1 U_{k-2})^T, (N_2 U_{k-2} + N_1 U_{k-1})^T)^T\,, \tag{4.4.5}$$

*with* $N_1 = \begin{pmatrix} 0_{n\times np} \\ -T\,\bar{\Sigma} \end{pmatrix}$ *and* $N_2 = \begin{pmatrix} T^2 \bar{M}^{-1}\,\bar{\Pi} \\ -T\,\bar{\Sigma} \end{pmatrix}$. *Moreover, given* $G = (0_{2n\times n}, \frac{1}{T}\,\mathbb{I}_{2n}, 0_{2n})$, *a 2-sample delayed input estimate* $\hat{w}_{k-2}$ *can be computed via the formula*

$$\hat{w}_{k-2} = G \begin{pmatrix} \hat{X}_{k-1} - A\,\hat{X}_{k-2} - B\,U_{k-2} \\ Y_k - C\hat{X}_{k-2} \end{pmatrix}. \tag{4.4.6}$$

*Proof.* The DUIO derivation can be achieved within the framework of delayed input-state observers (cf. e.g. Sec. 2.1), which can be done through the following three steps.

*1) Existence.* Recalling the results presented in chapter (2), the existence of the observer with a suitable delay $L$ is ensured if, and only if, the compound state dynamics in (4.4.1) is strongly observable with respect to all initial conditions and invertible with respect to the unknown input $w_k$ when the system output is $Y_k$. Referring to the conditions in prop. (2-3), the system dynamics has a null direct matrix, $D = 0_{2n}$, multiplying $w_k$, and hence the first three invertibility matrices in the

sequence are

$$\mathbb{V}_0 = 0_{2n}\,,\;\; \mathbb{V}_1 = \left(\begin{array}{cc|c} 0_{2n} & & 0_{2n} \\ \hline 0_n & 0_n & \multirow{2}{*}{$0_{2n}$} \\ 0_n & T\mathbb{I}_n & \end{array}\right)\,,$$

$$\mathbb{V}_2 = \begin{pmatrix} 0_{2n} & 0_{2n} & 0_{2n} \\ CW & 0_{2n} & 0_{2n} \\ CAW & CW & 0_{2n} \end{pmatrix} = \left(\begin{array}{cc|cc|c} 0_{2n} & & 0_{2n} & & 0_{2n} \\ \hline 0_n & 0_n & \multirow{2}{*}{$0_{2n}$} & & \multirow{2}{*}{$0_{2n}$} \\ 0_n & T\mathbb{I}_n & & & \\ \hline T^2\mathbb{I}_n & 0_n & 0_n & 0_n & \multirow{2}{*}{$0_{2n}$} \\ 0_n & T\mathbb{I}_n & 0_n & T\mathbb{I}_n & \end{array}\right)\,.$$

Given that the dimension of the unknown input $w_k$ is $m = 2n$ and that $\text{rank}(\mathbb{V}_0) = 0$, $\text{rank}(\mathbb{V}_1) = n$ and $\text{rank}(\mathbb{V}_2) = 3n$, the conditions in (2-3) are first satisfied with $L = 2$, which is the (minimum) delay of the observer.

*2a) State Estimation – Convergence Conditions.* Knowing that the required delay is $L = 2$, one can define the output history vector $\mathbb{Y}_k = (Y_{k-2}^T, Y_{k-1}^T, Y_k^T)^T$ — comprising the latest $L + 1 = 3$ output samples and being the one in the theorem statement — and assume a state estimate update rule as in (4.4.3), where $E$ and $F$ are matrices to be suitably chosen and where $\mathbb{N}_k$ is still a free vector. As the observer is meant to provide, at any step $k$, an estimate of the past compound state $X_{k-2}$, the current state estimation error can be defined as $e_k = \hat{X}_{k-2} - X_{k-2}$. Shifting backward in time of 2 steps the robot dynamics in (4.4.1) yields

$$X_{k-2+1} = A\,X_{k-2} + B\,U_{k-2} + W\,w_{k-2}\,,$$

which allows, along with the assumed observer's update rule, deriving the following state estimation error dynamics:

$$\begin{aligned} e_{k+1} &= \hat{X}_{k-2+1} - X_{k-2+1} = \\ &= E\,\hat{X}_{k-2} - A\,X_{k-2} + F\,\mathbb{Y}'_k - W\,w_{k-2} = \\ &= E\,e_k + (E - A)\,X_{k-2} + F\,\mathbb{Y}'_k - W\,w_{k-2}\,, \end{aligned} \tag{4.4.7}$$

where the addend $E\,X_{k-2}$ has been added and subtracted in the last line of (4.4.7), and where $\mathbb{Y}'_k = \mathbb{Y}_k + \mathbb{N}_k$.

Now, the observer's convergence must be guaranteed for all delayed states $X_{k-2}$ and all behaviors of the delayed unknown input $w_{k-2}$, and hence (4.4.7) should be made independent of them. A possible dynamics that has the desired convergence property and that is algebraically compliant with (4.4.7) is $e_{k+1} = E\, e_k$ with $E$ a Schur matrix. By comparing the two expressions one gets the condition

$$(E - A)\, X_{k-2} + F\, \mathbb{Y}'_k - W\, w_{k-2} = 0\,. \tag{4.4.8}$$

To remove the explicit dependency of this expression on the output history vector $\mathbb{Y}_k$, its entries can be expanded in terms of the delayed state $X_{k-2}$ and the latest unknown input samples $w_{k-2}$, $w_{k-1}$, and $w_k$. This leads to the three formulas:

$$\begin{aligned} Y_{k-2} &= C\, X_{k-2}\,, \\ Y_{k-1} &= CA\, X_{k-2} + CB\, U_{k-2} + CW\, w_{k-2}\,, \\ Y_k &= CA^2\, X_{k-2} + CAB\, U_{k-2} + CB\, U_{k-1} + \\ &\quad + CAW\, w_{k-2} + CW\, w_{k-1}\,, \end{aligned}$$

from which, after conveniently choosing matrix $\mathbb{N}_k$ as

$$\mathbb{N}_k = -\begin{pmatrix} 0_{2n} & 0_{2n} & 0_{2n} \\ CB & 0_{2n} & 0_{2n} \\ CAB & CB & 0_{2n} \end{pmatrix} \begin{pmatrix} U_{k-2} \\ U_{k-1} \\ U_k \end{pmatrix}\,,$$

whose direct computation leads to its expression in (4.4.5), with $N_1 = -CB$ and $N_2 = -CAB$, one can write

$$\begin{pmatrix} Y'_{k-2} \\ Y'_{k-1} \\ Y'_k \end{pmatrix} = \begin{pmatrix} C \\ CA \\ CA^2 \end{pmatrix} X_{k-2} + \begin{pmatrix} 0_{2n} & 0_{2n} & 0_{2n} \\ CW & 0_{2n} & 0_{2n} \\ CAW & CW & 0_{2n} \end{pmatrix} \begin{pmatrix} w_{k-2} \\ w_{k-1} \\ w_k \end{pmatrix}$$

or, in matrix form, $\mathbb{Y}'_k = \mathcal{O}_2\, X_{k-2} + \mathbb{V}_2\, \mathbb{W}_k$, where $\mathcal{O}_2$ is the 2-step observability matrix and $\mathbb{W}_k = \left(w_{k-2}^T, w_{k-1}^T, w_k^T\right)^T$. Consequently, (4.4.8) becomes

$$(E - A + F\mathcal{O}_2)\, X_{k-2} + (F\, \mathbb{H}_2 - (W, 0_{2n}, 0_{2n}))\, \mathbb{W}_k = 0\,.$$

Now, recalling the DUIO foundations theory, in order to satisfy this expression for every $X_{k-2}$ and $\mathbb{W}_k$, it must be that

$$E = A - F\mathcal{O}_2 \quad \text{and} \quad F\,\mathbb{V}_2 = (W, 0_{2n}, 0_{2n})\,. \tag{4.4.9}$$

*2b) State Estimation – Derivation of the Matrices.*

The second condition in (4.4.9) requires that $F$ is in the left-nullspace of the last $m$ columns of $\mathbb{V}_2$, that are $P = (0_{4n}, \mathbb{V}_1^T)^T$. Given a matrix $\bar{N}$ whose rows are a basis of the left-nullspace of $\mathbb{V}_1$, the rows of matrix $\mathrm{diag}(\mathbb{I}_{2n}, \bar{N})$ are a basis of the left-nullspace of $P$. Seeing the structure of $\mathbb{V}_1$, it suffices to choose $\bar{N} = (\mathbb{I}_{3n}, 0_{3n\times n})$. Moreover, given an invertible matrix $W^*$, we can define $N = W^*\mathrm{diag}(\mathbb{I}_{2n}, \bar{N})$, whose rows also form a basis of the left nullspace of $P$. Therefore, to find $W$, first note that $N \begin{pmatrix} 0_{2n} & 0_{2n\times 4n} \\ \mathcal{O}_1 W & \mathbb{V}_1 \end{pmatrix} = W^* \begin{pmatrix} 0_{2n} & 0_{2n} \\ \bar{N}\,\mathcal{O}_1\,W & 0_{2n} \end{pmatrix} = W^*\,V$, where $\mathcal{O}_1 = (C^T, (CA)^T)^T$. As the required delay is $L = 2$, the first $2n$ columns of $\mathbb{V}_2$ are linearly independent and hence $\mathrm{rank}(V) = 2n$. Matrix $W^*$ can be chosen so that its last $2n$ rows are a left-inverse of $V$, while the top ones are a basis of its left-nullspace. The choice

$$W^* = \left(\begin{array}{c|cc} \multicolumn{3}{c}{\mathbb{I}_{3n} \qquad\qquad 0_{3n\times 2n}} \\ \hline & 0_n & \mathbb{I}_n/T^2 \\ 0_{2n\times 3n} & & \\ & \frac{1}{T}\,\mathbb{I}_n & 0_n \end{array}\right),$$

leads to a matrix $N$ satisfying the expression $N\,\mathbb{V}_2 = \begin{pmatrix} 0_{2n} & 0_{2n} \\ \mathbb{I}_{2n} & 0_{2n} \end{pmatrix}$ and then $N = W^*$. Based again on the structure of (4.4.9) and the columns of $W$, $F$ can be factorized as $F = F^*N$, with $F^* = (F_1^*, F_2^*)$, so that (4.4.9) itself can be written as $(F_1^*, F_2^*) \begin{pmatrix} 0_{2n} & 0_{2n} \\ \mathbb{I}_{2n} & 0_{2n} \end{pmatrix} = (W, 0_{3n\times 2n})$, from which it follows $F_2^* = W$, while $F_1^*$ is still free. Plugging $F$ into the first condition in (4.4.9) yields $E = A - (F_1^*, W)\,N\mathcal{O}_2 = A - (F_1^*, W)(R^T, Q^T)^T$, with

$$R = \begin{pmatrix} \mathbb{I}_n & 0_n & 0_n \\ 0_n & 0_n & \mathbb{I}_n \\ \mathbb{I}_n & T\mathbb{I}_n & 0_n \end{pmatrix}, \quad Q = \begin{pmatrix} \frac{1}{T^2}\mathbb{I}_n & \frac{2}{T}\mathbb{I}_n & 0_n \\ 0_n & 0_n & \frac{1}{T}\mathbb{I}_n \end{pmatrix},$$

and then

$$E = A - WQ - F_1^* R = \\ = \begin{pmatrix} 0_n & \mathbb{I}_n & 0_n \\ -\frac{1}{T^2}\mathbb{I}_n & -\frac{2}{T}\mathbb{I}_n & 0_n \\ 0_n & 0_n & -\frac{1}{T}\mathbb{I}_n \end{pmatrix} - F_1^* \begin{pmatrix} \mathbb{I}_n & 0_n & 0_n \\ 0_n & 0_n & \mathbb{I}_n \\ \mathbb{I}_n & T\mathbb{I}_n & 0_n \end{pmatrix} .$$

To finally ensure that $E$ is Schur and diagonal as in (4.4.4), it suffices to choose $F_1^* = (A - WQ - \text{diag}(\lambda_1, \cdots, \lambda_{3n}))R$, which also leads to $F$'s expression in (4.4.4).

*3) Unknown Input Reconstruction.* Finally, an estimate, that is optimal in the least square sense, of the delayed unknown input $w_{k-2}$ can be retrieved from the conditions:

$$\hat{X}_{k-2+1} - X_{k-2+1} = \hat{X}_{k-2+1} - AX_{k-2} - B\,U_{k-2} - Ww_{k-2}\,, \\ \hat{Y}_{k-2} - Y_{k-2} = C\hat{X}_{k-2} - Y_{k-2}\,.$$

Once the delayed state estimate $\hat{X}_{k-2}$ has converged to $X_{k-2}$, the right hand-sides of these equations converge to zero; then the remaining expressions can be rearranges as follows:

$$\begin{pmatrix} W \\ 0_{2n} \end{pmatrix} w_{k-2} = \begin{pmatrix} \hat{X}_{k-2+1} - AX_{k-2} - B\,U_{k-2} \\ Y_{k-2} - C\hat{X}_{k-2} \end{pmatrix} .$$

Left-multiplying both sides of this equation by a matrix $G = (W^T W)^{-1}(W^T, 0_{2n})$, whose computation leads to the formula in theorem's statement, allows obtaining the sought (4.4.6), which concludes the proof. □

## 4.5 Robust Control and Closed-loop Stability

Given desired trajectories, $q_d(t)$ and $\sigma_d(t)$, for the compound configuration, define the desired state signal samples $X_{d,k} = (q_d(kT)^T, \dot{q}_d(kT)^T, S_d(kT)^T)^T$, with $S_d(t) = \int_0^t \sigma_d(\tau)d\tau$. Then, using the information retrieved by the DUIO, the following can be found:

**Theorem 9.** *Given an articulated soft robot as in* (4.3.1)*, the feedback-feedforward control law*

$$U_k = K(\hat{X}_{k-2} - X_{d,k}) + P(X_{d,k+1} - A\,X_{d,k} - W\,\hat{w}_{k-2})\,, \tag{4.5.1}$$

*where* $\hat{X}_{k-2}$ *and* $\hat{w}_{k-2}$ *are found using* (4.4.3) *and* (4.4.6)*,* $P = (B^T B)^{-1} B^T$*, and* $K$ *is such that* $A+BK$ *is Schur, ensures global and robust bounded stability for the tracking error of desired position and stiffness trajectories,* $q_d(t)$ *and* $\sigma_d(t)$*.*

*Proof.* The dynamics of the discrete-time tracking error, $Z_k = X_k - X_{d,k}$, reads

$$\begin{aligned} Z_{k+1} &= AX_k + BU_k + Ww_k - X_{d,k+1} = \\ &= AZ_k + BU_k - X_{d,k+1} + AX_{d,k} + Ww_k\,. \end{aligned} \tag{4.5.2}$$

A desired convergent dynamics for the state vector is $Z_{k+1} = A^*\,Z_k$, with $A^* = A + B\,K$, where $K \in \mathbb{R}^{2np\times 3n}$ is a free gain matrix that can be chosen to make matrix $A^*$ Schur. Comparing such desired expression with (4.5.2) yields the condition $BU_k = BKZ_k + X_{d,k+1} - AX_{d,k} - Ww_k$. In practice, as only the estimates of $X_k$ and $w_k$ are available with 2-sample delays, the following best-effort condition can be ensured:

$$BU_k = BK\hat{Z}_k + X_{d,k+1} - AX_{d,k} - W\hat{w}_{k-2}\,, \tag{4.5.3}$$

with $\hat{Z}_k = \hat{X}_{k-2} - X_{d,k}$. The overall closed-loop dynamics, including the tracking error dynamics in (4.5.2) and the estimation error $e_k$ from Theorem 8 reads

$$\begin{pmatrix} Z_{k+1} \\ e_{k+1} \end{pmatrix} = \begin{pmatrix} A^* & 0_{3n} \\ 0_{3n} & E \end{pmatrix} \begin{pmatrix} Z_k \\ e_k \end{pmatrix} + \begin{pmatrix} \varphi_k \\ 0_{3n} \end{pmatrix}\,, \tag{4.5.4}$$

with $\varphi_k = BK(\hat{Z}_k - Z_k) + W\tilde{w}_k$ and $\tilde{w}_k = w_k - \hat{w}_{k-2}$. It can be seen, as expected by its design, that the dynamics of the estimation error $e_k$ is independent of $U_k$ and $w_k$, and hence its closed-loop convergence is ensured by $E$ being Schur. That being so, after a transient in the observer estimates, $\hat{X}_{k-2} \simeq X_{k-2}$ and $\hat{w}_{k-2} \simeq w_{k-2}$. Moreover, considering the small delay $L = 2$ [66] and assuming a small enough sampling period $T$, it also holds $\hat{X}_{k-2} \simeq X_k$, $U_{k-2} \simeq U_k$, $w_{k-2} \simeq w_k$,

$Y_{k-2} \simeq Y_k$. As a result, $\hat{Z}_k \simeq Z_k$ and $\tilde{w}_k \simeq w_k - \hat{w}_k \simeq 0$ and the forcing term $\varphi_k$ in the closed-loop dynamics vanishes, i.e. $\varphi_k$ tends to zero. More precisely, it can be shown that $\hat{Z}_{k-1} - Z_{k-1} = A(\hat{Z}_{k-2} - Z_{k-2}) + W(\hat{w}_{k-2} - w_{k-2}) \simeq 0$, which in turn implies $\hat{Z}_k - Z_k = A(\hat{Z}_{k-1} - Z_{k-1}) + W(\hat{w}_{k-1} - w_{k-1}) \simeq W(\hat{w}_{k-1} - w_{k-1})$. As $(A, B)$ is controllable, a matrix $K$ making $A^*$ Schur always exists, thus ensuring $||A^* Z_k|| < ||Z_k||$. Also, for small $T$ [66], $\hat{w}_{k-1} \simeq \hat{w}_{k-2} \simeq w_{k-2}$. Then, from (4.5.4), $Z_k$ evolves with a stable dynamics subject to a forcing signal $\varphi$ such that $||\varphi|| = ||BKW(w_{k-2} - w_{k-1}) + W(w_k - w_{k-2})|| \leq T(||B||\,||K|| + 2)\gamma$, where $\gamma$ is the absolute maximum variation of $w_k$ between any two consecutive samples. A possible estimate for this quantity is $\gamma = \max(\ddot{q}_{max}, \dot{S}_{max}) = \max(\ddot{q}_{max}, \sigma_{max})$, where $\ddot{q}_{max}$ and $\sigma_{max}$ are the maximum reachable acceleration and stiffness. $Z_k$ converges to the equilibrium $Z_k = (\mathbb{I}_{3n} - A^*)^{-1}\varphi$, whose norm is $||Z_k|| \leq T\,||(\mathbb{I}_{3n} - A^*)^{-1}||(||B||\,||K|| + 2)\gamma$ and hence is upper bounded by a quantity proportional to $T$. Finally, left-multiplying both members of (4.5.3) by the pseudoinverse of $B$, the control law in (4.5.1) is obtained. □

## 4.6 Method Application and Evaluation

This section shows the performance of the proposed solution when applied to the 3-degree-of-freedom ASR in Fig. 4.1. In the considered hardware setup, each joint of the robot is driven by a *qbmove advanced* actuator [117] that allows simultaneous settings of link position and joint stiffness. The section is organized in three parts: 1) instances of the proposed estimator and robust controller are derived based on a coarse but very convenient simplification of the robot's compound dynamics; 2) their effectiveness and robustness are shown in simulation with large model uncertainty due to the few amount of information used for their derivation; 3) experimental test results with the adopted real hardware setup are reported.

### 4.6.1 Derivation of Estimator and Controller Components

To test the robustness of the method and to show also the few amount of information used to derive the corresponding estimator and controller, first of all, all links' interactions are completely neglected, thereby leading to a nominal inertia matrix inverse that is diagonal and given by $\bar{M}(q)^{-1} =$

Table 4.1: Nominal parameters of the VSA-driven robot

| | |
|---|---|
| Link masses | $m_1 = m_2 = m_3 = 0.45$ kg |
| Link inertia | $I_1 = I_2 = 0.0045$ kgm$^2$, $I_3 = 0.001125$ kgm$^2$ |
| Link lengths | $l_1 = l_2 = 0.1$ m, $l_3 = 0.05$ m |
| Agonistic | $k_a = 0.0026$ Nm, $a_a = 8.9995$ rad$^{-1}$ |
| Antagonistic | $k_b = 0.0011$ Nm, $a_b = 8.9989$ rad$^{-1}$ |

diag$(1/I_1, 1/I_2, 1/I_3)$ (cf. e.g. [118]), where $I_i$ are the solely link inertia constants whose values are reported in Table. 4.1. Secondly, from [117], the $i$-th VSA device can apply the total elastic torque and set the joint stiffness given by the following VSA-specific formulas

$$\begin{aligned} \tau_i^e &= k_{i,a} \sinh(u_{i,a}) + k_{i,b} \sinh(u_{i,b}) \,, \\ \sigma_i &= a_{i,a} k_{i,a} \cosh(u_{i,a}) + a_{i,b} k_{i,b} \cosh(u_{i,b}) \,, \end{aligned} \tag{4.6.1}$$

where $u_{i,a} = a_{i,a}\phi_{i,a}$, $u_{i,b} = a_{i,b}\phi_{i,b}$, and where $k_{i,a}$, $k_{i,b}$, $a_{i,a}$, and $a_{i,b}$ are suitable constants whose nominal values $k_a$, $k_b$, $a_a$, and $a_b$, experimentally identified by the manufacturer, are reported again in Table. 4.1. Given the convex behavior of such functions, one can expand them as

$$\tau_i^e = \pi_i(t)(u_{i,a} + u_{i,b}) \,, \; \sigma_i = \mu_i(t)(u_{i,a} + u_{i,b}) \,, \tag{4.6.2}$$

where $\pi_i(t)$ and $\mu_i(t)$ are time-varying yet bounded slope signals. While for our approach any positive constant value can be used in place of these signals, it is reasonable to conservatively tune them bargaining the maximum elastic torque $\tau^e_{\max}$ and stiffness $\sigma_{\max}$ demands. To do so, using the prosthaphaeresis formulas for hyperbolic functions, with $a_{i,a} = a_{i,b} = a$ and $k_{i,a} = k_{i,b} = k$, one can rewrite (4.6.1) as $\tau_i^e = 2k\,\kappa\,\omega$ and $\sigma_i = 2ak\,\varepsilon\,\omega$, with $\kappa = \sinh((u_{i,a} + u_{i,b})/2)$, $\omega = \cosh((u_{i,a} - u_{i,b})/2)$, and $\varepsilon = \cosh((u_{i,a} + u_{i,b})/2)$. The ratio $\varepsilon/\kappa = \coth((u_{i,a} + u_{i,b})/2) = \sigma_i/(a\tau_i^e)$ allows finding $(u_{i,a} + u_{i,b})/2 = (\sigma_i/(a\tau_i^e)) = \chi_1$. Then, from the relation $\omega = \tau_i^e/(2k\,\kappa)$, one also obtains $(u_{i,a} - u_{i,b})/2 = (\tau_i^e/(2k\,\sinh(\chi_1))) = \chi_2$, and finally $\begin{pmatrix} u_{i,a} \\ u_{i,b} \end{pmatrix} = \begin{pmatrix} \frac{1}{2} & \frac{1}{2} \\ \frac{1}{2} & -\frac{1}{2} \end{pmatrix}^{-1} \begin{pmatrix} \chi_1 \\ \chi_2 \end{pmatrix}$. Evaluating this last relation for the maximum torque and stiffness demands allows obtaining the maximum values for $u_{i,a}$ and $u_{i,b}$, which are then converted to the maximum of $\pi_i$ and $\mu_i$. For the

adopted qbmove actuators, it holds $\tau^e_{\max} = 7$ Nm and $\sigma_{\max} = 83.5$ Nm/rad, and hence it holds $\pi_i = 3.3416$ and $\mu_i = 37.2032$.

In accordance with this reasoning and the proposed formalization, the nominal matrices of the actuation-related terms are chosen as $\bar{\Pi} = \text{diag}(\bar{\Pi}_1, \bar{\Pi}_2, \bar{\Pi}_3)$, $\bar{\Sigma} = \text{diag}(\bar{\Sigma}_1, \bar{\Sigma}_2, \bar{\Sigma}_3)$, with $\bar{\Pi}_i = (\pi_i, \pi_i, 0, 0)$ and $\bar{\Sigma}_i = (0, 0, \mu_i, \mu_i)$, for all $i$, and the (manipulable) input vector is

$$\Gamma(\phi_a, \phi_b) = (\gamma_1^T(\phi_{1,a}, \phi_{1,b}), \gamma_2^T(\phi_{2,a}, \phi_{2,b}), \gamma_3^T(\phi_{3,a}, \phi_{3,b}))^T ,$$

with $\gamma_i = (u_{i,a}, u_{i,b})^T$, for all $i$. Accordingly, the (manipulable) input vector is $U_k = \Gamma(\phi_a(kT), \phi_b(kT))$ and the matrices of the estimator are of immediate writing from Theorem 8, while they are omitted here for the sake of space. Finally, it should be recalled, as stated in paragraph (4.3), that the actual inputs to the $i$-th VSA device are the motor positions, $\theta_{i,a}$ and $\theta_{i,b}$. They are finally determined by inverting (4.2.1) and are given by $\theta^c_{i,a} = q_i - u_{i,a}/a$ and $\theta^c_{i,b} = q_i - u_{i,b}/a$.

### 4.6.2 Effectiveness and Robustness Evaluation

To show its validity and robustness, the proposed approach is tested in Matlab/Simulink with parametric, nominal inertia matrix $\bar{M}$, and input matrix $B$ uncertainties. Nominal parameters are reported in Table 4.1. Nominal matrix $\bar{M}$ is set to be $\text{diag}(I_1, I_2, I_3)$ representing the case where all off-diagonal entries of $M(q)$ are neglected. Perturbation of parameters, $\bar{M}$, and $B$ range from a 25% to a 100% increase from their nominal values. Fig. 4.2 depicts the position and stiffness tracking errors for the robot's base segment, being the one with the most visible trends. A common behavior is that higher tracking errors appear with larger uncertainty, yet, the closed-loop performance is not significantly deteriorated even with substantial uncertainty. Noticeably, this shows that the method is robust with respect to the choice of $\bar{M}$ and $B$, which, in practice, allows neglecting all off-diagonal entries of $M(q)$ and approximating the diagonal ones even up to a relative error of 100%.

Moreover, the proposed solution is compared in Fig. 4.3 with an ESO-based one [119], initialized with position and stiffness tracking errors of $(0.1, 0.1, 0.1)$ rad and $(4, 4, 4)$ Nm/rad. The robust DUIO-based control law in (4.5.1) is used with the same control gains and, specifically, matrix $K$ is chosen so that the closed loop matrix $A^*$ are in the unit circle, and with desired references of the

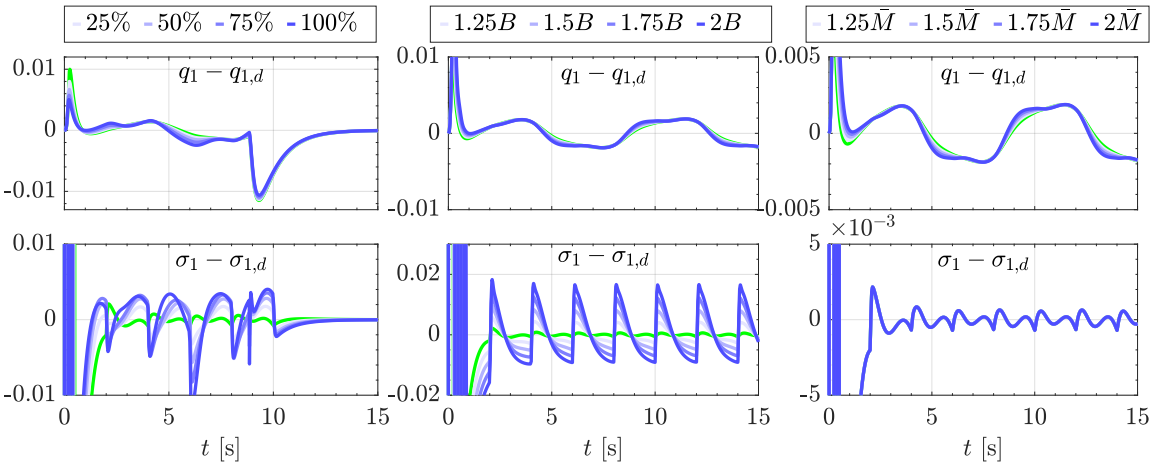


Figure 4.2: *Robustness to parametric (left), input matrix $B$ (middle) and inertia matrix $\bar{M}$ (right) uncertainties, ranging from* 25% *to* 100% *deviation from their nominal values.* Green indicates the closed-loop behavior with nominal choices for parameters, $B$ and $\bar{M}$. Position and stiffness tracking errors grow as uncertainty increases, yet, the closed-loop system performance does not deteriorate considerably. Tracking errors exist during time-varying references and are due to worse feedforward compensation, originating from larger parametric uncertainty and model simplification. Indeed, they nicely converge when references become still (last phase of left plots).

form $q_{i,d} = Q_i \sin \omega_{q_i} t$ and $\sigma_{i,d} = \epsilon_i + A_{\sigma_i} |\sin \omega_{\sigma_i} t|$, for $i \in \{1, 2, 3\}$. Fig. 4.3 shows that the UIO solution outperforms the ESO one, achieves a faster and more precise disturbance estimation and allows better tracking errors.

### 4.6.3 Experimental Validation

An experimental validation of the proposed solution is finally presented using the real hardware pictured in Fig. 4.1. Nominal geometric and inertial parameter values are in Table 4.1 and the desired trajectories have the same form as in the simulations, so as to capture similar behaviors, and have been chosen with various amplitudes and frequencies for each joint. The controller is also set as in Sec. 4.6.1. Link positions are measured through the encoders embedded in the *qbmove* actuators, while joint stiffness is obtained through the use of the stiffness estimator in [120]. As it can be seen in Fig. 4.4, the proposed solution robustly tracks the desired signals, and imperfect yet practically negligible tracking errors occur only very rarely, which is due to intrinsic slackness of the actuators. Noteworthy, despite the drastically simplified robot model, used to design the

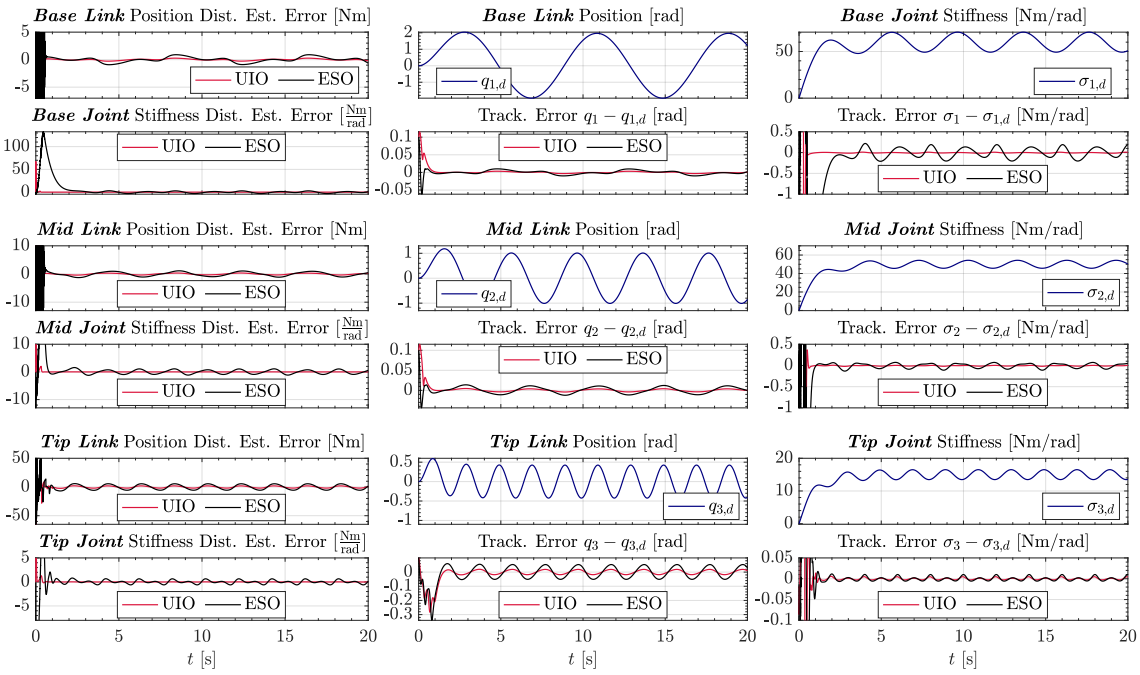


Figure 4.3: *Robustness to large uncertainty and comparison with ESO.* Results from typical simulation runs with 100% deviation of system parameters from the nominal values, as well as a drastic simplification of the system model. Despite the large uncertainty, when the proposed DUIO-solution is used, the desired trajectories are accurately tracked as a result of fast and precise estimation of the disturbance perturbing the nominal system. The ESO-based solution under-performs especially when the disturbance signals are rapidly changing.

estimator from Theorem 8 and the controller from Theorem 9, each link position and joint stiffness are smoothly and successfully controlled.

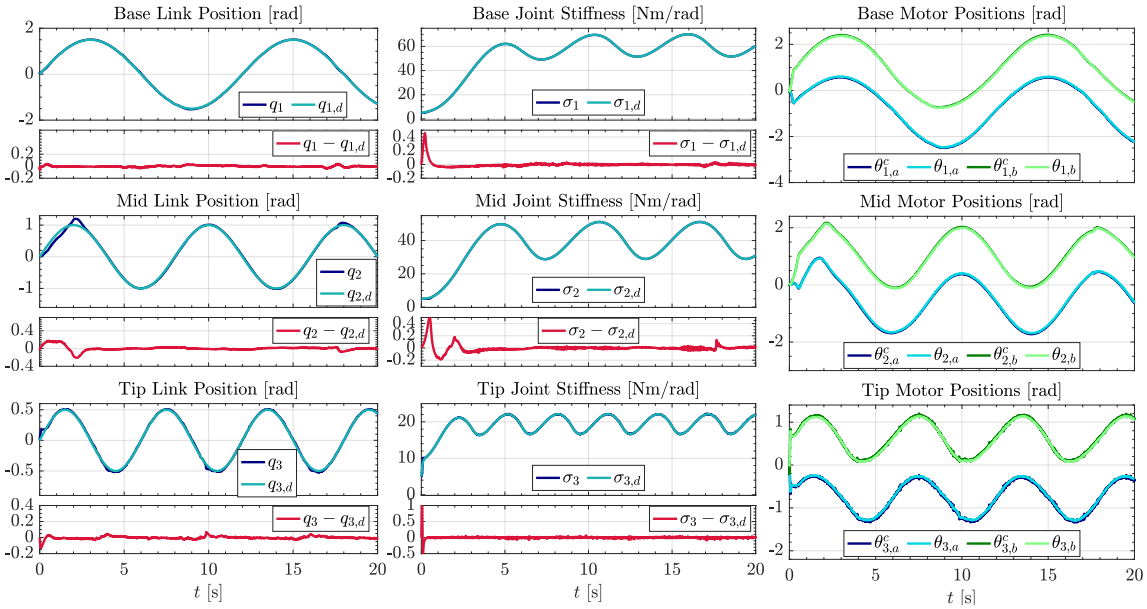


Figure 4.4: *Experimental validation.* Results from testing with real ASR pictured in Fig. 4.1, when the task is to simultaneously track sinusoidal position and stiffness trajectories. The position and stiffness tracking errors are reported in red for each degree-of-freedom. Despite the drastically simplified robot model, upon which the estimator from Theorem 8 and the controller from Theorem 9 are derived, the proposed solution can robustly track the desired signals. Commanded $\theta^c_{i,j}$ and executed $\theta_{i,j}$ motor angles are shown and largely within the available range of the involved VSA devices.

## 4.7 Conclusion

This work formulated the model of VSA-driven articulated soft robots with the factorized actuator matrix suitable for the decomposition into the nominal and uncertain dynamics, and it derived a novel solution for their control. Using delayed unknown input observer theory and disturbance-observer-based control, the proposed approach enables successful position and stiffness tracking, even with large disturbance due to the model uncertainty. Validation of the method was carried out in simulations and experiments, proving also its robustness to parametric and structural uncertainties. Future work will explore the advantages of information decoupling between possible external

interaction and uncertainty estimation, due to parametric changes and actuator failures.

# Chapter 5

# Conclusion and Future Works

This thesis addressed the robust control of complex systems via a Delayed Unknown Input Observer. First, through a suitable model dynamic reformulation, a generic nonlinear system has been described as the sum of two functions, the first linear and known and the second highly nonlinear and unknown. Subsequently, a discrete-time Delayed Unknown Input Observer has been designed to asymptotically estimate both system state and disturbance to ensure the necessary information to a controller that, exploiting them, actively compensates the estimated disturbance and asymptotically steers the system state to the desired one. This thesis also presents a closed-loop stability proof of the method and its effectiveness and superiority to existing methods are studied in theory and practice in two different contexts, i.e. self-driving racecars and articulated soft-robots. Future works will focus on improving the observer response in the presence of measurement noise and updating the estimates at the current time.

# Bibliography


[1] B.-Z. Guo and Z. Zhao, *Active Disturbance Rejection Control for Nonlinear Systems: An Introduction*. 10 2016.

[2] L. Shihua, J. Yang, W. Chen, and X. Chen, *Disturbance Observer-Based Control: Methods and Applications (1st ed.)*. CRC Press, 10 2014.

[3] J. Han, "From pid to active disturbance rejection control," *IEEE Transactions on Industrial Electronics*, vol. 56, no. 3, pp. 900–906, 2009.

[4] S. Sundaram and C. N. Hadjicostis, "Delayed observers for linear systems with unknown inputs," *IEEE Transactions on Automatic Control*, vol. 52, pp. 334–339, Feb 2007.

[5] J. Jin, M.-J. Tahk, and C. Park, "Time-delayed state and unknown input observation," *International Journal of Control*, vol. 66, no. 5, pp. 733–746, 1997.

[6] S. Pedone and A. Fagiolini, "Racecar longitudinal control in unknown and highly-varying driving conditions," *IEEE transactions on vehicular technology*, vol. 69, no. 11, pp. 12521–12535, 2020.

[7] S. Pedone and A. Fagiolini, "Robust discrete-time lateral control of racecars by unknown input observers," *IEEE Transactions on Control Systems Technology*, pp. 1–9, 2022.

[8] S. Pedone, M. Trumić, K. Jovanović, and A. Fagiolini, "Robust and decoupled position and stiffness control for electrically-driven articulated soft robots," *IEEE Robotics and Automation Letters*, vol. 7, no. 4, pp. 9059–9066, 2022.

[9] qbrobotics, "qbmove Advanced KIT - User Manual." Accessed: 2022-02-15.

[10] S. Sundaram and C. N. Hadjicostis, "Delayed observers for linear systems with unknown inputs," *IEEE Trans. Automat. Contr.*, vol. 52, no. 2, pp. 334–339, 2007.

[11] J. CHEN, R. J. PATTON, and H.-Y. ZHANG, "Design of unknown input observers and robust fault detection filters," *International Journal of Control*, vol. 63, no. 1, pp. 85–105, 1996.

[12] K. Katsaros and M. Dianati, "Evolution of vehicular communications within the context of 5g systems," *Enabling 5G Communication Systems to Support Vertical Industries*, pp. 103–126, 2019.

[13] A. Li and K. Luk, "Single-layer wideband end-fire dual-polarized antenna array for device-to-device communication in 5g wireless systems," *IEEE Transactions on Vehicular Technology*, vol. 69, no. 5, pp. 5142–5150, 2020.

[14] T. Hou, Y. Liu, Z. Song, X. Sun, and Y. Chen, "Uav-to-everything (u2x) networks relying on noma: A stochastic geometry model," *IEEE Transactions on Vehicular Technology*, pp. 1–1, 2020.

[15] F. Zhu, Z. Li, S. Chen, and G. Xiong, "Parallel transportation management and control system and its applications in building smart cities," *IEEE Transactions on Intelligent Transportation Systems*, vol. 17, no. 6, pp. 1576–1585, 2016.

[16] F.-Y. Wang and J. J. Zhang, "Transportation 5.0 in cpss: Towards acp-based society-centered intelligent transportation," in *2017 IEEE 20th International Conference on Intelligent Transportation Systems (ITSC)*, pp. 762–767, IEEE, 2017.

[17] A. Rucco, G. Notarstefano, and J. Hauser, "An efficient minimum-time trajectory generation strategy for two-track car vehicles," *IEEE Transactions on Control Systems Technology*, vol. 23, no. 4, pp. 1505–1519, 2015.

[18] J. Betz, A. Wischnewski, A. Heilmeier, F. Nobis, L. Hermansdorfer, T. Stahl, T. Herrmann, and M. Lienkamp, "A software architecture for the dynamic path planning of an autonomous

racecar at the limits of handling," in *2019 IEEE International Conference on Connected Vehicles and Expo (ICCVE)*, pp. 1–8, IEEE, 2019.

[19] A. Heilmeier, A. Wischnewski, L. Hermansdorfer, J. Betz, M. Lienkamp, and B. Lohmann, "Minimum curvature trajectory planning and control for an autonomous race car," *Vehicle System Dynamics*, pp. 1–31, 2019.

[20] Y. Lu, X. Huang, K. Zhang, S. Maharjan, and Y. Zhang, "Blockchain empowered asynchronous federated learning for secure data sharing in internet of vehicles," *IEEE Transactions on Vehicular Technology*, vol. 69, no. 4, pp. 4298–4311, 2020.

[21] R. Singh, D. Saluja, and S. Kumar, "Blind cancellation in radar based self driving vehicles," *IEEE Transactions on Vehicular Technology*, pp. 1–1, 2020.

[22] Y. Fu, C. Li, R. Yu, T. H. Luan, and Y. Zhang, "A decision-making strategy for vehicle autonomous braking in emergency via deep reinforcement learning," *IEEE Transactions on Vehicular Technology*, pp. 1–1, 2020.

[23] C. Li, H. Zhang, T. Zhang, J. Rao, L. Y. Wang, and G. Yin, "Cyber-physical scheduling for predictable reliability of inter-vehicle communications," *IEEE Transactions on Vehicular Technology*, vol. 69, no. 4, pp. 4192–4206, 2020.

[24] A. Fagiolini, G. Dini, and A. Bicchi, "Distributed intrusion detection for the security of industrial cooperative robotic systems," *IFAC Proceedings Volumes*, vol. 47, no. 3, pp. 7610–7615, 2014.

[25] J. Hu, X. Zhang, and S. Maybank, "Abnormal driving detection with normalized driving behavior data: A deep learning approach," *IEEE Transactions on Vehicular Technology*, pp. 1–1, 2020.

[26] G. De Nicolao, A. Ferrara, and L. Giacomini, "Onboard sensor-based collision risk assessment to improve pedestrians' safety," *IEEE transactions on vehicular technology*, vol. 56, no. 5, pp. 2405–2413, 2007.

[27] R. Hussain and S. Zeadally, "Autonomous cars: Research results, issues, and future challenges," *IEEE Communications Surveys & Tutorials*, vol. 21, no. 2, pp. 1275–1313, 2018.

[28] D. Caporale, A. Fagiolini, L. Pallottino, A. Settimi, A. Biondo, F. Amerotti, F. Massa, S. De Caro, A. Corti, and L. Venturini, "A planning and control system for self-driving racing vehicles," *IEEE 4th International Forum on Research and Technologies for Society and Industry, RTSI 2018 - Proceedings*, 2018.

[29] B. Chen, X. Li, S. A. Evangelou, and R. Lot, "Joint propulsion and cooling energy management of hybrid electric vehicles by optimal control," *IEEE Transactions on Vehicular Technology*, vol. 69, no. 5, pp. 4894–4906, 2020.

[30] L. Ulrich, "Top 10 tech cars: The scramble for electric dominance has begun," *IEEE Spectrum*, vol. 57, no. 4, pp. 30–39, 2020.

[31] N. A. Greenblatt, "Self-driving cars and the law," *IEEE spectrum*, vol. 53, no. 2, pp. 46–51, 2016.

[32] F. Bohm and K. Häger, *Introduction of autonomous vehicles in the Swedish traffic system: Effects and changes due to the new self-driving car technology.* PhD thesis, University of Uppsala, 2015.

[33] F. Tian, Y. Yu, X. Yuan, B. Lyu, and G. Gui, "Predicted decoupling for coexistence between wifi and lte in unlicensed band," *IEEE Transactions on Vehicular Technology*, vol. 69, no. 4, pp. 4130–4141, 2020.

[34] E. Awad, S. Dsouza, R. Kim, J. Schulz, J. Henrich, A. Shariff, J.-F. Bonnefon, and I. Rahwan, "The moral machine experiment," *Nature*, vol. 563, no. 7729, pp. 59–64, 2018.

[35] S. Nyholm, "The ethics of crashes with self-driving cars: A roadmap, i," *Philosophy Compass*, vol. 13, no. 7, p. e12507, 2018.

[36] M. Guiggiani, "The science of vehicle dynamics," *Pisa, Italy: Springer Netherlands*, 2014.

[37] M. Burckhardt, "Abs und asr, sicherheitsrelevantes, radschlupf-regel system," *Lecture Scriptum, University of Braunschweig*, 1987.

[38] H. Pacejka, "Tire and vehicle dynamics," *Butterworth-Heinemann*, 2012.

[39] S. Watkins, S. Toksoy, and J. Saunders, "On the generation of tunnel turbulence for road vehicles," *11th AFMC, Hobart, Australia*, 1992.

[40] Z. Liang, J. Zhao, Z. Dong, Y. Wang, and Z. Ding, "Torque vectoring and rear-wheel-steering control for vehicle's uncertain slips on soft and slope terrain using sliding mode algorithm," *IEEE Transactions on Vehicular Technology*, vol. 69, no. 4, pp. 3805–3815, 2020.

[41] H. Guo, Z. Yin, D. Cao, H. Chen, and C. Lv, "A review of estimation for vehicle tire-road interactions toward automated driving," *IEEE Transactions on Systems, Man, and Cybernetics: Systems*, vol. 49, no. 1, pp. 14–30, 2018.

[42] C. Diaz, V. Quintero, A. Perez, F. Jaramillo, C. Burgos-Mellado, H. Rozas, M. E. Orchard, D. Saez, and R. Cardenas, "Particle-filtering-based prognostics for the state of maximum power available in lithium-ion batteries at electromobility applications," *IEEE Transactions on Vehicular Technology*, pp. 1–1, 2020.

[43] C. Huang, L. Li, Y. Liu, and L. Xiao, "Robust observer based intermittent forces estimation for driver intervention identification," *IEEE Transactions on Vehicular Technology*, vol. 69, no. 4, pp. 3628–3640, 2020.

[44] S.-K. Chen, N. Moshchuk, F. Nardi, and J. Ryu, "Vehicle rollover avoidance," *IEEE Control System*, vol. 30, no. 4, pp. 70–85, 2010.

[45] K. Nam, S. Oh, H. Fujimoto, and Y. Hori, "Estimation of sideslip through rls and kalman filter approaches," *IEEE Trans. Ind. Electron.*, vol. 60, no. 3, pp. 988–1000, 2013.

[46] M. Doumiati, A. Victorino, D. Lechner, G. Baffet, and A. Charara, "Observers for vehicle tyre/road forces estimation: Experimental validation," *Vehicle System Dynamics*, vol. 48, no. 11, pp. 1345–1378, 2010.

[47] M. Doumiati, A. Victorino, A. Charara, and D. Lechner, "Onboard real-time estimation of vehicle lateral tire road forces and sideslip angle," *IEEE/ASME Trans. Mechatronics*, vol. 16, no. 4, pp. 601–614, 2011.

[48] J. Dakhlallah, S. Glaser, S. Mammar, and Y. Sebsadji, "Tire-road forces estimation using extended kalman filter and sideslip angle evaluation," *American Control Conference*, 2008.

[49] M. Best, T. Gordon, and P. Dixon, "An extended adaptive kalman filter for real-time state estimation of vehicle handling dynamics," *Vehicle System Dynamics*, vol. 1, no. 34, pp. 55–75, 2000.

[50] B.-Z. Guo and Z.-L. Zhao, *Active disturbance rejection control for nonlinear systems: An introduction*. John Wiley & Sons, 2016.

[51] S. You, J. Gil, and W. Kim, "Fixed-time slip control with extended-state observer using only wheel speed for anti-lock braking systems of electric vehicles," *IEEE Transactions on Intelligent Transportation Systems*, pp. 1–11, 2021.

[52] H. Wang, Z. Zuo, Y. Wang, H. Yang, and S. Chang, "Composite nonlinear extended state observer and its application to unmanned ground vehicles," *Control Engineering Practice*, vol. 109, p. 104731, 2021.

[53] S. E. Talole, J. P. Kolhe, and S. B. Phadke, "Extended-state-observer-based control of flexible-joint system with experimental validation," *IEEE Trans. on Industrial Electronics*, vol. 57, no. 4, pp. 1411–1419, 2009.

[54] Y. Wu, L. Wang, J. Zhang, and F. Li, "Path following control of autonomous ground vehicle based on nonsingular terminal sliding mode and active disturbance rejection control," *IEEE Transactions on Vehicular Technology*, vol. 68, no. 7, pp. 6379–6390, 2019.

[55] H. Yang, L. Cheng, Y. Xia, and Y. Yuan, "Active disturbance rejection attitude control for a dual closed-loop quadrotor under gust wind," *IEEE Transactions on Control Systems technology*, vol. 26, no. 4, pp. 1400–1405, 2017.

[56] Y. Xia, F. Pu, S. Li, and Y. Gao, "Lateral path tracking control of autonomous land vehicle based on adrc and differential flatness," *IEEE Transactions on Industrial Electronics*, vol. 63, no. 5, pp. 3091–3099, 2016.

[57] W. Xue, W. Bai, S. Yang, K. Song, Y. Huang, and H. Xie, "Adrc with adaptive extended state observer and its application to air–fuel ratio control in gasoline engines," *IEEE Transactions on Industrial Electronics*, vol. 62, no. 9, pp. 5847–5857, 2015.

[58] B. Goldfain, P. Drews, C. You, M. Barulic, O. Velev, P. Tsiotras, and J. M. Rehg, "Autorally: An open platform for aggressive autonomous driving," *IEEE Control Systems Magazine*, vol. 39, no. 1, pp. 26–55, 2019.

[59] R. Rajamani, *Vehicle dynamics and control*. Springer Science & Business Media, 2011.

[60] H. Guo, R. Yu, W. Qiang, and H. Chen, "Optimal slip based traction control for electric vehicles using feedback linearization," in *2014 International Conference on Mechatronics and Control (ICMC)*, pp. 1159–1164, IEEE, 2014.

[61] O. Walter, J. Schmalenstroeer, A. Engler, and R. Haeb-Umbach, "Smartphone-based sensor fusion for improved vehicular navigation," in *2013 10th Workshop on Positioning, Navigation and Communication (WPNC)*, pp. 1–6, IEEE, 2013.

[62] F. Massa, L. Bonamini, A. Settimi, L. Pallottino, and D. Caporale, "Lidar-based gnss denied localization for autonomous racing cars," *Sensors*, vol. 20, no. 14, p. 3992, 2020.

[63] R. No, "Regulation no 39 of the economic commission for europe of the united nations (un/ece), uniform provisions concerning the approval of vehicles with regard to the speedometer equipment including its installation," *L*, vol. 120, p. 40, 39.

[64] K. A. Al-Gaadi, "Testing the accuracy of autonomous gps in ground speed measurement," *J. Appl. Sci*, vol. 5, pp. 1518–1522, 2005.

[65] R. N. Jazar, "Driveline dynamics," in *Vehicle Dynamics*, pp. 173–223, Springer, 2017.

[66] K. Youcef-Toumi and O. Ito, "A time delay controller for systems with unknown dynamics," in *1988 American Control Conference*, pp. 904–913, 1988.

[67] G. Welch and G. Bishop, "An introduction to the kalman filter," *University of North Carolina at Chapel Hill*, 2006.

[68] L. Biagiotti, "State estimation in presence of disturbances: The kalman filter," *Lectures Slided on Control and System Theory*, 2016.

[69] S. G. Mohinder and A. P. Andrews, "Kalman filtering, theory and practice using matlab, third edition," *WILEY*, 2008.

[70] F. Naets, S. Van Aalst, B. Boulkroune, N. El Ghouti, and W. Desmet, "Design and experimental validation of a stable two-stage estimator for automotive sideslip angle and tire parameters," *IEEE Transactions on Vehicular Technology*, vol. 66, no. 11, 2017.

[71] M. Dousti, S. C. Baslamısli, E. T. Onder, and S. Solmaz, "Design of a multiple-model switching controller for abs braking dynamics," *Transactions of the Institute of Measurement and Control*, vol. 37, no. 5, pp. 582–595, 2015.

[72] A. Ružinskas and H. Sivilevičius, "Magic formula tyre model application for a tyre-ice interaction," *Procedia Eng*, vol. 187, pp. 335–341, 2017.

[73] T. M. I. Hakim and O. Arifianto, "Implementation of drydend continuos turbulence model into simulink for lsa-02 flight test simulation," *5th International Seminar of Aerospace Science and Technology*, 2018.

[74] L. Li, F.-Y. Wang, and Q. Zhou, "Integrated longitudinal and lateral tire/road friction modeling and monitoring for vehicle motion control," *IEEE Transactions on intelligent transportation systems*, vol. 7, no. 1, pp. 1–19, 2006.

[75] J. Katz, *Race car aerodynamics: designing for speed*. R. Bentley, 1995.

[76] G. Genta, *Motor vehicle dynamics: modeling and simulation*, vol. 43. World Scientific, 1997.

[77] A. Radke and Zhiqiang Gao, "A survey of state and disturbance observers for practitioners," in *2006 American Control Conference*, pp. 6 pp.–, 2006.

[78] S. Rouhani, T.-C. Tsao, and J. L. Speyer, "Robust disturbance estimation-an integrated game theoretic and unknown input observer approach," in *2019 American Control Conference (ACC)*, pp. 5077–5082, IEEE, 2019.

[79] A. Oveisi, M. Aldeen, and T. Nestorović, "Disturbance rejection control based on state-reconstruction and persistence disturbance estimation," *Journal of the Franklin Institute*, vol. 354, no. 18, pp. 8015–8037, 2017.

[80] D. Rotondo, M. Witczak, V. Puig, F. Nejjari, and M. Pazera, "Robust unknown input observer for state and fault estimation in discrete-time takagi–sugeno systems," *International Journal of Systems Science*, vol. 47, no. 14, pp. 3409–3424, 2016.

[81] S. G. Mohinder and A. Andrews, "Kalman filtering, theory and practice using matlab, third edition," *Wiley*, 2008.

[82] D. Caporale, A. Settimi, F. Massa, F. Amerotti, A. Corti, A. Fagiolini, M. Guiggian, A. Bicchi, and L. Pallottino, "Towards the design of robotic drivers for full-scale self-driving racing cars," in *2019 International Conference on Robotics and Automation (ICRA)*, pp. 5643–5649, IEEE, 2019.

[83] T. Hakim and O. Arifianto, "Implementation of drydend continuos turbulence model into simulink for lsa-02 flight test simulation," 2018.

[84] "Vehicle dynamics blockset - model and simulate vehicle dynamics in a virtual 3d environment."

[85] M. Guiggiani, "The science of vehicle dynamics," *Pisa, Italy: Springer Netherlands*, 2014.

[86] R. Rajamani, *Vehicle dynamics and control*. Springer Science & Business Media, 2011.

[87] J. Chen and R. J. Patton, "Robust model-based fault diagnosis for dynamic systems," *Springer Science & Business Media, LLC*, vol. 223(1), 1999.

[88] S. Sundaram and C. N. Hadjicostis, "Delayed observers for linear systems with unknown inputs," *IEEE Transactions on Automatic Control*, vol. 52, no. 2, pp. 334–339, 2007.

[89] T. D. Gillespie, *Fundamentals of vehicle dynamics*, vol. 400. Society of automotive engineers Warrendale, PA, 1992.

[90] M. Krstic, P. V. Kokotovic, and I. Kanellakopoulos, *Nonlinear and adaptive control design*. John Wiley & Sons, Inc., 1995.

[91] H. K. Khalil, *Nonlinear systems*. Prentice Hall Upper Saddle River, NJ, 3 ed., 2002.

[92] "Spatial dual - advanced navigation positioning everywhere," 2020.

[93] A. Norouzi, M. Masoumi, A. Barari, and S. Farrokhpour Sani, "Lateral control of an autonomous vehicle using integrated backstepping and sliding mode controller," *Proceedings of the Institution of Mechanical Engineers, Part K: Journal of Multi-body Dynamics*, vol. 233, no. 1, pp. 141–151, 2019.

[94] M. Guiggiani, "The science of vehicle dynamics," *Pisa, Italy: Springer Netherlands*, p. 15, 2014.

[95] D. Caporale, A. Fagiolini, L. Pallottino, A. Settimi, A. Biondo, F. Amerotti, F. Massa, S. De Caro, A. Corti, and L. Venturini, "A planning and control system for self-driving racing vehicles," in *2018 IEEE 4th International Forum on Research and Technology for Society and Industry (RTSI)*, pp. 1–6, IEEE, 2018.

[96] H. B. Pacejka, "Chapter 4 - semi-empirical tyre models," in *Tyre and Vehicle Dynamics (Second Edition)* (H. B. Pacejka, ed.), pp. 156–215, Oxford: Butterworth-Heinemann, second edition ed., 2006.

[97] T. M. I. Hakim and O. Arifianto, "Implementation of dryden continuous turbulence model into simulink for lsa-02 flight test simulation," in *Journal of Physics*, vol. 1005, p. 012017, IOP Publishing, 2018.

[98] A. H. Al-Bayati and Z. Skaf, "A comparative study of linear observers applied to a dc servo motor," in *Proceedings of the 2010 International Conference on Modelling, Identification and Control*, pp. 785–790, IEEE, 2010.

[99] R. Van Ham *et al.*, "Maccepa, the mechanically adjustable compliance and controllable equilibrium position actuator: Design and implementation in a biped robot," *Robot. Auton. Syst.*, vol. 55, no. 10, pp. 761–768, 2007.

[100] F. Wu and M. Howard, "Energy regenerative damping in variable impedance actuators for long-term robotic deployment," *IEEE Trans. Robot.*, vol. 36, no. 6, pp. 1778–1790, 2020.

[101] R. Mengacci *et al.*, "Stiffness bounds for resilient and stable physical interaction of articulated soft robots," *IEEE Robot. Autom. Lett.*, vol. 4, no. 4, pp. 4131–4138, 2019.

[102] S. Wolf, G. Grioli, O. Eiberger, W. Friedl, M. Grebenstein, H. Höppner, E. Burdet, D. G. Caldwell, R. Carloni, M. G. Catalano, *et al.*, "Variable stiffness actuators: Review on design and components," *IEEE/ASME Trans. Mechatron.*, vol. 21, no. 5, pp. 2418–2430, 2015.

[103] G. Palli, C. Melchiorri, and A. De Luca, "On the feedback linearization of robots with variable joint stiffness," in *Int. Conf. Robot. Autom. (ICRA)*, pp. 1753–1759, IEEE, 2008.

[104] R. Mengacci *et al.*, "On the motion/stiffness decoupling property of articulated soft robots with application to model-free torque iterative learning control," *The Int. J. Rob. Res.*, vol. 40, no. 1, pp. 348–374, 2021.

[105] M. Trumić, K. Jovanović, and A. Fagiolini, "Decoupled nonlinear adaptive control of position and stiffness for pneumatic soft robots," *The Int. J. of Rob. Research*, vol. 40, no. 1, pp. 277–295, 2021.

[106] S. S. M. Salehian, M. Khoramshahi, and A. Billard, "A dynamical system approach for softly catching a flying object: Theory and experiment," *IEEE Trans. Robot.*, vol. 32, no. 2, pp. 462–471, 2016.

[107] R. Mengacci *et al.*, "Overcoming the torque/stiffness range tradeoff in antagonistic variable stiffness actuators," *Trans. Mechatr,*, vol. 26, no. 6, pp. 3186–3197, 2021.

[108] A. Albu-Schäffer and A. Bicchi, "Actuators for soft robotics," in *Handbook of robotics* (B. Siciliano and O. Khatib, eds.), ch. 21, pp. 243–282, Springer, 2016.

[109] M. Ruderman, T. Bertram, and M. Iwasaki, "Modeling, observation, and control of hysteresis torsion in elastic robot joints," *Mechatronics*, vol. 24, no. 5, pp. 407–415, 2014.

[110] I. Sardellitti *et al.*, "Gain scheduling control for a class of variable stiffness actuators based on lever mechanisms," *Trans. Robot.*, vol. 29, no. 3, pp. 791–798, 2013.

[111] F. Petit *et al.*, "Backstepping control of variable stiffness robots," *Trans. Control Syst. Technol.*, vol. 23, no. 6, pp. 2195–2202, 2015.

[112] M. Keppler, D. Lakatos, C. Ott, and A. Albu-Schäffer, "Elastic structure preserving (esp) control for compliantly actuated robots," *IEEE Trans. Robot.*, vol. 34, no. 2, pp. 317–335, 2018.

[113] F. Angelini *et al.*, "Decentralized trajectory tracking control for soft robots interacting with the environment," *IEEE Trans. on Robot.*, vol. 34, no. 4, pp. 924–935, 2018.

[114] F. Petit and A. Albu-Schäffer, "State feedback damping control for a multi dof variable stiffness robot arm," in *2011 Int. conf. Robot. Autom*, pp. 5561–5567, IEEE, 2011.

[115] T. H. Chong, V. Chalvet, and D. J. Braun, "Analytical conditions for the design of variable stiffness mechanisms," in *Int. Conf. Robot. Autom. (ICRA)*, pp. 1241–1247, IEEE, 2017.

[116] M. Mattioni, A. Moreschini, S. Monaco, and D. Normand-Cyrot, "On feedback passivation under sampling," in *American Control Conf.*, pp. 3578–3583, IEEE, 2021.

[117] qbrobotics, "qbmove Advanced KIT - User Manual." Accessed: 2022-02-15.

[118] J. Kim *et al.*, "Dynamic modeling and motion control of a three-link robotic manipulator," *Intl. Conf. on Artif. Life and Robotics*, vol. 22, pp. 380–383, 01 2017.

[119] S. E. Talole, J. P. Kolhe, and S. B. Phadke, "Extended-state-observer-based control of flexible-joint system with experimental validation," *IEEE Trans. Ind. Electron.*, vol. 57, no. 4, pp. 1411–1419, 2010.

[120] A. Fagiolini, M. Trumić, and K. Jovanović, "An input observer-based stiffness estimation approach for flexible robot joints," *IEEE Robot. Autom. Lett.*, vol. 5, no. 2, pp. 1843–1850, 2020.